Modeling and Application of Piezoelectric Materials in Repair of Engineering Structures

By

Nan Wu

A thesis submitted to
the Faculty of Graduate Studies of
The University of Manitoba
in partial fulfilment of the requirements for the degree of
Doctor of Philosophy

Department of Mechanical and Manufacturing Engineering
Faculty of Engineering
University of Manitoba
Winnipeg, Manitoba

Abstract

The shear horizontal wave propagation and vibration of piezoelectric coupled structures under an open circuit electrical boundary condition are studied. Following the studies on the dynamic response of piezoelectric coupled structures, the repair of both crack/notch and delaminated structures using piezoelectric materials are conducted. The main contribution was the proposed the active structural repair design using piezoelectric materials for different structures.

An accurate model for the piezoelectric effect on the shear wave propagation is first proposed to guide the application of piezoelectric materials as sensors and actuators in the repair of engineering structures. A vibration analysis of a circular steel substrate surface bonded by a piezoelectric layer with open circuit is presented. The mechanical models and solutions for the wave propagation and vibration analysis of piezoelectric coupled structures are established based on the Kirchhoff plate model and Maxwell equation.

Following the studies of the dynamic response of piezoelectric coupled structures, a close-loop feedback control repair methodology is proposed for a vibrating delaminated beam structure by using piezoelectric patches. The electromechanical characteristic of the piezoelectric material is employed to induce a local shear force above the delamination area via an external actuation voltage, which is designed as a feedback of the deflection of a vibrating beam and a delaminated plate, to reduce the stress singularity around the delamination tips. Furthermore, an experimental realization of an effective repair of a notched cantilever beam structure subjected to a dynamic loading by use of piezoelectric patches is reported. A small piezoelectric patch used as a sensor

is placed on the notch position to monitor the severity of the stress singularity around the notch area by measuring the charge output on the sensor, and a patch used as an actuator is located around the notch area to generate a required bending moment by employing an actuation voltage to reduce the stress singularity at the notch position. The actuation voltage on the actuator is designed from a feedback circuit process. Through the analytical model, FEM simulation and experimental studies, the active structural repair method using piezoelectric materials is realized and proved to be feasible and practical.

Acknowledgments

I would like to take this opportunity to thank my advisor, Prof. Abraham Q. Wang for his great teaching and warm help in both of my study and living. Without his constant support, guidance and encouragement, this thesis would not been possibly completed. It is a great honor for me to work under his supervision.

I am grateful to express my appreciations to professors, who gave me great help during my PhD study. Many thanks to Prof. Ehab EI-Salakawy, Prof. Qingjin Peng and Prof. Yunhua Luo. I also appreciate the following colleagues in the Structural Mechanical Lab. of the University of Manitoba: Hongxi Chen, Zhaoyang Liang and Dai Shi for their cooperation and support in my research.

Finally, I owe my deepest gratitude to my parents for their unconditional love and support throughout my work.

Contents

List of Tables

List of Figures

List of Copyrighted Material

Fig. 1-3 is adopted from the reference:

Wang Q., Quek S.T. and Liew K.M., On the repair of a cracked beam via piezoelectric patches, *Smart Mater. Struct.* **11** (2002) 404-410.

Fig. 1- 4 is adopted from the reference:

Wang Q., Duan W.H. and Quek S.T., Repair of notched beam under dynamic load using piezoelectric patch, *International Journal of Mechanical Science* **46** (2004) 1517-1533.

Fig. 1-5 is adopted from the reference:

Platz R., Stapp C. and Hanselka H., Statistical approach to evaluating reduction of active crack propagation in aluminum panels with piezoelectric actuator patches, *Smart Materials and Structures* **20** (2011) 085009. Copyright has been obtained.

Fig. 1- 6 is adopted from the reference:

Duan W.H., Quek S.T. and Wang Q., Finite element analysis piezoelectric-based repair of a delaminated beam, *Smart Mater. Struct.* **17** (2008) 015017.

List of Symbols

G : Shear Modulus

E : Young's modulus

ρ' : Mass density of host structures

υ : Poisson ratio of host structures

∇^2 : Laplace operator (Δ)

c_{ji} : Elastic modulus of piezoelectric materials (C_{ij}^{E})

e_{ij} : Stress-Charge form piezoelectric coefficient

d_{ij} : Strain-Charge form piezoelectric coefficient

Ξ_{ij} : Dielectric constant

ρ : Mass density of the piezoelectric layer

ϕ : Electric potential

$\varphi(i)$: Electric field along i direction

ω : Frequency

v' : Phase velocity in the host structure

c : Phase velocity in the piezoelectric coupled structure

v : Phase velocity in the piezoelectric material

w : Deflection

$\hat{w}$: Amplitude of vibration deflection

n : Thickness ratio between the piezoelectric patches and the host structure

H : Thickness of host structures (H=2h)

h_1 : Thickness of piezoelectric patches

E_i : Electric field along *i* direction

D_i : Electric displacement along *i* direction

M_{rr}, $M_{\theta\theta}$, $M_{r\theta}$: Bending moments

$J(\circ)$: First type Bessel function

$I(\circ)$: Modified first type Bessel function

V_o : Output voltage of piezoelectric patches

C_v : Electric capacitance of piezoelectric patches

G : Voltage gain factor

p : Repair coefficient

t : Thickness of the upper delamination layer

P_{xu} : Compression or tensile axial force on the upper delamination layer along X direction

P_{xl} : Compression or tensile axial force on the lower delamination layer along X direction

P_{yu} : Compression or tensile axial force on the upper delamination layer along Y direction

P_{yl} : Compression or tensile axial force on the lower delamination layer along Y direction

$N\&M$: Numbers of discrete electrodes

P_{xu}^i : Compression or tensile axial force on the ith section of the upper delamination layer along X direction

P_{xl}^i : Compression or tensile axial force on the ith position of the lower delamination layer along X direction

P_{yu}^{i} : Compression or tensile axial force on the jth position of the upper delamination layer along Y direction

P_{yl}^{i} : Compression or tensile axial force on the jth position of the lower delamination layer along Y direction

S_{xu}^{i} / S_{xl}^{i} : Shear force between the host structure and piezoelectric patches generated by the input voltage along X direction

S_{yu}^{i} / S_{yl}^{i} : Shear force between the host structure and piezoelectric patches generated by the input voltage along Y direction

V : Voltage applied to the surface of piezoelectric layer

V_i &V_j : Voltages applied to distributed electrodes

L1&L2 : Length and width of the delaminated plate

a&b : Length and width of the rectangular delamination

c&d : Transverse loading positions on the delaminated plate

L : Length of the host beam structure

dn : Depth of the notch on a beam structure

l_1 : Length of the piezoelectric patch mounted above the notch area

b_s : Width of the piezoelectric sensor

b_a : Width of the piezoelectric actuator

1 Introduction

1.1 Background

Damages such as a crack, notch or delamination in aerospace, mechanical, civil and offshore structures due to fatigue, corrosion or accidence are inevitable during services. Such damages will grow at an alarming rate due to the stress/strain concentration around the damage locations and cause possible failures of structures (Jones and Callinan 1981, Suiker and Fleck 2006, Zou *et al* 2000, Tay *et al* 2003, Kitamura *et al* 2003, Turon *et al* 2006). Fig. 1-1 shows typical structural failures on a vehicle chassis and a delaminated structure due to the existence of the crack and delamination, respectively. Thus, structural repair has become an important and practical research topic since the last several decades and attracted much attention in academy and industry. The effective repair method is to reduce the stress/strain concentration at the damaged location so as to control the growth of the damage and reinforce the damaged structures.

Structural repair with bonded materials has been the most traditionally used technology to increase the service life of damaged structures (Baker and Jones 1988). The traditional method was to meld or mount additional high stiffness patches onto the damaged area to improve the mechanical function of a damaged structure. The major problem of the repair process is that additional stress concentration may possibly be induced at the bonding area (Sun *et al* 1996). Different numerical simulations, such as boundary element method and finite element method

(FEM) (Young *et al* 1992, Chue *et al* 1994), have been conducted to investigate this issue. Moreover, the repair method using normal additional patch cannot adjust newly induced damage due to unexpected external loadings.

In view of the limitations of structural repair with traditional methods, smart materials have been employed in applications of structural enhancement and repair due to their adjustable mechanical property. Applications of smart materials in engineering structures have drawn serious attentions recently. Smart materials are the materials that have one or more properties that can be significantly changed in a controlled fashion by external stimuli, such as stress, temperature, electric, or magnetic fields. Piezoelectric material is one of the mostly common used smart materials. Different patches made of Lead zirconate titanate (PZT), which is the most commonly used piezoelectric material, are shown in Fig. 1-2. Piezoelectric materials refer to substances that have the electro-mechanical coupling effect: i.e. an electric charge will be produced when an external load is applied on a piezoelectric material, and conversely a mechanical force will be generated by applying an electric field to the piezoelectric material. Owning to the active electro-mechanical property, piezoelectric materials have been widely used as sensors and actuators in engineering structures.

Due to the active electric-mechanical coupling effect that can be significantly changed in a controlled fashion, the piezoelectric material has been widely used in structural control and repair. Meressi and Paden (1993) investigated the buckling control of flexible beams using piezoelectric materials. The principle of their work is to apply a controlled voltage to piezoelectric materials to induce a reactive moment at the beam centre. Wang (2001) presented an analytical model to investigate the potential of piezoelectric materials on buckling

enhancement of column structures subjected to compressive loadings. The principle of the work, however, was to apply a pre-determined follower tensile force, based on an analytical model, excited by a pair of piezoelectric patches mounted on the surface of a column structure to counteract the external compressive force so as to enhance the buckling capacity of the column. Applications of piezoelectric materials have also been considered in structural repair. The key objective on repair of cracked/notched and delaminated structures introduced in this work is to reduce the stress/strain concentration at the damaged part so that possible propagation or growth of the crack/notch and delamination can be restrained and the function of the damaged structures can be reinstated. Wang *et al* (2002) first presented a study on repair of a cracked beam under a static transverse loading. A voltage, which was obtained from a analytical model of a simply supported beam, was applied to a piezoelectric patch bonded on the beam to ensure the reduction of the stress around the crack. Liu (2008) used the plane strain finite element method to analyze the crack repair via a piezoelectric actuator estimated by slope continuity and facture mechanics. Moreover, the electromechanical characteristics of piezoelectric materials were also employed for repair of notched and cracked structures under dynamic loadings. A feedback control repair methodology for a vibrating notched beam structure using a piezoelectric patch was induced by Wang *et al* (2004). The resonant frequency of the noted beam after repair was employed as the criterion for identifying the actuation voltage applied to the piezoelectric patch. In addition, repair of delaminated structures has also attracted much attention. In composite materials, delamination is a major damage that requires intense attention. Studies on delaminated composites have been broadly reviewed by Wilkins *et al* (1982). Wang and Quek (2004) presented a analytical model for repair of a delaminated beam subjected to a static loading with piezoelectric patches.

To apply piezoelectric materials for the repair of damaged structures under both static and dynamic loadings, piezoelectric patches usually need to be bounded on the surface or embedded in the host structure to induce shear force between the piezoelectric patch and the host structure. Particularly when the damaged structure is under dynamic loading, the analysis of wave propagation and vibration of structures bonded with the piezoelectric layer is indispensible for researchers to understand the electrical and mechanical dynamic responses of piezoelectric coupled structures well and will provide guidance on the design of the structural repair via piezoelectric materials. Following investigations of the wave propagation and vibrations analysis of piezoelectric coupled structures, different repair methods via piezoelectric materials on delaminated beam and plate structures subjected to static and dynamic loadings are proposed. In addition, an accurate criterion for the repair of a cracked beam structure, and an experimental verification for this process are studied as well in this thesis.

1.2 Constitutive relations of piezoelectric materials

In this section, the linear piezoelectric constitutive equations, which are most commonly used in engineering applications discussed in the review, are introduced briefly. The well known man made piezoelectric materials include Gallium orthophosphate, Barium titanate and Lead zirconate titanate (PZT).

1.2.1 Various forms of piezoelectric materials

Piezoelectric materials have been known as a simple, low cost, light weight and easy-to-control smart material for the structural actuation application. For its diverse applications in different structures, piezoelectric materials can be manufactured into various forms such as patches, thin

films, stack cylinders and fibers. De Faria and Donadon (2010) proposed different designs of the surface mounted piezo-patch actuators to study the effects of the shape of the piezo-patch to its actuation behaviour. Maukherjee and Chaudhuri (2002) used a stack multi-layered piezoelectric film as both the sensor and actuator to enhance the stability of column structures. Both FEM and experimental studies were carried out to show the effect of axial force on sensing and actuation mechanisms of piezoelectric materials and to demonstrate the active control of column type structures using these materials. As an ideal embedded material for the reinforcement of different structures, the study on piezoelectric fibers has also been studied. Etches *et al* (2006) presented an exploiting functional piezoelectric fiber by inducing hard magnetic powder materials into the hollow glass fiber cores to provide an active ferromagnetic function. Their study outlined the feasibility of embedding piezoelectric fibers directly into a composite lay-up, thereby allowing a composite laminate to deform due to internal actuation.

1.2.2 Linear piezoelectric constitutive equations (LPCE)

Studies on nonlinear theory of dielectrics were proposed by Nelson (1978) and Baumhaue and Tiersten (1973). According to Ehlers and Weisshaar (1990), nonlinear piezoelectric effects become significant only in applications involving high electric fields and cyclic fields which result in hysteresis. In addition, the constitutive equations are greatly simplified since the gradient of polarization and magnetization is zero within the scope of the linear piezoelectric theory and the body force generated by the electric field will also be ignored. Thus, only the linear piezoelectric constitutive equations, which are most related to the research works reviewed in this paper, are briefly outlined in this section.

LPCE can be derived from the macroscopic/phenomenological theory of piezoelectricity based on thermodynamic principles (Chee *et al* 1998). From energy considerations (Tiersten 1969), we can have following expressions,

$$\begin{aligned} dG &= SdT + DdE \\ dH &= TdS - DdE \end{aligned}, \tag{1-1}$$

where G and H are the Gibbs free energy and enthalpy, respectively; T and S stand for the mechanical stress and strain vectors, respectively. E and D are the electric field and electric displacement vectors.

Based on eq. (1-1), two common formulations of the linear constitutive model can be established to illustrate the piezoelectric effect, in which the mechanical and electrical variables contribute independently. The stress formulation is given as:

$$\begin{aligned} \sigma_i &= C_{ij}\varepsilon_j - e_{ki}E_k \\ D_l &= e_{lj}\varepsilon_j + \Xi_{lk}^S E_k \end{aligned}, \tag{1-2}$$

while the strain formulation can be expressed as:

$$\begin{aligned} \varepsilon_i &= S_{ij}\sigma_j - d_{ki}E_k \\ D_l &= d_{lj}\sigma_j + \Xi_{lk}^T E_k \end{aligned}. \tag{1-3}$$

where σ_i and ε_j are the stress and strain vectors; E_k is the electric field vector; D_l is the electric displacement vector; C_{ij} is the elastic stiffness matrix; S_{ij} is the elastic compliance matrix; e_{ij} and d_{ki} are the piezoelectric stress/charge and strain/charge vectors, respectively; and Ξ_{lk}^S and Ξ_{lk}^T are the piezoelectric permittivity matrices in stress and strain form, respectively.

Both stress and strain formulations describe the same physical model and are easily interchangeable. The two sets of material parameters are related as follows:

$$\begin{aligned} d_{lj}C_{ij} &= e_{lj} \\ e_{li}S_{ij} &= d_{lj} \\ e_{lj}d_{nj} &= d_{lj}e_{nj} \\ (C)_{ij}^{-1} &= S_{ij} \end{aligned} \quad . \tag{1-4}$$

The relationships in eq. (1-4) are valid provided that the compliance or stiffness matrix is non-singular. The stress formulation is often applied in finite element calculations, where the strain is the natural variable. In studies involving other physical models or when using plane stress assumptions in plate/laminate models, the strain formulation is preferred.

1.3 Literature review

In this section, the previous studies on the surface wave propagation and vibration of the piezoelectric coupled structures are reviewed first. The accurate analytical models of dynamic responses of the piezoelectric coupled plate with an open electrical boundary condition are found to be desirable. The review of previous repair works of different damaged structures using piezoelectric materials is followed.

1.3.1 Surface wave propagation in piezoelectric coupled structures

Surface wave propagation in a piezoelectric plate has become a topic of practical importance, as piezoelectric materials are used as sensors and wave actuators more and more commonly for the applications of the health monitoring and the dynamic repair in engineering structures (Viktorov 1967 and 1981 and Curtis and Redwood 1973). One of the applications of using surface wave propagation in piezoelectric materials and structures is to achieve time delay effect for acoustic application. Wave propagation and vibration analysis in a pure piezoelectric plate have received considerable attention previously as exhibited by the work of Mindlin (1951), Tiersten (1963c

and 1963d) and Bleustein (1969). Parton and Kudryavtser (1988) studied the piezoelectric surface wave in a semi-infinite piezoelectric media surface covered with a layer of isotropic conducting material. Cheng and Sun (1975) presented plane strain wave propagation in a two-layered piezoelectric plate by three-dimensional theory of piezoelectricity and approximation theories.

The use of piezoelectric sensor and actuator patches has been widely studied (Kim *et al* 1996, Crawley and Deluis 1987, Sun and Zhang 1995 and Varadan *et al* 1996). Wang and Quek (2000e and 2000f) presented the model of wave propagation in piezoelectric coupled beams and plates by different kinematics assumptions. The embedded and surface mounted sensor and actuator patches have been used in engineering applications such as health monitoring of structures by MEMS-IDT sensors (Varadan V.K. and Varadan V.V. 2000). An accurate model for the piezoelectric effect in a coupled structure is significant to the application of piezoelectric materials as sensors and actuators in engineering structures.

The linear response of piezoelectric materials is related to electrical boundary conditions significantly (Jaffe 1971). Chang and Ouyang (2002) have conducted the open-circuit test on a PZT. Their research concentrated on electrical characteristic of the PZT vibrator. The result showed that open circuit condition should be proposed aiming to test the surface current and the amplitude of transient response. Accordingly, under high-power excitation, an open-circuit test was proposed to elucidate complete terminal transient responses of vibrators (Chang and Ouyang 2002). Guillon *et al* (2004) conducted the research about the tensile behaviours of a PZT in both short and open circuit conditions. It has been found that nonlinear stress–strain curves are greatly affected by the electric field which appears in the open circuit condition. Recently, the dynamic property of piezoelectric sensors with preamplifiers has been studied by Liu *et al* (2007) in open

and short circuit states. Their research demonstrated that the stiffness of piezoelectric materials is rather different when the electrodes are in different states. As an actuator, the piezoelectric material would have different working ranges at different electrode states also. This could be easily understood while the PZT has different resonant frequencies with shorted and open circuit states (Liu *et al* 2007). Wang and Varadan did research on SH wave propagation in piezoelectric coupled plates using an interdigital transducer (Wang and Varadan 2002g). In addition, further research on wave propagation in piezoelectric coupled plates with short circuit was carried out (Wang and Varadan 2002h). Note that the wave propagation in a piezoelectric layer with open-circuit should have different characteristics compared with the shorted piezoelectric layer.

1.3.2 Vibration of piezoelectric coupled structures

A metal substrate surface bonded or embedded by a piezoelectric layer has been intensely studied during last two decades for practical designs of actuators, sensors and absorbers because of the electromechanically coupling characteristics. Examples include the actuation analysis of piezoelectric fiber composites (Bent *et al* 1995), vibration and buckling of piezoelectric coupled laminated structures (Heyliger and Ramirez 1999 and Varelis and Saraanos 2004), and wave propagation in piezoelectric coupled cylinder structures (Wang and Liew 2003). The analyses about the structural vibration and control were also conducted with different piezoelectric coupled structures (Kapuria *et al* 2003, Duan *et al* 2005, Liew *et al* 2002, Liew *et al* 2004 and Zhang *et al* 2006).

Fundamental mechanical models for analysis of piezoelectric coupled structures are indispensable and have been attracted much attention. Crawley and deLius (1987) developed a uniform strain model for a beam with surface bonded and embedded piezoelectric actuator

patches accounting for the shear lag effects of the adhesive layer between the piezoelectric actuator and the host beam. A model to account for the coupling effect was later proposed based on the Euler beam assumption (1989). Based on Hamilton's principle, Leibowitz and Vinson (2003) derived a model in which the elastic layers, soft-core layers or piezoelectric layers are included. A meshfree model was constructed by Liew *et al.* (2002) for the static analysis of laminated composite beams and plates with integrated piezoelectric layer based on the element-free Galerkin (EFG) method.

Piezoelectric materials with both closed and open circuit boundary conditions are widely applied in engineering applications. For example, the closed circuit piezoelectric materials are mostly used for the design of ultrasonic motors and resonators, and the open circuit piezoelectric materials are employed for the design of vibration sensors, actuators and absorbers. Wang and Quek (2000e) presented a study of a free vibration of a piezoelectric sandwich beam structure, in which the piezoelectric effect on resonance frequencies of the structure and the distribution of the electric potential were investigated and analyzed. In addition, a quadratic electrical distribution in thickness direction of the piezoelectric layer was proposed by Wang *et al*. (2001) in analysis of a piezoelectric coupled circular plate with closed circuit condition. In analysis of the open circuit piezoelectric materials, Davis and Lesieutre (2000) studied a vibration absorber using a piezoelectric material, and found the effective stiffness of the piezoelectric material would increase when the electric surface condition changes from closed to open circuit. Corr and Clark (2002) employed the high stiffness of the structure induced by the open circuit piezoelectric material to increase the structure damping and potential energy. Chevallier *et al* (2008) experimentally presented a benchmark for free vibration and effective coupling of thick piezoelectric smart structures. Liu, Pan, Heyliger and Ding (Liu 2001, Pan and Heyliger 2002,

Heyliger and Saravanos 1995 and Ding *et al* 2000) studied the free vibration process of piezoelectrically coupled plate with both open and closed circuit electric surface conditions based on the basic study of free vibration of piezo-plate given by Tiersten (1969). Their research showed that the coupled plate vibration response with open circuit piezoelectric layer is far different from the one with closed circuit piezoelectric layer. Most of the available research studied the open circuit piezoelectric coupled plates through finite element method (FEM) simulations and experimental investigations. An accurate physical model of the piezoelectric coupled plate with open circuit electric boundary condition, especially the electrical potential distribution along the thickness direction of the piezoelectric layer, needs to be developed.

1.3.3 Structural repair using piezoelectric materials

As an efficient structural maintenance process, repair of damaged structures to reinstate them to their normal function and to avoid possible structure failures has been widely studied during the last few decades. A key objective in a repair design is to lessen the stress/strain concentration at the damaged part of a structure to reinforce the damaged structure. With the development of smart materials and structures, the employment of piezoelectric materials in structural repair has been investigated with remarkable and interesting research findings. This section is to introduce the recent developments on applications of piezoelectric materials in repair of cracked, notched and delaminated structures.

I. Repair of cracked and notched structures

A notch is defined as a geometric discontinuity that has a definite depth and root radius, whereas a crack is the geometric discontinuity with its root radius approaching a mathematical zero (in

the engineering terms, 10^{-9}m) (Wang 1996). However, the main reason leading to a material failure due to the two types of damage is similar, i.e. the stress concentration, only with different severity, at the crack/notch root. For the repair aim of both cracked and notched structures, a piezoelectric patch used as an actuator is located around the crack/notch area to generate the active counteracting bending moment to decrease the stress concentration at the crack/notch tip. Since both notches and cracks induce stress concentration leading a possible structural failure, repair works of cracked and notched structures using piezoelectric materials will be discussed simultaneously in this section. Details of technologies are introduced and different repair processes for the cracked and notched beams subjected to static and dynamic loadings are provided and reviewed.

(i) Repair of cracked/notched beams under static loading. In this section, research findings on repair of cracked beams under static compressive and transversal loadings are introduced, respectively. When a compressive force reaches the critical buckling load of a beam, a bending shape is identified at its buckling mode. The critical buckling load of a cracked beam due to the crack effect will be decreased compared with the healthy one. The piezoelectric material was employed for the repair of a cracked beam structure under a compressive loading by Wang and Quek (2005). In the research, an analytical model for the design of the actuation voltage applied to the piezoelectric patches for repair of the cracked column with different boundary conditions was introduced. The decreased buckling capacity of the cracked column was efficiently compensated due to the local bending moment induced by the actuated piezoelectric patch. This approach offered significant advantages over passive repair design methods with the ability to use a wide variety of applied voltages to repair column structures with cracks with various locations, depths and intensities.

In repair of carked structures subjected to transverse loadings, Wang *et al* (2002) studied repair of a cracked simply supported beam under an external transversal loading by employing a piezoelectric material to induce a local moment following the principle introduced based on eq. (7). The Euler-Bernoulli beam theory was employed in modelling. An external actuation voltage, which was obtained from an equation containing variables such as the applied force and the geometric and material properties of the beam and the piezoelectric material, was applied to a piezoelectric patch bonded on the beam to decrease the stress concentration induced by the crack. Fig. 1-3 shows the slop profile of a cracked simply supported beam before and after the repair using a piezoelectric patch. It can be seen that the slop difference at the crack position due to bending of the beam structure can be erased efficiently by the piezoelectric patch subjected to a suitable actuation voltage. Furthermore, no discontinuities of the deflection and slope of the beam were observed with the applied repair method and hence the stress concentration at the crack/notch position is removed.

It was further pointed out that the actuation voltage can be adjusted to follow the variation of the external loading and boundary conditions. This proposed method realized an active repair for cracked structures under different working conditions. On the other hand, it has to be noted that using higher voltage that is larger than the required one may induce reverse effect because it will enlarge the stress concentration near the crack tip in the opposite direction of the beam before repair. The problem was pointed out in the studies by Liu (2007 and 2008). Therefore, a proper model in obtaining an appropriate actuation voltage is indispensable in repair of cracked structures. A new fracture mechanics repair criterion was proposed in Liu's papers. Crack contact analyses and fracture mechanics in the crack tip field were considered in the plane strain finite element analyses.

The above studies are based on the assumption that piezoelectric patches are bonded perfectly on the surface of the host structures. Alaimo *et al* (2009) used boundary element method to analyse bonding of piezoelectric patches on the host structures. The fracture mechanics behaviour of the structures was analyzed for both perfect and imperfect interface between the piezoelectric patches and the host beams. It was concluded that the adhesive condition affects the repair performance significantly as any loss of the shear stress transfer at the imperfect interface between the host structure and the patch would bring a reduction of the actuation capability of a piezoelectric patch.

(ii) Repair of cracked and notched beams under dynamic loading. The electromechanical characteristics of piezoelectric materials can also be employed for repair of cracked and notched structures under dynamic loading as the voltage applied on the piezoelectric actuator can be real-time adjusted to reduce the stress concentration at the crack/notch tip in a vibrating structure. A study on smart-patch repair of cracked aircraft panels was addressed by Sekine (2006). The patching efficiency in cracked aircraft panels repaired with piezoelectric patches was examined, and the enhancement of patching efficiency due to the activation of piezoelectric actuators was presented. A close-loop feedback control repair method using piezoelectric patch for repair of a notched beam subjected to a dynamic loading was proposed by Wang *et al* (2004) and is introduced and reviewed here. The piezoelectric patch was used for both vibration sensor and repair actuator in the close-loop feedback control process. A feedback factor was defined as a value to be multiplied to the feedback voltage developed on the sensor to generate the actuation voltage on the actuator. The actuation voltage was applied to the piezoelectric patch bonded around the notch area of the beam to decrease the stress/strain concentration at the notch tip under dynamic loading. Such a process would lead the strengthening of the notched beam and

hence increase its resonant frequency back to the frequency of its healthy counterpart. Hence the adjustment of the resonant frequency of the notched beam by employment of the piezoelectric patch was measured to evaluate the effectiveness of the repair strategy. A cantilever beam used in reference is employed to demonstrate the repair methodology. The dynamic response of the tip displacements before and after repair predicted by the proposed model is shown in Fig. 1-4 (a) and (b). It can be seen that the vibration amplitude of the notched beam before repair is around two times larger than that of the healthy one because of the softening effect by the notch. The dynamic response of the notched beam after repair and its difference from that of the healthy one are shown in Fig. 1-4 (c) and (d), respectively. The largest difference of the vibration deflection of the notched beam after repair and that of the healthy one is only 2.14% showing the recovery of the stiffness of the beam structure with the use of the piezoelectric patch. Although the recovery of the stiffness or the adjustment of the resonant frequency of the notched beam can be viewed as an indication of reinforcement of the structure, a complete reduction of the stress/strain concentration at the notch tip cannot be viewed or guaranteed with the model, and further the possible reduction of the stress concentration was not verified.

To overcome the above problem, a new experimental study was conducted by Wu and Wang (2011). In the research, a dynamic analytical model of a notched beam bonded with a piezoelectric patch was first built to find the vibration deflection of the notched beam subjected to a dynamic loading. The reduction of the slop discontinuity at the notch position, which directly represented the intensity of the stress concentration at the notch tip, was to be achieved in finding the feedback factor that was to be multiplied to the feedback voltage from the vibration sensor for an actuation voltage. Details of this research will be given in chapter eight. Another study on active reduction of the crack propagation using piezoelectric patch was

proposed by Platz *et al* (2011). As shown in Fig. 1-5 (a), piezoelectric patch was applied directly to the crack area to lower the cyclic stress intensity factor at the crack tip so that the crack propagation can be reduced. Fig. 1-5 (b) shows a significant statistically assessed reduction rate of about 20% in crack propagation when an acted piezoelectric actuator patch was mounted near the crack tip with respect to an applied but passive actuator on a similar specimen under similar boundary conditions.

In addition, Ariaei *et al* (2010) developed a method for repair of cracked beams subjected to a moving mass with piezoelectric materials. The adjustment of the resonant frequency of the cracked beam was also used as the criterion of the repair to find the suitable actuation voltage.

II. Repair of delaminated structures

Delamination is another common damage type especially in composite structures. Studies on delaminated materials have been extensively reviewed by Wilkins *et al* (1982) and the accompanying problems of instability of delaminated composites have been widely studied. In this section, research findings on repair of delaminated beams and plates, mainly by the first author and his research group, are particularly introduced.

(i) Repair of delaminated beams.

(a) Repair of delaminated beams under static loading. In this section, research findings on repair of delaminated beams subjected to both the compressive force and transversal force are introduced. The application of piezoelectric materials in repair of delaminated beam structures subjected to a compressive loading was investigated by Wang *et al* (2005). A comprehensive mechanical analysis was provided to calculate the actuation voltages on the piezoelectric layers to erase the shear stress discontinuity at the tips of the

delamination. From the numerical simulations, the derivation of the buckling load of the delaminated beam with different boundary conditions and the actuation voltages applied to the piezoelectric patches were conducted. This research first highlighted the practical potential of piezoelectric materials in repair of delaminated beam structures under the compressive force.

The repair of a delaminated beam subjected to a transversal static loading with a piezoelectric patch was studied by Wang and Quek (2004). According to eq. (9), the repair force induced by the piezoelectric patch was identified to be equal to the negative value of the compressive/tensile force generated on the delamination layer due to the bending of the delaminated structure. Although the research provides a guideline on repair of delaminated beams, the verification of the proposed repair methodology based on theoretical work needs to be provided either by FEM or experimental work. Duan *et al* (2008) employed an FEM model to facilitate a design of repair of delaminated beams with piezoelectric patches. Based on both the analytical and the FEM modal, parametric studies on the delaminated beam and piezoelectric materials with various geometry and material properties were performed numerically to demonstrate the effectiveness of the proposed repair methodology. Fig. 1-6 illustrates the FEM simulation on the stress concentration at the delamination tip. It can be found that the stress concentration can be reduced efficiently when a suitable actuation voltage was applied to the piezoelectric patches. The repair method for the delaminated beam structures under static load via the piezoelectric materials proposed in the references (Wang *et al* 2004, Duan *et al* 2008) was proven to be efficient and practical from the FEM simulation.

(b) Repair of vibrating delaminated beams. Based on the repair principle of the delaminated structures provided by Wang and Quek (2004), repair of a vibrating delaminated beam structure with piezoelectric materials was investigated by Wu and Wang (2010f). In the research, piezoelectric patches were employed to be bonded above the delamination area to reduce the shear stress discontinuity at the delamination tips of the bending beam. A close-loop feedback control repair methodology for the vibrating delaminated beam structure by use of piezoelectric patches was presented. Details of this research will be discussed in chapter six.

(ii) Repair of delaminated plates. Wu and Wang (2010e) developed a repair design of a delaminated plate under a static loading with piezoelectric patches by an analytical model and FEM. Unlike the repair of delaminated beam structures, the repair for the delaminated plate involves an analysis on a two dimensional problem. The stress concentrations of a bending delaminated plate are not uniformly distributed along the delamination edges when the plate was under a point loading. Thus, an analytical model was first built to obtain the distributions of the tensile and compressive forces on the upper and lower layers of the delamination. Then, a design of discrete electrodes on the patches was developed, and the voltages on the electrodes were calculated based on the analytical model for repair of the delaminated plate by eliminating the tensile and compressive forces along the edges of delamination layers. Details of this research will be given in chapter seven. It is noted the analytical model provided is only suitable for the static analysis. An accurate model for repair of the delaminated plate under dynamic loading with piezoelectric materials needs to be developed. Actually, a dynamic finite element model based on the refined higher-order-theory has already been developed for modeling the dynamic response of delaminated smart composite plates by Chattopadhyay *et al* (1999). This theory provided an

accurate description of displacement field and the satisfaction of stress-free boundary conditions at all free surfaces including delamination interfaces. The results proposed by Chattopadhyay can be a reference to study the repair of the delaminated plate under dynamic loading using the FEM.

Repair of other damaged structures have also been studied by researchers using piezoelectric materials. Rabinovitch (2007c) proposed an analytical model of piezoelectric control of edge deboning in beams strengthened with composite materials. The original contribution of the study was in addressing the challenge of using piezoelectric active materials in presenting a potential solution to the edge-debonding failure problem. From an analytical model, the response of a full-scale strengthened beam to mechanical loads and to different schemes of piezoelectric actuation was investigated in terms of the localized stresses near the edge of the bonded composite strip. Following this research, Rabinovitch (2007d) also presented the failure criteria and optimization design of the piezoelectric control of the edge debonding failure in the reinforcement beam by composite patches. A numerical optimization study that focused on the ability of different combinations of piezoelectric actuators to control the edge debonding failure was presented. A systematic approach was provided to optimize the piezoelectric control under different debonding failure criteria and in demonstrating the feasibility of using the piezoelectric system in the full-scale civil engineering structure.

Future works on structural repair using piezoelectric materials may focus on the following issues. Stronger piezoelectric materials, such as stack piezoelectric patches, need to be employed for repair of thicker damaged structures, which requires larger repair forces or moments. In addition, for structures with multiple delaminations, the use of piezoelectric patches embedded in the structure would be a more effective and efficient way.

1.4 Objectives and scope of studies

Owing to the active electro-mechanical property of piezoelectric materials, the shear force generated by a piezoelectric patch is expected to be used for repair of damaged structures subjected to static and dynamic loadings. From literature review, it can be seen that most of previous studies of dynamic responses of piezoelectric coupled structures with open circuit electric boundary condition were conducted with FEM simulations or experiments and could not provide the accurate electric distribution along the thickness of the piezoelectric layer. Thus, the studies of wave propagation and vibration of structures bonded with piezoelectric layers under open circuit electric boundary condition using an accurate numerical model are desired to help to understand the dynamic responses of piezoelectric coupled structures. The electro-mechanical coupling effect and the interaction between the host structure and piezoelectric layers with open circuit electric boundary condition found in the studies will provide a guidance on the design of the structural repair. Form table 1-1, it is found that all previous repair methods using piezoelectric materials were applied mainly to beam structures. The active repair for a delaminated plate using piezoelectric materials has not been studied. In addition, there is few studies on repair methods developed for vibrating delaminated beam structures, and the criterion for repair of a cracked beam under dynamic loadings still needs to be improved. From the discussion given above, the scope of this PhD study mainly concentrate on: (a) studies on the wave propagation and vibration of piezoelectric coupled structures; (b) studies on structural repair of delaminated beam and plate structures under static and dynamic loading via piezoelectric materials with the analytical model and the finite element model (FEM); (c) studies on structural repair of cracked beam structures under dynamic loading with a new criterion, which is defined as the slop discontinuity at the crack position, and verifications of the

effectiveness of the proposed repair methodology through an experimental process. Experimental verification focuses on the repair of the cracked beam using the piezoelectric layer mounted on the crack area. The contributions of this research work include the followings: (a) developing accurate numerical models of piezoelectric coupled structures with open circuit electric boundary condition to analyse the piezoelectric effect on the dynamic responses of the piezo-coupled structures so as to guide the design of structural repair using piezoelectric materials; (b) providing an active feedback control repair method and an accurate criterion for the structural repair via piezoelectric materials for different damages on different structures; (c) proving the efficiency and feasibility of the active structural repair via piezoelectric materials experimentally.

Table1- 1 Most related studies of the structural repair using piezoelectric materials

Resources	Contributions	Applications & Limitations
Liew *et al* (2002)	A dynamic control method was proposed by using self-monitoring sensor and self-controlling actuators.	Only FEM simulation is proposed.
Varelis and Saravanos (2003 and 2004)	The effects of the adhesive properties on the variation of the stress concentration at the crack tip were highlighted.	No accurate numerical model, passive repair.
Alaimo et al (2009)	Acitive repair on a cracked structure via piezoelectric patch was analyzed by the boundary element method	The method is Applied to a cracked structure. No accurate analytical model to explain the repair process.
Wang and Quek (2004)	An accurate analytical model for the repair of a delaminated beam was developed.	This study is on the repair of a delaminated beam under static loading.
Duan *et al* (2008)	FEM was employed to prove the efficiency of the repair of a delaminated beam using piezoelectric patches.	This study is on the repair of a delaminated beam under static loading.
Duan *et al* (2005)	A analytical model was built to analysis the repair for a notched beam under dynamic loading via a piezoelectric patch.	Resonant frequency of the repaired beam was used as criterion of the repair, which is still needed to be improved.

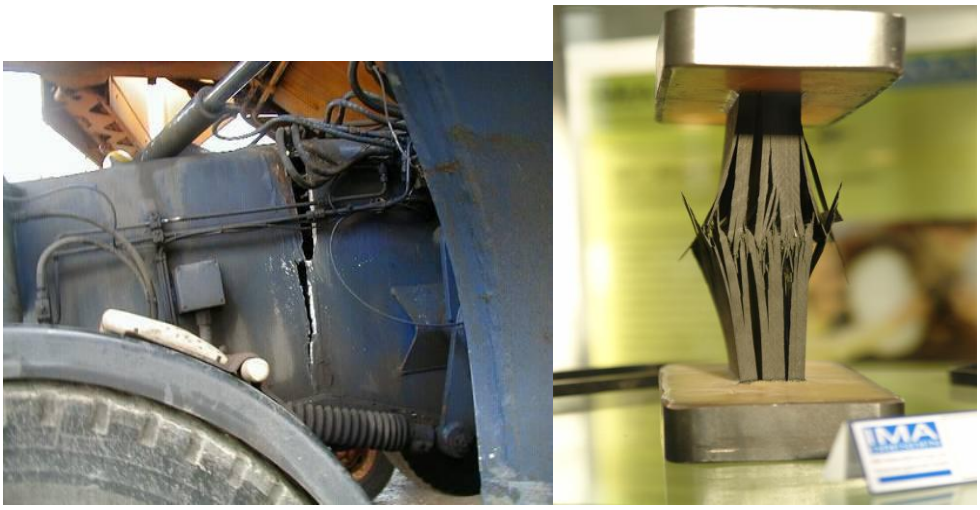

(a) (b)

Fig. 1- 1 Structure failure on (a) a vehicle chassis and (b) a delaminated structure.

Fig. 1- 2 Smart materials: PZT patches.

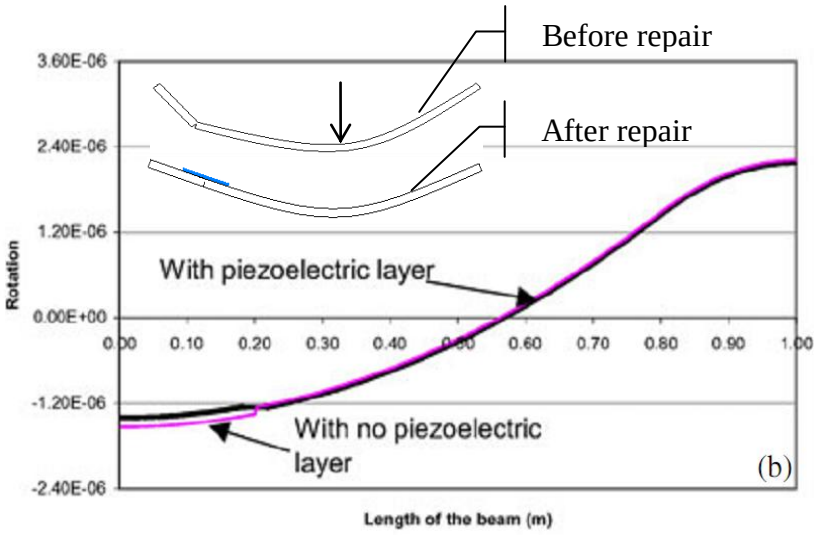

Fig. 1- 3 Slop of a cracked beam before and after repair (adopted from Fig. 4 (b) in Wang *et al* 2002)

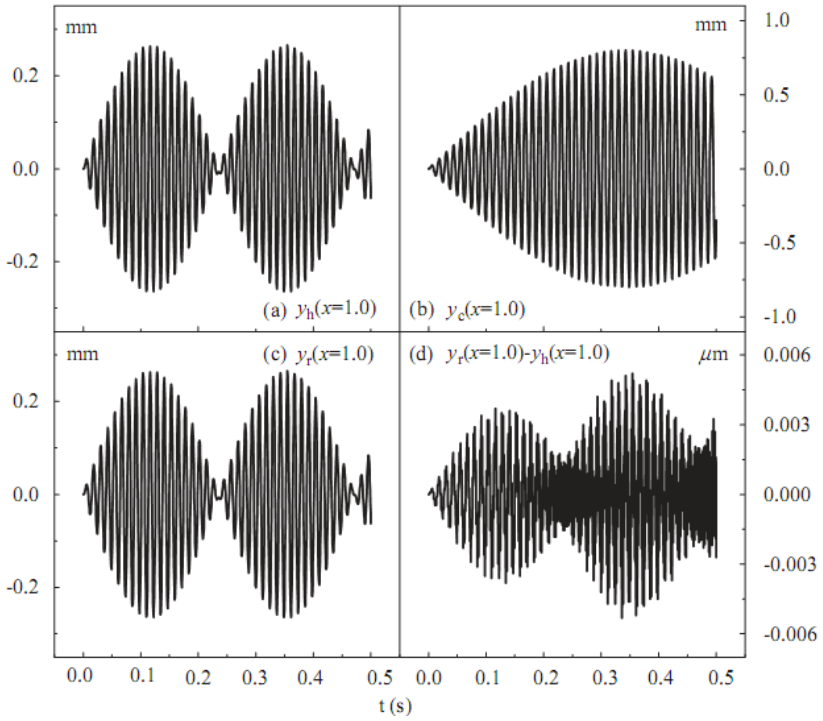

Fig. 1- 4 Dynamic response of the tip displacement predicted by the proposed model for (a) the healthy beam, (b) the notched beam before repair, (c) the notched beam after repair, and (d) the difference between the notched beam after repair and the healthy beam. (Adopted from Fig. 4 in Wang *et al* 2004)

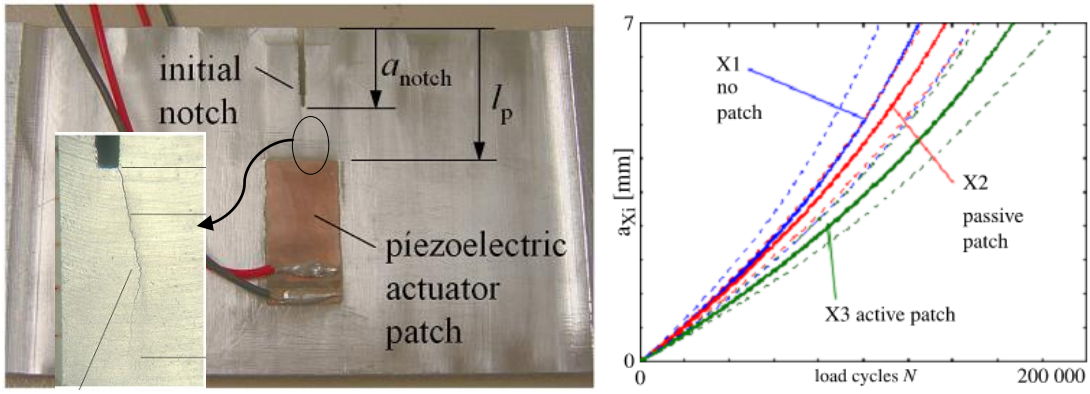

(a) (b)

Fig. 1- 5 (a) cracked specimen mounted with piezoelectric actuator (adopted from figure 6 and Fig. 7, Platz *et al* 2011), (b) Summarized mean (——) and mean deviation (– – –) curves of crack length propagation versus load cycles before and after repair (adopted from Fig. 14, Platz *et al* 2011).

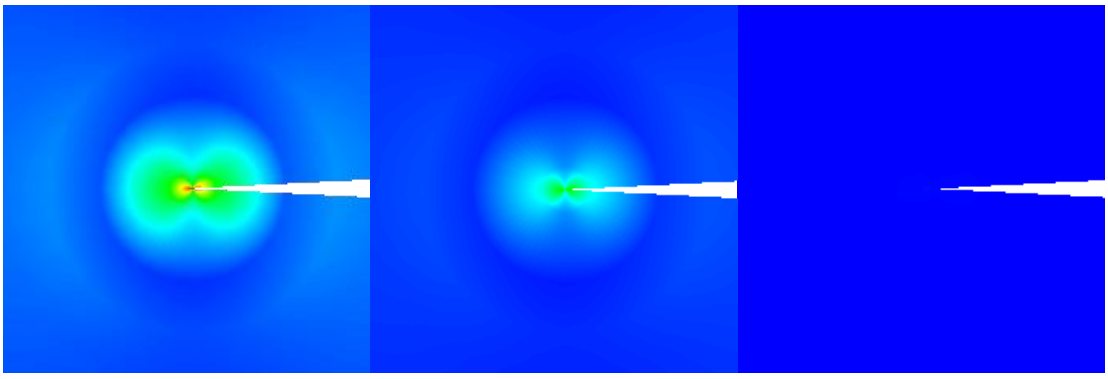

(a) (b) (c)

Fig. 1- 6 Von-Mises stress distribution around the crack tip at different applied voltages on the piezoelectric patches (a) 0 V, (b) 300 V and (c) 480 V. (Adopted from Fig. 5 in Duan *et al* 2008)

2 Study on wave propagation in a piezoelectric coupled structure

Shear force is generated between the piezoelectric patch and the host structure when deformation takes place on the piezoelectric coupled structure or an extra voltage is applied to the piezoelectric material. This could be used as an active repair force for a damaged structure under both static and dynamic loading. Thus, an accurate model for the piezoelectric effect during the shear wave propagation is significant to the application of piezoelectric materials as sensors and actuators in engineering structures. Simulation of shear horizontal (SH) wave propagation in an infinite metal plate surface bonded by a piezoelectric layer with open electrical circuit is presented. The objective is to study the mode shapes and dispersion characteristics of the shear horizontal wave propagated in a metal core bonded by a layer of piezoelectric material for the potential of health monitoring and repair of structures. The dispersive characteristics and mode shapes of the deflection, electric potential and electric displacement of the piezoelectric layer are theoretically derived. The results from numerical simulations show that the phase velocity of the piezoelectric coupled plate tends to the bulk shear wave velocity of the substrate at high wavenumbers. It is also found that thinner piezoelectric layer in the steel-PZT coupled plates will increase the phase velocity and frequency of the structure especially at smaller wave numbers, whereas the effect by the thickness of the PZT layer plays less role in the gold-PZT coupled plate.

This will help to design piezo-actuator for the structural repair with different host materials. The mode shapes of electric potential and deflection of the piezoelectric layer with steel substrates change from a shape with few zero nodes to a shape with more zero nodes at higher wavenumbers and with thicker piezoelectric layer. For the coupled plate with gold substrates at higher wavenumbers, the electric potential is found to jump from null at the interface of the piezoelectric layer and the substrate to a constant at the surface of the piezoelectric layer along the thickness direction. The electric potential and deflection are found to be closer to be linearly distributed along the thickness direction of the piezoelectric layer when thinner piezoelectric layer is mounted on the host structure. Results from the numerical simulation could be used as a guidance for the design of the structural repair using piezoelectric materials.

2.1 Numerical modeling for a piezoelectric coupled plate

2.1.1 Analytical model of a piezoelectric coupled plate

Consider a metal plate covered by a layer of piezoelectric material as illustrated in Fig. 2-1. The propagation of SH wave in the host metal is governed by:

$$c'_{44}\nabla^2 u'_3 = \rho' \frac{\partial^2 u'_3}{\partial t^2} \tag{2-1}$$

where $c'_{44} = 2G = \frac{E}{(1+\upsilon)}$ is the shear modulus, ρ' the mass density, υ the Poisson ratio, E the Young's modulus of the host medium, u'_3 the deflection of the host medium in the x_3-direction, and ∇^2 the Laplace operator given by $\nabla^2 = \frac{\partial^2}{\partial x_1^2} + \frac{\partial^2}{\partial x_2^2}$. The shear stress can be written as:

$$\sigma'_{23} = c'_{44} \frac{\partial u'_3}{\partial x_2} \tag{2-2}$$

The poling direction of the piezoelectric layer is in the flexural x_3-direction, thus the coupling equation for the piezoelectric layer is written as (Viktorov 1981),

$$c_{44}\nabla^2 u_3 + e_{15}\nabla^2 \phi = \rho \frac{\partial^2 u_3}{\partial t^2} \tag{2-3a}$$

$$e_{15}\nabla^2 u_3 - \Xi_{11}\nabla^2 \phi = 0 \tag{2-3b}$$

where $c_{44} = (c_{11} - c_{22})/2$ is the elastic modulus, e_{15} the piezoelectric coefficient, Ξ_{11} the dielectric constant, and ρ the mass density of the piezoelectric layer, u_3 the deflection of the piezoelectric layer in the x_3 direction, and ϕ the electric potential. The shear stress in the piezoelectric layer is expressed by,

$$\sigma_{23} = c_{44} \frac{\partial u_3}{\partial x_2} + e_{15} \frac{\partial \phi}{\partial x_2} \tag{2-4}$$

Since the piezoelectric layer is surface bonded on the metal substrate, the electric potential on the interface of the layer and substrate is null. Meanwhile, since the piezoelectric layer abuts the vaccum, i.e. the surface of the piezoelectric layer is totally isolated and insulated, it is

appropriate to model the electric displacement approximately to be zero at the surface. Thus, the boundary condition at the surface of the piezoelectric layer could be expressed as

$$D_2 = 0, \sigma_{23} = 0.(x_2 = -h_1)\,. \tag{2-5}$$

The boundary conditions of the interface between the piezoelectric layer and the host plate and the surface of host plate could be expressed as

$$u_3 = u_3', \sigma_{23} = \sigma_{23}', \phi = 0.(x_2 = 0) \tag{2-6}$$

$$\sigma_{23}' = 0.(x_2 = \mathrm{H}) \tag{2-7}$$

The solution of wave propagation in x_1-direction for the metal core can be solved following the calculation process in (Wang and Varadan 2002),

$$u_3' = \left(A_1 \sin \alpha x_2 + A_2 \cos \alpha x_2\right) e^{i\omega\left(t - \frac{x_1}{c}\right)}\ , \tag{2-8}$$

where $\alpha^2 = \dfrac{\omega^2}{v'^2} - \dfrac{\omega^2}{c^2}$, $v'^2 = c_{44}'/\rho'$. Substituting Eq. (2-3b) into (2-3a) gives

$$\bar{c}_{44} \nabla^2 u_3 = \rho \frac{\partial^2 u_3}{\partial t^2} \tag{2-9}$$

where $\bar{c}_{44} = c_{44} + \dfrac{e_{15}^2}{\Xi_{11}}$ is the piezoelectrically stiffened elastic constant. The solution of Eq. (2-9) for the piezoelectric layer can be obtained as

$$u_3 = \left(C_1 e^{-\chi_2 x_2} + C_2 e^{\chi_2 x_2}\right) e^{i\omega\left(t - \frac{x_1}{c}\right)} \qquad \text{when } v' < c < v \tag{2-10a}$$

$$u_3 = \left(D_1 \cos \chi_2 x_2 + D_2 \sin \chi_2 x_2\right) e^{i\omega\left(t - \frac{x_1}{c}\right)} \quad \text{when } c > v' > v \text{ or } c > v > v' \tag{2-10b}$$

where $\chi_2 = \frac{\omega}{c}\sqrt{\left|1-\left(\frac{c}{v}\right)^2\right|}$ and $v^2 = \frac{\bar{c}_{44}}{\rho}$. The electric displacement along x_2 direction is expressed as:

$$D = e_{15}\frac{\partial u_3}{\partial x_2} - \Xi_{11}\frac{\partial \phi}{\partial x_2} = -\Xi_{11}\frac{\partial \psi}{\partial x_2} = \Xi_{11}\chi_1\left(B_1 e^{-\chi_1 x_2} - B_2 e^{\chi_1 x_2}\right) \tag{2-11}$$

where $\psi = \left(B_1 e^{-\chi_1 x_2} + B_2 e^{\chi_1 x_2}\right)e^{i\omega\left(t-\frac{x_1}{c}\right)}$ and $\chi_1 = \omega / c$ (Parton and Kudryavtser 1988). The electric potential and shear stress components can be solved by substituting Eqs. (2-10) and (2-8) into Eqs. (2-2~2-4),

$$\phi = \left[\left(B_1 e^{-\chi_1 x_2} + B_2 e^{\chi_1 x_2}\right) + \frac{e_{15}}{\Xi_{11}}\left(C_1 e^{-\chi_2 x_2} + C_2 e^{\chi_2 x_2}\right)\right]e^{i\omega\left(t-\frac{x_1}{c}\right)} \tag{2-12}$$

$$\sigma'_{23} = c'_{44}\alpha\left(A_1 \cos\alpha x_2 - A_2 \sin\alpha x_2\right)e^{i\omega\left(t-\frac{x_1}{c}\right)} \tag{2-13}$$

$$\sigma_{23} = \left[\left(-\chi_2\right)\bar{c}_{44}\left(C_1 e^{-\chi_2 x_2} - C_2 e^{\chi_2 x_2}\right) + \left(-\chi_1\right)e_{15}\left(B_1 e^{-\chi_1 x_2} - B_2 e^{\chi_1 x_2}\right)\right]e^{i\omega\left(t-\frac{x_1}{c}\right)} \tag{2-14}$$

when $v' < c < v$,

$$\phi = \left[\left(B_1 e^{-\chi_1 x_2} + B_2 e^{\chi_1 x_2}\right) + \frac{e_{15}}{\Xi_{11}}\left(D_1 \cos\chi_2 x_2 + D_2 \sin\chi_2 x_2\right)\right]e^{i\omega\left(t-\frac{x_1}{c}\right)} \tag{2-15}$$

$$\sigma_{23} = \left[\left(-\chi_2\right)\bar{c}_{44}\left(D_1 \sin\chi_2 x_2 - D_2 \cos\chi_2 x_2\right) + \left(-\chi_1\right)e_{15}\left(B_1 e^{-\chi_1 x_2} - B_2 e^{\chi_1 x_2}\right)\right]e^{i\omega\left(t-\frac{x_1}{c}\right)} \tag{2-16}$$

when $c > v' > v$ or $c > v > v'$.

2.1.2 Dispersion relations of a piezoelectric coupled plate

Substituting the solutions for the metal core and the piezoelectric layer in eqs. (2-8), (2-10) and (2-12)-(2-16) into the boundary conditions in eqs. (2-5)-(2-7) will result in an eigen-value problem from which the dispersive characteristics for this piezoelectric coupled plate may be deduced.

For the case when $v' < c < v$, the condition of non-trivial solutions for A_i, B_i, and C_i $(i = 1,2)$ can be studied via an eigen-value problem, whose solution can be directly provided following the similar process in (Wang and Varadan 2002):

$$-\frac{c'_{44}\alpha}{2\bar{c}_{44}\chi_2}\left(e^{\chi_2 h1}+e^{-\chi_2 h1}\right)\sin\alpha H+\left(\frac{\frac{e_{15}^2\chi_1\left(1-e^{2\chi_1 h_1}\right)}{\Xi_{11}\bar{c}_{44}\chi_2\left(1+e^{2\chi_1 h_1}\right)}+1}{2}e^{\chi_2 h_1}-\frac{1-\frac{e_{15}^2\chi_1\left(1-e^{2\chi_1 h_1}\right)}{\Xi_{11}\bar{c}_{44}\chi_2\left(1+e^{2\chi_1 h_1}\right)}}{2}e^{-\chi_2 h_1}\right)\cos\alpha H=0. \quad (2\text{-}17)$$

For the case of $c > v' > v$ or $c > v > v'$, we can have the following equation for the condition of nontrivial solutions of A_i, B_i, and C_i $(i = 1,2)$:

$$\frac{c'_{44}\alpha}{\bar{c}_{44}\chi_2}\cos\chi_2 h_1\sin\alpha H+\cos\alpha H\left(-\frac{e_{15}^2\chi_1\left(1-e^{2\chi_1 h_1}\right)}{\Xi_{11}\bar{c}_{44}\chi_2\left(1+e^{2\chi_1 h_1}\right)}\cos\chi_2 h_1+\sin\chi_2 h_1\right)=0 \qquad (2\text{-}18)$$

2.1.3 Mode shapes in a piezoelectric layer

The mode shapes of the deflection, electric potential, and electric displacement in thickness direction of piezoelectric layer may be obtained from characteristic equation of eq. (2-17) or (2-18) as follows, when $v' < c < v$, eqs. (7) and (13) imply

$$A_1 = A_2 \tan \alpha H \tag{2-19}$$

Thus C_1 and C_2 can all be expressed in term of A_2, and the mode shapes of the host plate and piezoelectric layer can be derived in term of eqs. (2-8), (2-10a), (2-11) and (2-12) as follows,

$$\overline{u}_3' = A_2\left(\tan \alpha H \sin \alpha x_2 + \cos \alpha x_2\right) \tag{2-20}$$

$$\overline{u}_3 = A_2 e^{-\chi_2 x_2}\left(\frac{M_1}{2}\tan \alpha H + \frac{M_2 + 1}{2}\right) + A_2 e^{\chi_2 x_2}\left(-\frac{M_1}{2}\tan \alpha H + \frac{1 - M_2}{2}\right) \tag{2-21}$$

$$\overline{\phi} = -A_2 \frac{e_{15}}{\Xi_{11}\left(1 + e^{2\chi_1 h_1}\right)}\left(e^{-\chi_1 x_2} + e^{2\chi_1 h_1} e^{\chi_1 x_2}\right) + \frac{e_{15}}{\Xi_{11}}\overline{u}_3 \tag{2-22}$$

$$\overline{D}_2 = -A_2 \frac{e_{15}\chi_1}{\Xi_{11}\left(1 + e^{2\chi_1 h_1}\right)}\left(e^{-\chi_1 x_2} - e^{2\chi_1 h_1} e^{\chi_1 x_2}\right) \tag{2-23}$$

where the over bar indicates the spatial components of the variables.

When $c > v' > v$ or $c > v > v'$, mode shape of the host plate remain the same with that in eq. (2-20), and the mode shapes of the piezoelectric layer are obtained as follows in the similar ways,

$$\overline{u}_3 = A_2\left[\cos \chi_2 x_2 + \sin \chi_2 x_2\left(-M_2 + \tan \alpha H \frac{c_{44}'\alpha}{\overline{c}_{44}\chi_2}\right)\right] \tag{2-24}$$

$$\overline{\phi} = -A_2 \frac{e_{15}}{\Xi_{11}\left(1 + e^{2\chi_1 h_1}\right)}\left(e^{-\chi_1 x_2} + e^{2\chi_1 h_2} e^{\chi_1 x_2}\right) + \frac{e_{15}}{\Xi_{11}}\overline{u}_3 \tag{2-25}$$

$$\overline{D}_2 = -A_2 \frac{e_{15}\chi_1}{\Xi_{11}\left(1 + e^{2\chi_1 h_1}\right)}\left(e^{-\chi_1 x_2} - e^{2\chi_1 h_2} e^{\chi_1 x_2}\right) \tag{2-26}$$

It is noted that the electric potential and electric displacement in eqs. (2-25) and (2-26) have the same expressions with eqs. (2-22) and (2-23).

Numerical simulations were performed to illustrate the results of the dispersive characteristics and the mode shapes obtained above and presented in the following section.

2.2 Numerical simulations and discussions

The bulk shear wave velocities of steel, aluminium and gold as substrates and PZT-4 surface bonded on the substrates are calculated as $v'|_{steel} = 3216 m/s$, $v'|_{al} = 3066\, m/s$, $v'|_{gold} = 1202 m/s$ and $v|_{PZT4} = 2352\, m/s$ from the material properties provided in Table 2-1.

The dispersion curves for the steel-PZT-4, aluminium-PZT-4 and gold-PZT-4 piezoelectric coupled plates are plotted in Figs. 2-2 to 2-4. The non-dimensional phase velocity is taken as $\bar{c} = c/v'$ and the non-dimensional wave number as $\bar{\xi} = \xi h_1 / 2\pi$. The ratio of the thickness of the PZT-4 layer to that of the host metal is taken as 0.1, i.e. $n = \frac{h_1}{H} = 0.1$. The dispersion curves for the first five modes of wave propagation for all the three cases indicate that the wave phase velocity approaches the bulk-shear wave velocity of the host metal at high wavenumbers. This conclusion is consistent with the fact that when the wavelength is much smaller compared to the thickness of the plate, the behaviour of wave propagation in the piezoelectric plate will be similar to that in an infinite metal media. Figs. 2-2 to 2-5 and 2-2 to 2-6 plot the dispersion curves of the steel-PZT and gold-PZT plates at different ratios of the thickness of the piezoelectric layer. It is noted from Fig. 2-5 that the phase velocity decreases very slightly with increase of the thickness of the piezoelectric layer as the stiffness of PZT is smaller than that of steel. Nevertheless, the thickness of the piezoelectric layer has less effect on the dispersion characteristics of the plate

with gold as core material, seen from Fig. 2-6. The asymptotic velocities at high wavenumbers for all thickness remain to be the bulk shear wave velocity of the metal core.

The first mode shapes of the deflection, electric potential and electric displacement in the piezoelectric layer for steel-PZT-4 coupled plate with thickness ratio of 0.3 are presented in Figs. 2-7 and 2-8 at the non-dimensional wavenumber of 0.3 and 2.3, respectively, along the thickness direction. It can be seen that all the boundary conditions related to the electric potential and electric displacement are satisfied completely. At the higher non-dimensional wave number of 2.3, more zero nodes in the distribution of the electric potential and deflection are observed, consistent with the finding by Wang and Quek [30].The thickness of the piezoelectric layer also affects the distribution of the above variables, seen from Figs. 2-9 and 2-10 in which the fifth mode shapes are plotted for non-dimensional wave number of 2.3 with thickness ratios of 0.3 and 0.1. More zero nodes are observed for the thicker piezoelectric layer. From Figs. 2-7 to 2-10, it can also be found that the mode shapes of the deflection and electric potential are consistent especially near the PZT surface, which is a characteristic of piezoelectric material with open circuit. The result is obviously different from the finding by Wang and Varadan (2002) of a piezoelectric plate with short circuit condition. In the study of the close circuit condition, the mode shapes of the deflection and electric potential all keep similar close to the interface of piezoelectric layer and the host metal for a wide region of wave numbers before breaking away to approach to a shape with large gradient near the surface of electric layer. In addition, our current research shows that the SH wave propagation presents higher wave velocity in open circuit piezoelectric coupled plates than in the short circuit plate, when the same wave number is considered. That means the frequency of wave propagation in open circuit piezoelectric coupled plate is higher than the one with short circuit condition as well.

For the gold-PZT-4 coupled plate, Figs. 2-11 and 2-12 show the first mode shapes at n=0.3 and non-dimensional wavenumber of 0.5 and 2.0, respectively. Different from the results in steel-PZT-4 coupled plate, the zero nodes of the distribution of the electric potential and deflection do not increase with higher wave numbers. Besides, the results show that even at the high non-dimensional wave number of 2.0, the electric potential is found to jump from null at the interface of the piezoelectric layer and gold to a constant at the surface of the piezoelectric layer along the thickness direction.

It is concluded from the simulations that close to surface of the piezoelectric layer of the gold-PZT coupled plate, the electric potential reaches an almost maximal constant and such a characteristic is indispensable for a possible displacement sensor design based on the coupled plate structure as the electrical potential can be used as an output and viewed as a representative index of the displacement variation on the surface of an engineering plate.

2.3 Conclusions

This chapter presents the research on SH wave propagation in a piezoelectric coupled plate with open circuit. The dispersion characteristics of the coupled structure and the mode shape of the deflection, electric potential and electric displacement of the piezoelectric layer are investigated by numerical simulations. The results show that the asymptotic solution of wave propagation in the plate with steel, aluminium, and gold as core plates is the bulk shear wave velocity of the substrate. The effect of the ratio of thickness of the piezoelectric layer is studied as well. It shows that thicker piezoelectric layer in the steel-PZT coupled plates will reduce the phase velocity of the structure, whereas the effect by the thickness of the PZT layer plays less role in the gold-PZT coupled plate.

In the study of the mode shapes of the piezoelectric layer of steel-PZT coupled plates, it is found that the zero nodes of the mode shapes of the electric potential and deflection along the thickness of the piezoelectric increase at higher wavenumbers and with thicker piezoelectric layer. Otherwise, the mode shapes of deflection and electric potential are accordant especially near the PZT surface. For the gold-PZT 4 coupled plate even at higher wavenumbers, the electric potential is found to jump from null at the interface of the piezoelectric layer and gold to a constant at the surface of the piezoelectric layer along the thickness direction.

Table 2- 1 Material properties and geometric size of the piezoelectric coupled plate

	Host Structure (Steel)	Host Structure (Aluminum)	Piezoelectric layer
Young's module (N/m^2)	$E = 200\times10^9$	$E = 70\times10^9$	$C_{11}^E = c_{11} = 132\times10^9$ $C_{12}^E = c_{12} = 71\times10^9$ $C_{33}^E = c_{33} = 115\times10^9$ $C_{13}^E = c_{13} = 73\times10^9$ $C_{44}^E = c_{44} = 26\times10^9$ $E_p = 78.6\times10^9$
Poisson ratio	$\upsilon = 0.3$	$\upsilon = 0.3$	–
Mass density (kg/m^3)	7.8×10^3	2.8×10^3	7.5×10^3
e_{31} (C/m^2)	–		-4.1
e_{33} (C/m^2)	–		14.1
e_{15} (C/m^2)	–		10.5
Ξ_{11} (F/m)	–		7.124×10^{-9}
Ξ_{33} (F/m)	–		5.841×10^{-9}
r_0 (mm)	600		
H (2*h) (mm)	10		
h_1 (mm)	2		

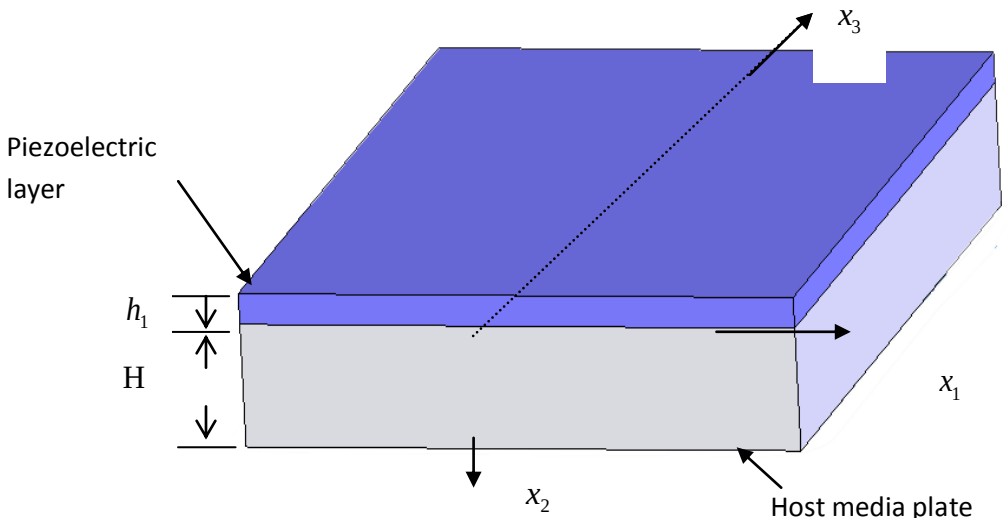

Fig. 2- 1 A semi-infinite metal plate surface covered by a layer of piezoelectric material with open circuit. (the plate is semi-infinite along x_3 direction)

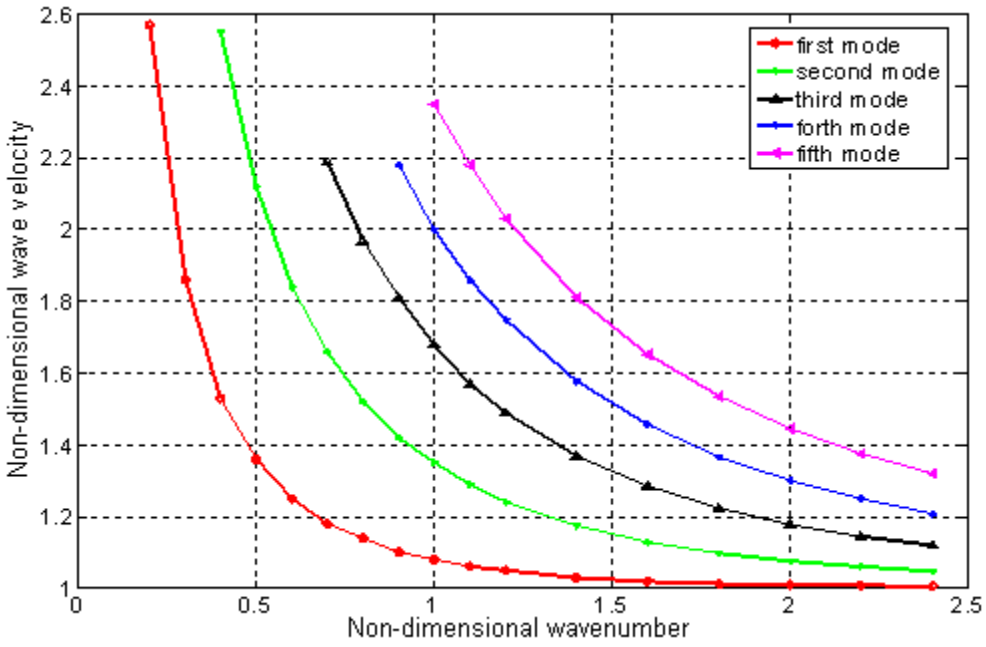

Fig. 2- 2 Dispersion Curves for steel-PZT at n=0.1.

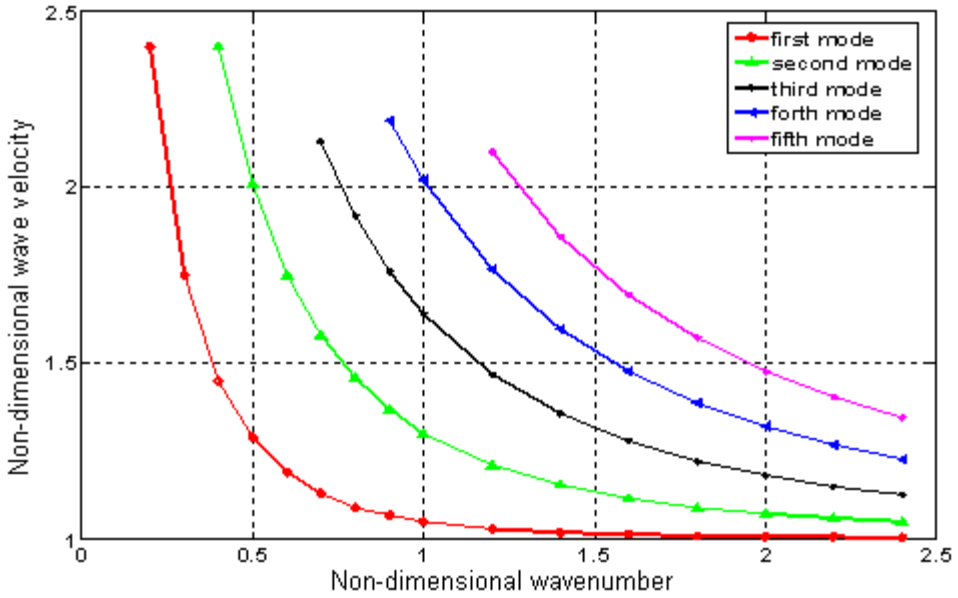

Fig. 2- 3 Dispersion curves for aluminium-PZT at n=0.1.

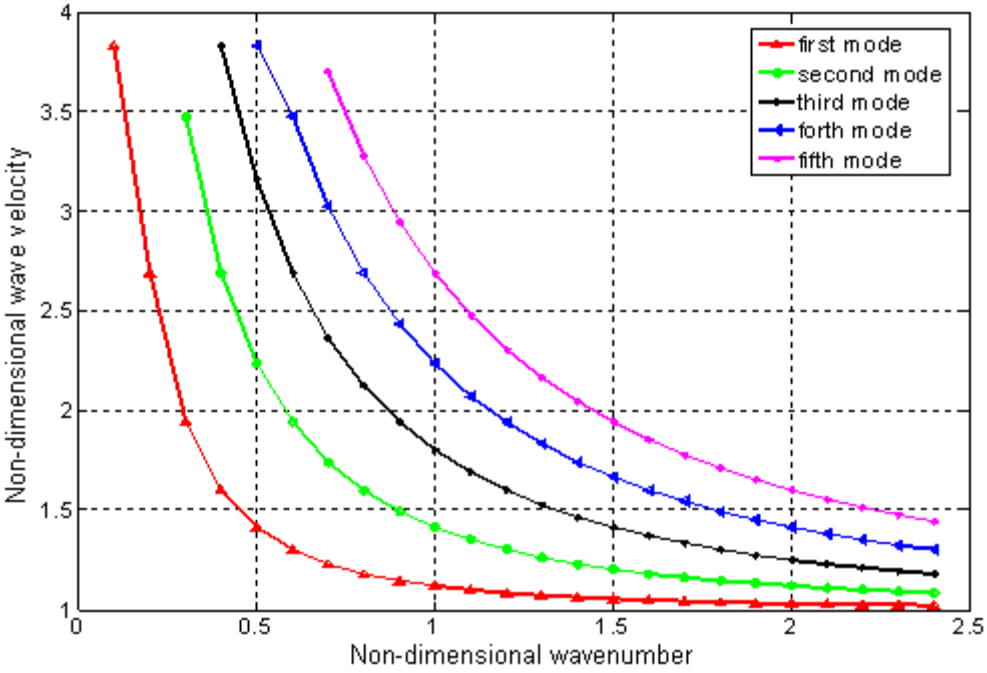

Fig. 2- 4 Dispersion curves for a gold-PZT coupled plate at n=0.1.

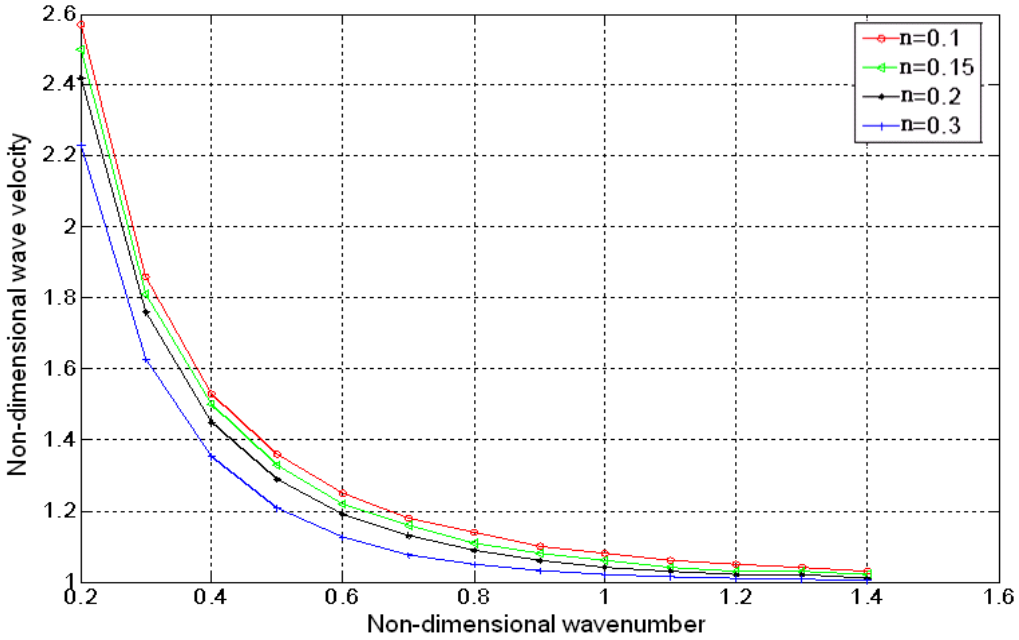

Fig. 2- 5 Variation of dispersion characteristics of a Steel-PZT plate by different thickness rates.

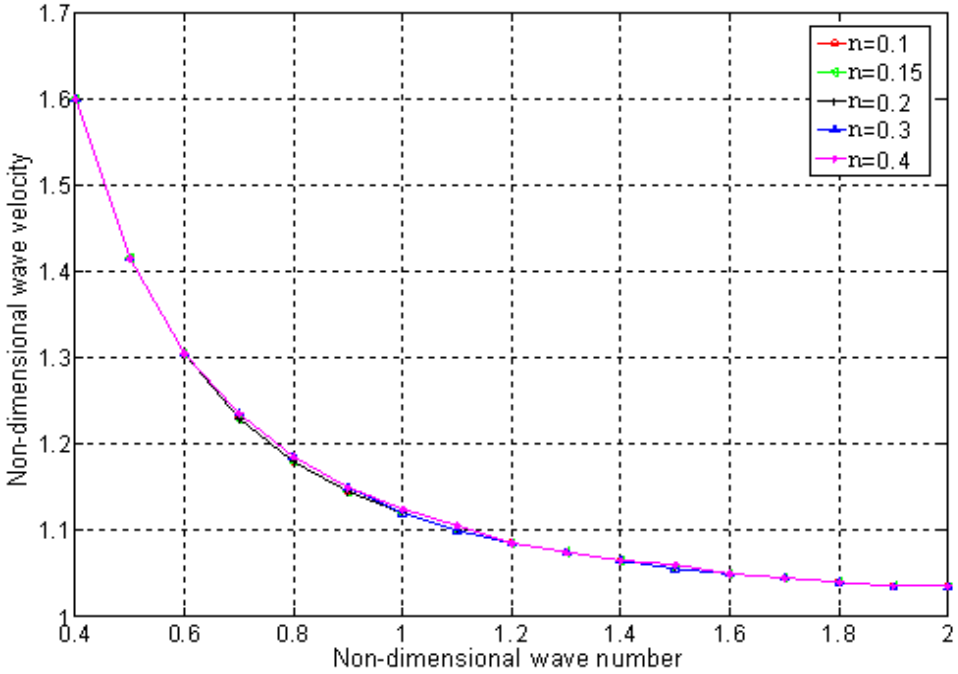

Fig. 2- 6 Variation of dispersion characteristics of a Gold-PZT plate by different thickness rates.

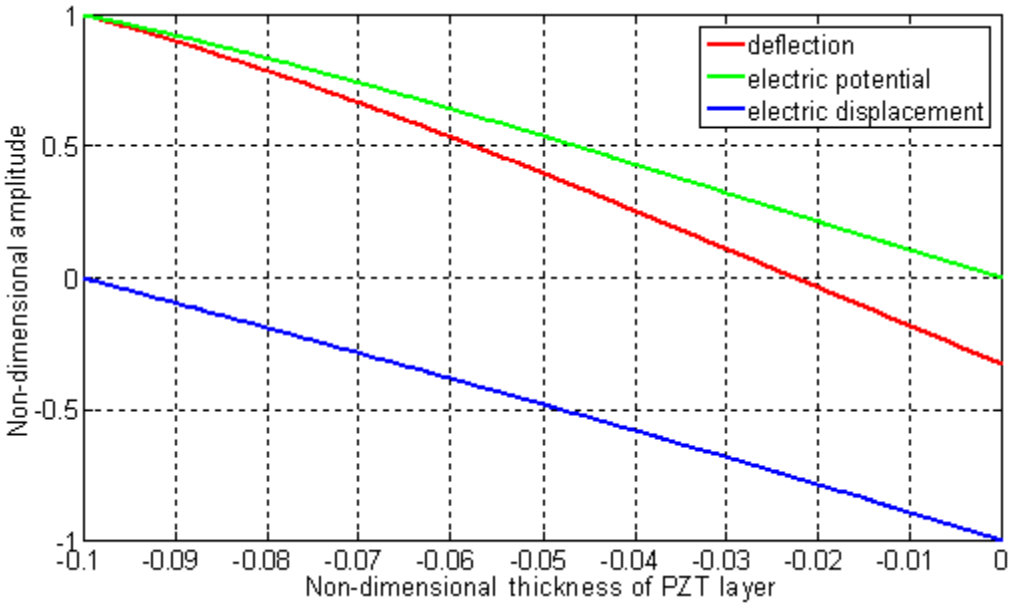

Fig. 2- 7 First mode shape of the PZT layer in a steel-PZT coupled plate at n=0.3 and non-dimensional wave number 0.3.

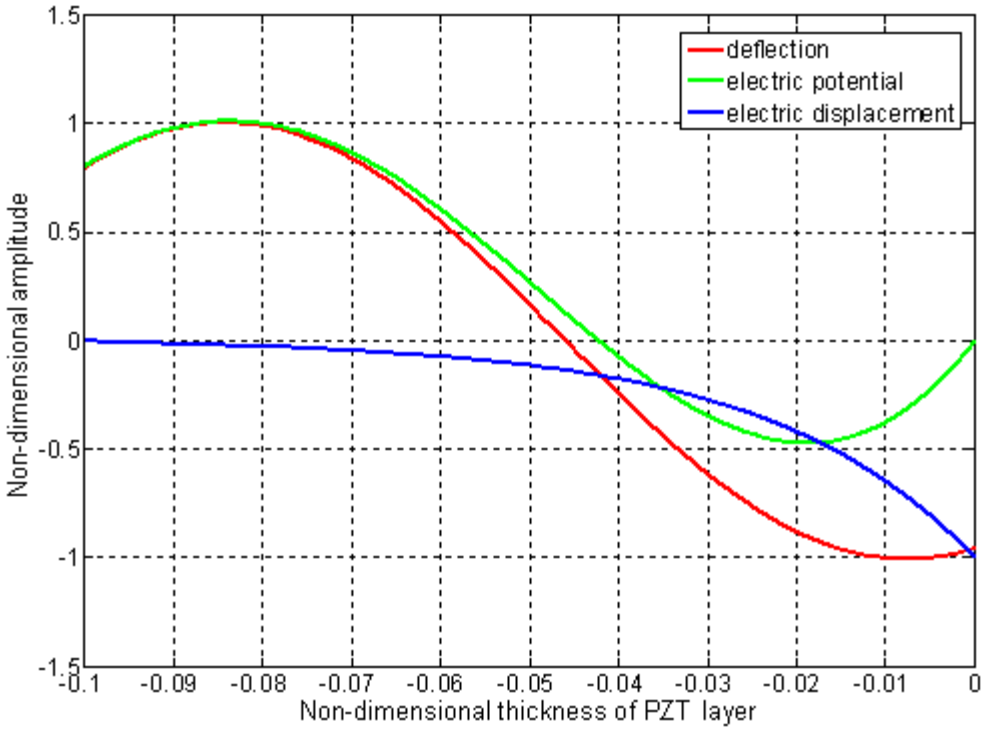

Fig. 2- 8 First mode shape of the PZT layer in a steel-PZT coupled plate at n=0.3 and non-dimensional wave number 2.3.

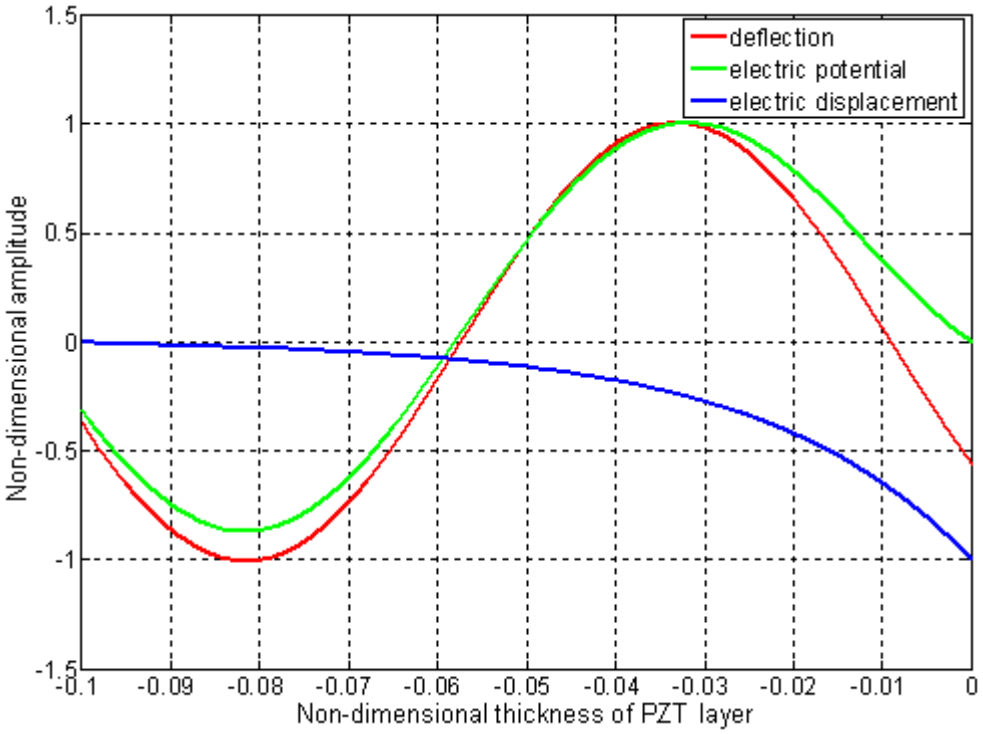

Fig. 2- 9 Fifth mode shape of the PZT layer in a steel-PZT coupled plate at n=0.3 and non-dimensional wave number 2.3.

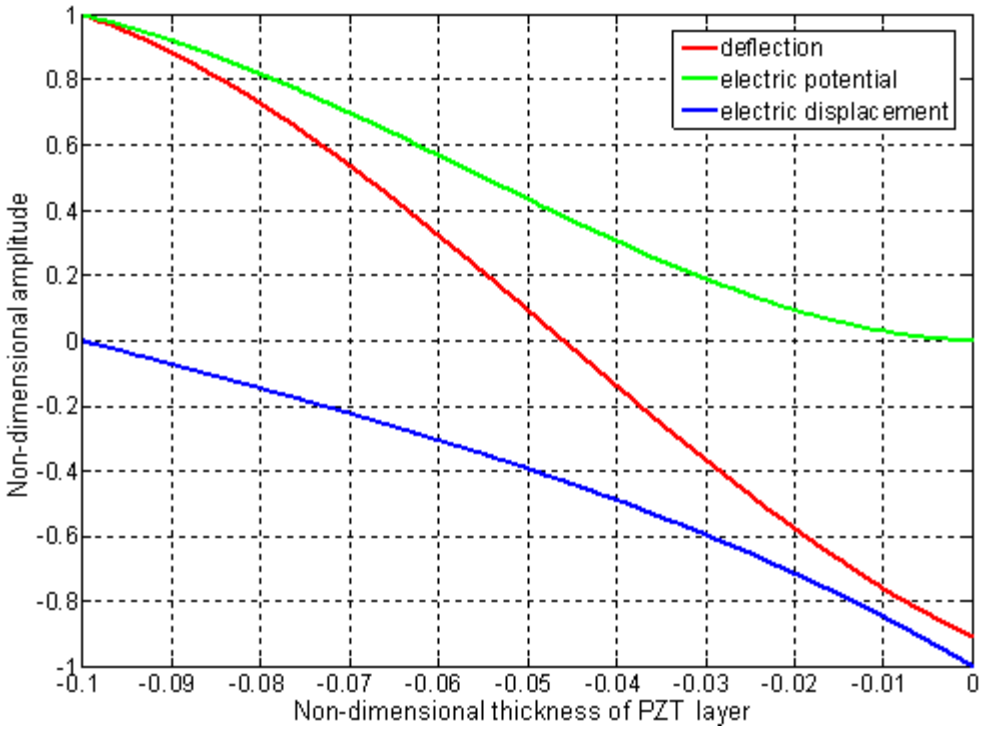

Fig. 2- 10 Fifth mode shape of the PZT layer in a steel-PZT coupled plate at n=0.1 and non-dimensional wave number 2.3.

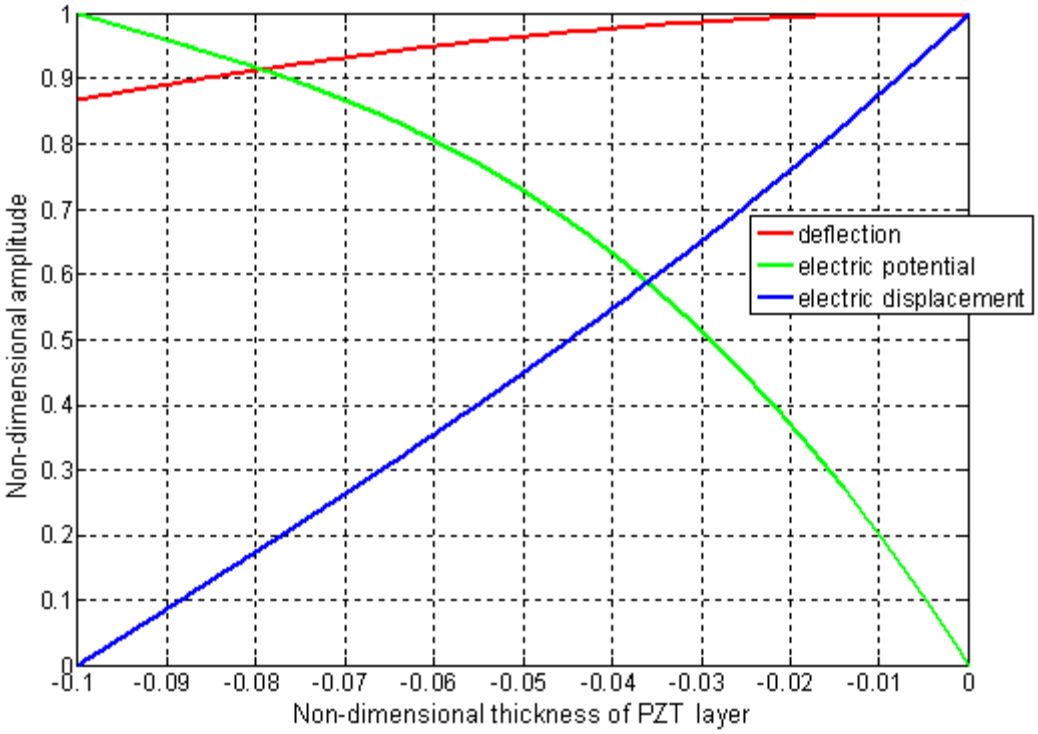

Fig. 2- 11 First mode shape of the PZT layer in a gold-PZT coupled plate for the second type of wave propagation at n=0.3 and non-dimensional wave number 0.5.

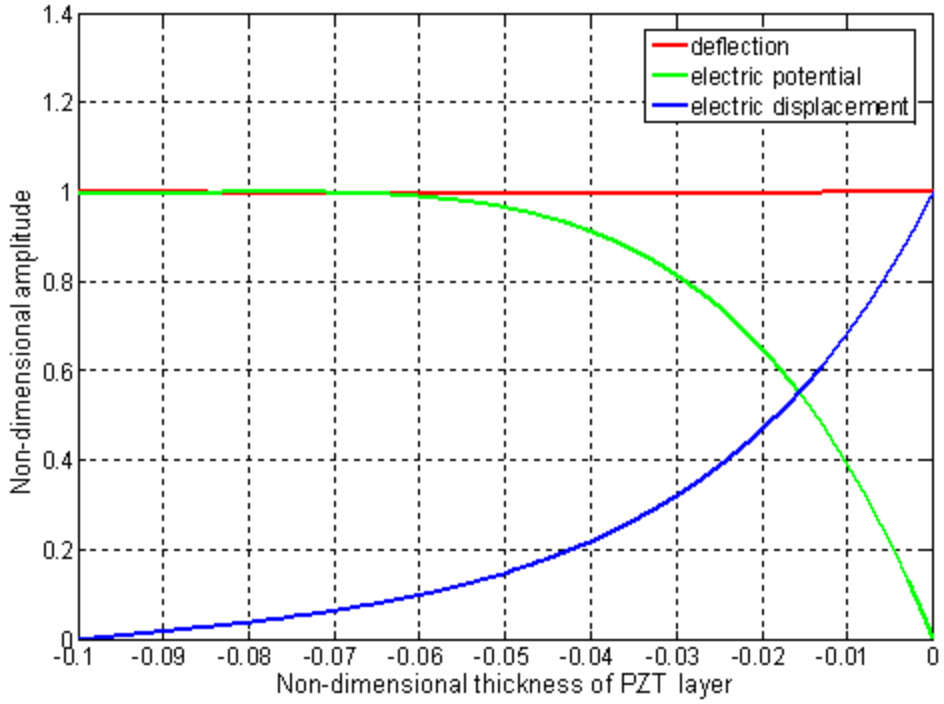

Fig. 2- 12 First mode shape of the PZT layer in a gold-PZT coupled plate for the second type of wave propagation at n=0.3 and non-dimensional wave number 2.0.

3 Free vibration analysis of a piezoelectric coupled plate

Because of the active electro-mechanical property, piezoelectric materials are usually used as sensors and actuators for the dynamic repair of damaged structures. The analysis of both electrical and mechanical dynamic responses of piezoelectric coupled structures is significant for the design of structural repair via piezoelectric materials. A vibration analysis of a circular steel substrate surface bonded by a piezoelectric layer with open circuit is presented to study the piezoelectric effect on the dynamic response of the host structure. A solution for the electrical potential along the thickness direction of the piezoelectric layer satisfying the open circuit electric boundary condition is developed for the first time. The mechanical model and solutions for the vibration analysis of the piezoelectric coupled circular plate are then established based on the developed electrical potential, Kirchhoff plate model, and Maxwell equation. The first four mode shapes and the corresponding resonant frequencies of the plate with two standard boundary conditions are presented in numerical simulations and compared with those of a piezoelectric coupled plate with the closed circuit condition. The simulations show that the resonant frequencies of the open circuit piezoelectric coupled plate are higher than those of the closed circuit piezoelectric coupled plate. In additional, the electric potential is approximately to be linear distributed along the thickness direction of the piezoelectric layer at the first vibration

mode of the piezoelectric coupled plate, while non-linear electric potential distributions are found at higher modes.

3.1 Mechanical models for a piezoelectrically coupled circular plate with open circuit condition

In the following vibration analysis of the cylinder plate, the cylindrical coordinate system is adopted. Axis z indicates the thickness direction.

3.1.1 Kinematics and constitutive relations

In this section, basic kinematics and constitutive equations of the piezoelectric layer and the host plate are simply provided for derivations of the free vibration of the coupled plate in later sections. The structure of a piezoelectric coupled circular plate with radius r_0 is shown in Fig. 3-1. The thickness of piezoelectric layer and the half thickness of the host plate are denoted as h_1 and H. In application of Kirchhoff thin plate theory, the displacements and strains of the plate are provided:

$$u_z = u_z(r,\theta,t) = w(r,\theta,t) \tag{3-1}$$

$$u_r = u_r(r,\theta,t) = -z\frac{\partial u_z}{\partial r} \tag{3-2}$$

$$u_\theta = u_\theta(r,\theta,t) = -z\frac{\partial u_z}{r\partial \theta} \tag{3-2}$$

$$\varepsilon_{rr} = \frac{\partial u_r}{\partial r} = -z\frac{\partial^2 w}{\partial r^2} \tag{3-4}$$

$$\varepsilon_{\theta\theta} = \frac{\partial u_\theta}{r\partial\theta} + \frac{u_r}{r} = -z(\frac{\partial^2 w}{r^2\partial\theta^2} + \frac{\partial w}{r\partial r}) \tag{3-5}$$

$$\varepsilon_{r\theta} = \frac{1}{2}(\frac{\partial u_r}{r\partial\theta} + \frac{\partial u_\theta}{\partial r} - \frac{u_\theta}{r}) = -z(\frac{\partial^2 w}{r\partial r\partial\theta} - \frac{\partial w}{r^2\partial\theta}) \tag{3-6}$$

where u_z, u_r, and u_θ are the displacements in the transverse z-direction, radial r-direction and tangential θ-direction of the plate, respectively.

The stress components in the host plate are thus expressed as

$$\sigma_{rr}^1 = \frac{E}{1-\upsilon^2}(\varepsilon_{rr} + \upsilon\varepsilon_{\theta\theta}) = -\frac{E}{1-\upsilon^2}[\frac{\partial^2 w}{\partial r^2} + \upsilon(\frac{\partial^2 w}{r^2\partial\theta^2} + \frac{\partial w}{r\partial r})] \tag{3-7}$$

$$\sigma_{\theta\theta}^1 = \frac{E}{1-\upsilon^2}(\varepsilon_{\theta\theta} + \upsilon\varepsilon_{rr}) = -\frac{E}{1-\upsilon^2}(\upsilon\frac{\partial^2 w}{\partial r^2} + \frac{\partial^2 w}{r^2\partial\theta^2} + \frac{\partial w}{r\partial r}) \tag{3-8}$$

$$\tau_{r\theta}^1 = -\frac{Ez}{1+\upsilon}(\frac{\partial^2 w}{r\partial r\partial\theta} - \frac{\partial w}{r^2\partial\theta}) \tag{3-9}$$

The piezoelectric material is assumed to be polarized in the z-direction. The stress components in piezoelectric layer can be written as

$$\sigma_{rr}^2 = \bar{C}_{11}^E\varepsilon_{rr} + \bar{C}_{12}^E\varepsilon_{\theta\theta} - \bar{e}_{31}E_z \tag{3-10}$$

$$\sigma_{\theta\theta}^2 = \bar{C}_{12}^E\varepsilon_{rr} + \bar{C}_{11}^E\varepsilon_{\theta\theta} - \bar{e}_{31}E_z \tag{3-11}$$

$$\tau_{r\theta}^2 = (\bar{C}_{11}^E - \bar{C}_{12}^E)\varepsilon_{r\theta} = -z(\bar{C}_{11}^E - \bar{C}_{12}^E)(\frac{\partial^2 w}{r\partial r\partial\theta} - \frac{\partial w}{r^2\partial\theta}) \tag{3-12}$$

where the superscripts 1 and 2 represent the variables in the host structure and the piezoelectric material, respectively; $\bar{C}_{11}^{E}$, $\bar{C}_{12}^{E}$ and $\bar{e}_{31}$ are transformed reduced material constants of piezoelectric medium for plane stress problem, and are given by $\bar{C}_{11}^{E} = C_{11}^{E} - \frac{\left(C_{13}^{E}\right)^2}{C_{33}^{E}}$, $\bar{C}_{12}^{E} = C_{12}^{E} - \frac{\left(C_{13}^{E}\right)^2}{C_{33}^{E}}$, $\bar{e}_{31} = e_{31} - \frac{C_{13}^{E} e_{33}}{C_{33}^{E}}$ [56]. E is the Young's modulus of beam material; C_{11}^{E} and C_{12}^{E} are the elastic modulus of piezoelectric material in the radial and tangential directions measured at constant electric field; and e_{31} is the piezoelectric constant of the piezoelectric layer.

3.1.2 Electric potential distribution in the piezoelectric layer

Each piezoelectric layer has electrodes mounted on both surfaces to facilitate the application of voltage to actuate the structure. When an external voltage is applied, the electric potential distribution on the surface of the electrode remains constant. When electrodes at the two surfaces of the piezoelectric layer are shortly connected, the electric potential is zero throughout the surfaces.

In the research of Wang *et al* (2001), they proposed a quadratic variation of the electric potential in the transverse direction of close circuit piezoelectric layer. The assumption was verified by finite element analysis in their paper. Thus, potential distribution function in thickness direction of close circuit piezoelectric layer can be written as

$$\phi = \left[1 - \left(\frac{z - h - h_1/2}{h_1/2}\right)^2\right] \cdot \varphi(r, \theta, t), \tag{3-13}$$

where z is measured from the mid-plane of the host plate in the global z-direction, h_1 is the thickness of the piezoelectric layer, and $\phi(r,\theta,t)$ is the electric potential on the mid-surface of the piezoelectric layer.

Since the piezoelectric layer is surface bonded on the metal substrate, the electric potential on the interface of the layer and substrate is null. However, for the open-circuit condition, the electric potential on the surface opposite to the interface is not zero. Thus the quadratic variation of the electric potential is not applicable for un-shorted connected piezoelectric layer. The potential function in thickness direction of open-circuit piezoelectric layer is assumed as

$$\phi = \left[1 - \left(\frac{z - h - h_1/2}{h_1/2}\right)^2\right] \cdot \varphi(r,\theta,t) + X \,, \tag{3-14}$$

where X is a linear function of z, $X = A \cdot z + B$. A and B are the parameters which should satisfy the open-circuit electric boundary condition. For the open-circuit piezoelectric plate, the electric displacement at the surface can be approximated to be zero. Eq. (3-14) should satisfy the following boundary condition,

$$\begin{aligned} \phi|_{z=h} &= 0 \\ D_z|_{z=h+h1} &= 0 \end{aligned} \tag{3-15}$$

where ϕ is the electric potential, and D_z is the corresponding electric displacement along z direction. The components of electric field E and electric displacement D as well as the satisfied electric boundary condition will be discussed as follow.

Submitting Eq. (3-14) into the functions of the components of the electric field E and electric displacement D, E and D can be written as

$$E_r = -\frac{\partial \phi}{\partial r} = -\left[1-\left(\frac{z-h-h_1/2}{h_1/2}\right)^2\right]\cdot\frac{\partial \varphi}{\partial r} - \frac{\partial X}{\partial r} \tag{3-16}$$

$$E_\theta = -\frac{\partial \phi}{r\partial \theta} = -\left[1-\left(\frac{z-h-h_1/2}{h_1/2}\right)^2\right]\cdot\frac{\partial \varphi}{r\partial \theta} - \frac{\partial X}{r\partial \theta} \tag{3-17}$$

$$E_z = -\frac{\partial \phi}{\partial z} = \frac{8(z-h-h_1/2)}{{h_1}^2}\cdot\varphi - \frac{\partial X}{\partial z} \tag{3-18}$$

$$D_r = \bar{\bar{\Xi}}_{11}E_r = -\bar{\bar{\Xi}}_{11}\left[1-\left(\frac{z-h-h_1/2}{h_1/2}\right)^2\right]\cdot\frac{\partial \varphi}{\partial r} - \bar{\bar{\Xi}}_{11}\frac{\partial X}{\partial r} \tag{3-19}$$

$$D_\theta = \bar{\bar{\Xi}}_{11}E_\theta = -\bar{\bar{\Xi}}_{11}\left[1-\left(\frac{z-h-h_1/2}{h_1/2}\right)^2\right]\cdot\frac{\partial \varphi}{r\partial \theta} - \bar{\bar{\Xi}}_{11}\frac{\partial X}{r\partial \theta} \tag{3-20}$$

$$D_z = \bar{\bar{\Xi}}_{33}E_z + \bar{e}_{31}(\varepsilon_{rr}+\varepsilon_{\theta\theta}) = \bar{\bar{\Xi}}_{33}\frac{8(z-h-h_1/2)}{{h_1}^2}\cdot\varphi - \bar{\bar{\Xi}}_{33}\frac{\partial X}{\partial z} + \bar{e}_{31}(\varepsilon_{rr}+\varepsilon_{\theta\theta}) \tag{3-21}$$

where $\bar{\bar{\Xi}}_{11}$ and $\bar{\bar{\Xi}}_{33}$ are reduced dielectric constant of the piezoelectric layer for plane stress problem, which are given by $\bar{\bar{\Xi}}_{11} = \Xi_{11}$, $\bar{\bar{\Xi}}_{33} = \Xi_{33} + \frac{e_{33}^2}{C_{33}^E}$, E_r, E_θ, and E_z are the electric field intensity in the *r*, θ and z directions, respectively; D_r, D_θ and D_z are the corresponding electric displacements; Ξ_{11} and Ξ_{33} are the dielectric constants of the piezoelectric layer; Δ is Lapace operator and is given by $\Delta = \frac{\partial^2}{\partial r^2} + \frac{\partial}{r\partial r} + \frac{\partial^2}{r^2\partial \theta^2}$.

Submitting Eqs. (3-14) and (3-21) into electric boundary condition Eq. (3-15), the unknown constants A and B in Eq. (3-14) can be solved out. Then, Eq. (3-14) is transformed to

$$\phi = \left[1-\left(\frac{z-h-h_1/2}{h_1/2}\right)^2\right]\cdot\varphi(r,\theta,t)+\frac{4(z-h)}{h_1}\cdot\varphi(r,\theta,t)-\frac{\bar{e}_{31}}{\bar{\Xi}_{33}}(h+h_1)(z-h)\Delta w \ , \quad (3\text{-}22)$$

Eq. (3-22) is the electric distribution function along the thickness direction of open-circuit piezoelectric layer.

Submitting Eq. (3-22) into Eqs. (3-16)-(3-21), the components of the electric field E and electric displacement D are rewritten as

$$E_r = -\frac{\partial\phi}{\partial r} = -\left[1-\left(\frac{z-h-h_1/2}{h_1/2}\right)^2\right]\cdot\frac{\partial\varphi}{\partial r}-\frac{4(z-h)}{h_1}\cdot\frac{\partial\varphi}{\partial r}+\frac{\bar{e}_{31}}{\bar{\Xi}_{33}}(h+h_1)(z-h)\frac{\partial\Delta w}{\partial r} \quad (3\text{-}23)$$

$$E_\theta = -\frac{\partial\phi}{r\partial\theta} = -\left[1-\left(\frac{z-h-h_1/2}{h_1/2}\right)^2\right]\cdot\frac{\partial\varphi}{r\partial\theta}-\frac{4(z-h)}{h_1}\cdot\frac{\partial\varphi}{r\partial\theta}+\frac{\bar{e}_{31}}{\bar{\Xi}_{33}}(h+h_1)(z-h)\frac{\partial w}{r\partial\theta} \quad (3\text{-}24)$$

$$E_z = -\frac{\partial\phi}{\partial z} = \frac{8(z-h-h_1/2)}{h_1^{\,2}}\cdot\varphi-\frac{4}{h_1}\varphi+\frac{\bar{e}_{31}}{\bar{\Xi}_{33}}(h+h_1)\Delta w \quad (3\text{-}25)$$

$$D_r = \bar{\Xi}_{11}E_r = -\bar{\Xi}_{11}\left[1-\left(\frac{z-h-h_1/2}{h_1/2}\right)^2\right]\cdot\frac{\partial\varphi}{\partial r}-\bar{\Xi}_{11}\frac{4(z-h)}{h_1}\cdot\frac{\partial\varphi}{\partial r}+\frac{\bar{e}_{31}\bar{\Xi}_{11}}{\bar{\Xi}_{33}}(h+h_1)(z-h)\frac{\partial\Delta w}{\partial r} \quad (3\text{-}26)$$

$$D_\theta = \bar{\Xi}_{11}E_\theta = -\bar{\Xi}_{11}\left[1-\left(\frac{z-h-h_1/2}{h_1/2}\right)^2\right]\cdot\frac{\partial\varphi}{\partial\theta}-\bar{\Xi}_{11}\frac{4(z-h)}{h_1}\cdot\frac{\partial\varphi}{r\partial\theta}+\frac{\bar{e}_{31}\bar{\Xi}_{11}}{\bar{\Xi}_{33}}(h+h_1)(z-h)\frac{\partial\Delta w}{r\partial\theta} \quad (3\text{-}27)$$

$$\begin{aligned} D_z &= \bar{\Xi}_{33}E_z+\bar{e}_{31}(\varepsilon_{rr}+\varepsilon_{\theta\theta}) \\ &= \bar{\Xi}_{33}\frac{8(z-h-h_1/2)}{h_1^{\,2}}\cdot\varphi-\bar{\Xi}_{33}\frac{4}{h_1}\varphi+\frac{\bar{e}_{31}\bar{\Xi}_{33}}{\bar{\Xi}_{33}}(h+h_1)\Delta w+\bar{e}_{31}(\varepsilon_{rr}+\varepsilon_{\theta\theta}) \end{aligned} \quad (3\text{-}28)$$

3.2 Analysis of piezoelectric coupled circular plate

Submitting electrical field E_z given by Eq. (3-25) into Eqs. (3-10~3-12), the stress components of piezoelectric layer can be solved as

$$\sigma_{rr}^{2} = \overline{C}_{11}^{E}\varepsilon_{rr} + \overline{C}_{12}^{E}\varepsilon_{\theta\theta} - \overline{e}_{31}\left(\frac{8(z-h-h_1/2)}{h_1^{\,2}}\cdot\varphi - \frac{4}{h_1}\varphi + \frac{\overline{e}_{31}}{\overline{\Xi}_{33}}(h+h_1)\Delta w\right) \tag{3-29}$$

$$\sigma_{\theta\theta}^{2} = \overline{C}_{12}^{E}\varepsilon_{rr} + \overline{C}_{11}^{E}\varepsilon_{\theta\theta} - \overline{e}_{31}\left(\frac{8(z-h-h_1/2)}{h_1^{\,2}}\cdot\varphi - \frac{4}{h_1}\varphi + \frac{\overline{e}_{31}}{\overline{\Xi}_{33}}(h+h_1)\Delta w\right) \tag{3-30}$$

$$\tau_{r\theta}^{2} = (\overline{C}_{11}^{E} - \overline{C}_{12}^{E})\varepsilon_{r\theta} = -z(\overline{C}_{11}^{E} - \overline{C}_{12}^{E})\left(\frac{\partial^2 w}{r\partial r\partial\theta} - \frac{\partial w}{r^2\partial\theta}\right) \tag{3-31}$$

Thus, the moments of coupled plate could be expressed as

$$\begin{aligned} M_{rr} &= \int_{-h-h_1}^{h+h_1} z\sigma_{rr}dz = \int_{-h}^{h} z\sigma_{rr}^{1}dz + 2\int_{h}^{h+h_1} z\sigma_{rr}^{2}dz \\ &= -[(D_1+D_2)\frac{\partial^2 w}{\partial r^2} + (\mu D_1 + \frac{\overline{C}_{12}^{E}}{\overline{C}_{11}^{E}}D_2)(\frac{\partial w}{r\partial r} + \frac{\partial^2 w}{r^2\partial\theta^2}) + \frac{4}{3}h_1\overline{e}_{31}\varphi] \\ &+ \frac{4\overline{e}_{31}}{h_1}[(h+h_1)^2 - h^2]\varphi - \frac{\overline{e}_{31}^{\,2}(h+h_1)}{\overline{\Xi}_{33}}[(h+h_1)^2 - h^2]\Delta w \end{aligned} \tag{3-32}$$

$$\begin{aligned} M_{\theta\theta} &= \int_{-h-h_1}^{h+h_1} z\sigma_{\theta\theta}dz = \int_{-h}^{h} z\sigma_{\theta\theta}^{1}dz + 2\int_{h}^{h+h_1} z\sigma_{\theta\theta}^{2}dz \\ &= -[(\mu D_1 + \frac{\overline{C}_{12}^{E}}{\overline{C}_{11}^{E}}D_2)\frac{\partial^2 w}{\partial r^2} + (D_1+D_2)(\frac{\partial w}{r\partial r} + \frac{\partial^2 w}{r^2\partial\theta^2}) + \frac{4}{3}h_1\overline{e}_{31}\varphi] \\ &+ \frac{4\overline{e}_{31}}{h_1}[(h+h_1)^2 - h^2]\varphi - \frac{\overline{e}_{31}^{\,2}(h+h_1)}{\overline{\Xi}_{33}}[(h+h_1)^2 - h^2]\Delta w \end{aligned} \tag{3-33}$$

$$\begin{aligned} M_{r\theta} &= \int_{-h-h_1}^{h+h_1} z\tau_{r\theta}dz = \int_{-h}^{h} z\tau_{r\theta}^{1}dz + 2\int_{h}^{h+h_1} z\tau_{r\theta}^{2}dz \\ &= -[(1-\mu)D_1 + (1-\frac{\overline{C}_{12}^{E}}{\overline{C}_{11}^{E}})D_2](\frac{\partial^2 w}{r\partial r\partial\theta} - \frac{\partial w}{r^2\partial\theta}) \end{aligned} \tag{3-34}$$

where *2h* is the thickness of the host plate is, h_1 is the thickness of piezoelectric layer; the piezoelectric layer is measured from $z = h$ to $z = h+h_1$ and $D_1 = \frac{2Eh^3}{3(1-\mu^2)}$,

$D_2 = \frac{2}{3}h_1(3h^2 + 3hh_1 + h_1^2)\bar{C}_{11}^E$.

The resultant shear forces are herein written as:

$$q_r = \frac{\partial M_{rr1}}{\partial r} + \frac{\partial M_{r\theta 1}}{r\partial\theta} + \frac{M_{rr1} - M_{\theta\theta 1}}{r} = -[(D_1 + D_2)\frac{\partial}{\partial r}(\Delta w) + \frac{4}{3}h_1\bar{e}_{31}\frac{\partial\varphi}{\partial r}] + \frac{4\bar{e}_{31}}{h_1}[(h+h_1)^2 - h^2]\frac{\partial\varphi}{\partial r} - \frac{\bar{e}_{31}{}^2(h+h_1)}{\bar{\Xi}_{33}}[(h+h_1)^2 - h^2]\frac{\partial\Delta w}{\partial r} \quad (3\text{-}35)$$

$$q_\theta = \frac{\partial M_{r\theta 1}}{\partial r} + \frac{M_{\theta\theta 1}}{r\partial\theta} + \frac{2M_{r\theta 1}}{r} = -\frac{1}{r}[(D_1 + D_2)\frac{\partial}{\partial\theta}(\Delta w) + \frac{4}{3}h_1\bar{e}_{31}\frac{\partial\varphi}{\partial\theta}] + \frac{4\bar{e}_{31}}{h_1}[(h+h_1)^2 - h^2]\frac{\partial\varphi}{r\partial\theta} - \frac{\bar{e}_{31}{}^2(h+h_1)}{\bar{\Xi}_{33}}[(h+h_1)^2 - h^2]\frac{\partial\Delta w}{r\partial\theta} \quad (3\text{-}36)$$

Substituting Eqs. (3-35) and (3-36) into governing equation of Kirchhoff plate model,

$$\frac{\partial q_r}{\partial r} + \frac{\partial q_\theta}{r\partial\theta} + \frac{q_r}{r} - (\int_{-h}^{h}\rho_1\frac{\partial^2 u_z}{\partial t^2}dz + 2\int_{h}^{h+h_1}\rho_2\frac{\partial^2 u_z}{\partial t^2}dz) = 0. \quad (3\text{-}37)$$

We can get the governing equation for open-circuit piezoelectric couple plate,

$$(D_1 + D_2 + D_4)\Delta\Delta w + (\frac{4}{3}h_1\bar{e}_{31} + D_3)\Delta\varphi + 2(\rho_1 h + \rho_2 h_1)\frac{\partial^2 w}{\partial t^2} = 0 \quad (3\text{-}38)$$

where $D_3 = -4\bar{e}_{31}(2h + h_1)$, $D_4 = \frac{\bar{e}_{31}(h+h_1)[(h+h_1)^2 - h^2]}{\bar{\Xi}_{33}}$; ρ_1 and ρ_2 are material densities of the host plate and piezoelectric layer, respectively.

Submitting Eqs. (3-26~3-28) into Maxwell equation,

$$\int_{h}^{h+h_1}\left[\frac{\partial(rD_r)}{r\partial r}+\frac{\partial(D_\theta)}{r\partial\theta}+\frac{\partial D_z}{\partial z}\right]dz=0\,. \tag{3-39}$$

Then an electric filed differential equation can be found,

$$B_1\Delta\varphi+B_2\Delta\Delta w+\frac{8\bar{\bar{\Xi}}_{33}}{h_1}\varphi-\bar{e}_{31}h_1\Delta w=0 \tag{3-40}$$

where $B_1=\frac{4}{3}[(h+h_1)^3-h^3]\frac{\bar{\bar{\Xi}}_{11}}{h_1^2}-2[(h+h_1)^2-h^2]\frac{\bar{\bar{\Xi}}_{11}}{h_1}-\frac{2(2h+h_1)}{h_1^2}[(h+h_1)^2-h^2]\bar{\bar{\Xi}}_{11}$
$-\left[1+\frac{4(h+h_1/2)^2}{h_1}\right]h_1\bar{\bar{\Xi}}_{11}+4h\bar{\bar{\Xi}}_{11}$,

$B_2=[(h+h_1)^2-h^2]\frac{\bar{e}_{31}(h+h_1)\bar{\bar{\Xi}}_{11}}{2\bar{\bar{\Xi}}_{33}}-\frac{\bar{e}_{31}h(h+h_1)\bar{\bar{\Xi}}_{11}h_1}{\bar{\bar{\Xi}}_{33}}$.

φ is solved by Eqs. (3-38) and (3-40),

$$\varphi=\frac{\bar{e}_{31}h_1^2}{8\bar{\bar{\Xi}}_{33}}\Delta w-\frac{C_1h_1}{8\bar{\bar{\Xi}}_{33}}\Delta\Delta w-\frac{C_2h_1}{8\bar{\bar{\Xi}}_{33}}\frac{\partial^2 w}{\partial t^2} \tag{3-41}$$

where $C_1=B_2-B_1\frac{D_1+D_2+D_4}{\frac{4}{3}h_1\bar{e}_{31}+D_3}$, $C_2=-B_1\frac{2(\rho_1h+\rho_2h_1)}{\frac{4}{3}h_1\bar{e}_{31}+D_3}$.

Applying Lapace operator to Eq. (3-41), we get

$$\Delta\varphi=\frac{\bar{e}_{31}h_1^2}{8\bar{\bar{\Xi}}_{33}}\Delta\Delta w-\frac{C_1h_1}{8\bar{\bar{\Xi}}_{33}}\Delta\Delta\Delta w-\frac{C_2h_1}{8\bar{\bar{\Xi}}_{33}}\Delta\left(\frac{\partial^2 w}{\partial t^2}\right). \tag{3-42}$$

Submitting Eq. (3-42) into Eq. (3-38), we get the deflection differential equation,

$$P_3\Delta\Delta\Delta w - P_2\Delta\Delta w + P_1\Delta(\frac{\partial^2 w}{\partial t^2}) - P_0\frac{\partial^2 w}{\partial t^2} = 0 \quad , \tag{3-43}$$

where $P_0 = 2(\rho_1 h + \rho_2 h_1)$, $P_1 = (\frac{4}{3}h_1\bar{e}_{31} + D_3)\frac{C_1 h_1}{8\bar{\Xi}_{33}}$, $P_2 = D_1 + D_2 + D_4 + (\frac{4}{3}h_1\bar{e}_{31} + D_3)\frac{\bar{e}_{31}h_1^2}{8\bar{\Xi}_{33}}$,

$P_3 = (\frac{4}{3}h_1\bar{e}_{31} + D_3)\frac{C_1 h_1}{8\bar{\Xi}_{33}}$.

For wave propagation in the circumferential plate, the deflection $w(r,\theta,t)$ can be written as,

$$w(r,\theta,t) = \hat{w}(r)e^{i(p\theta-\omega t)} \tag{3-44}$$

where $\hat{w}(r)$ is the amplitude of the z-direction displacement as a function of radial distance only; ω is the natural frequency of the coupled plate; and p is the wave number in θ-direction. Eq. (3-43) in terms of $\hat{w}(r)$ can be rewritten as,

$$P_3\bar{\Delta}\bar{\Delta}\bar{\Delta}w - P_2\bar{\Delta}\bar{\Delta}w - \omega^2 P_1\bar{\Delta}w + \omega^2 P_0 w = 0, \tag{3-45}$$

where the operator $\bar{\Delta}$ is given by $\bar{\Delta} = \frac{d^2}{dr^2} + \frac{d}{rdr} - \frac{p^2}{r^2}$.

Using the principle of superposition, the solution to Eq. (3-45) can be written as the sum of terms governed by three different types of Bessel equation as follows:

$$w = w_1 + w_2 + w_3 \tag{3-46}$$

$$\left(\bar{\Delta} - x_1\right)\hat{w}_1 = 0 \tag{3-47}$$

$$\left(\bar{\Delta} - x_2\right)\hat{w}_2 = 0 \tag{3-48}$$

$$\left(\bar{\Delta} - x_3\right)\hat{w}_3 = 0 \tag{3-49}$$

x_i (*i=1,2,3*) are roots of the following cubic characteristic equation,

$$P_3x^3 - P_2x^2 - \omega^2 P_1 x + \omega^2 P_0 = 0 \tag{3-50}$$

Use the following transformation,

$$y = x - \frac{P_2}{3P_3} \tag{3-51}$$

the Eq. (3-50) can be written in a reduced form as follow

$$y^3 + by + c = 0 \tag{3-52}$$

where $b = -\frac{P_2^2}{3P_3^2} - \frac{P_1\omega^2}{P_3}$, $c = -\frac{2P_2^3}{27P_3^3} - \frac{P_1P_2\omega^2}{3P_3^2} + \frac{P_0\omega^2}{P_3}$.

The discriminate of the cubic equation in Eq. (3-52) is

$$\begin{aligned}\delta &= (\frac{c}{2})^2 + (\frac{b}{3})^3 \\ &= -\frac{P_0P_2^3\omega^2}{27P_3^4} + \frac{(27P_0^2P_3^2 - P_1^2P_2^2 - 18P_0P_1P_2P_3)\omega^4}{108P_3^4} - \frac{P_1^3\omega^6}{27P_3^3}\end{aligned} \tag{3-53}$$

It is can be proven that δ<0 can always be satisfied. Thus, according to Cardano's formula (Wang *et al* 2001), the characteristic equation shown in Eq. (3-50) has three distinct real roots as follows

$$x_1 = 2S\cos\frac{\psi}{3} + \frac{P_2}{3P_3} \tag{3-54}$$

$$x_2 = 2S\cos\frac{\psi + 2\pi}{3} + \frac{P_2}{3P_3} \tag{3-55}$$

$$x_3 = 2S\cos\frac{\psi + 4\pi}{3} + \frac{P_2}{3P_3} \tag{3-56}$$

where $S = \frac{1}{3P_3}\sqrt{P_2^2 + 3P_1P_3\omega^2}$, $\psi = \arccos(-\frac{c}{2\sqrt{(-\frac{b}{3})^3}})$.

In view of the non-singularity of $\hat{w}$ at the center of the plate, the solution of Eq. (3-45) can be written as

$$\hat{w}(r) = A_1 Z_1(\alpha_1 r) + A_2 Z_2(\alpha_2 r) + A_3 Z_3(\alpha_3 r) \tag{3-57}$$

A_i is the unknown parameter.

where $\alpha_1 = \sqrt{|x_1|}$, $\alpha_2 = \sqrt{|x_2|}$, $\alpha_3 = \sqrt{|x_3|}$, and

$$Z_i(\alpha_i r) = \begin{cases} J(\alpha_i r), x_i < 0 \\ I(\alpha_i r), x_i > 0 \end{cases} (i = 1,2,3) \tag{3-58}$$

where J $(\circ)$ is the first type Bessel function and I $(\circ)$ is the modified first type Bessel function.

$\bar{\Delta}\hat{w}$ and $\bar{\Delta}\bar{\Delta}\hat{w}$ can be written as

$$\bar{\Delta}\hat{w} = A_1 Z_1(\alpha_1 r) s_1 \alpha_1^2 + A_2 Z_2(\alpha_2 r) s_2 \alpha_2^2 + A_3 Z_3(\alpha_3 r) s_3 \alpha_3^2 \tag{3-59}$$

$$\bar{\Delta}\bar{\Delta}\hat{w} = A_1 Z_1(\alpha_1 r) \alpha_1^4 + A_2 Z_2(\alpha_2 r) \alpha_2^4 + A_3 Z_3(\alpha_3 r) \alpha_3^4 \tag{3-60}$$

where s_1, s_2 and s_3 are the signs of the x_1, x_2 and x_3.

The resonance frequencies and mode shapes for the coupled plate structure can be solved as an eigen value problem based on certain boundary condition. $\varphi(r,\theta,t)$ can be expressed as following when wave propagation is studied,

$$\varphi(r,\theta,t) = \hat{\varphi}(r) e^{j(p\theta - \omega t)} \tag{3-61}$$

where $\hat{\varphi}(r)$ is the spatial variation of the electric potential in the radial direction. Submitting Eqs. (3-61) and (3-44) into Eq. (3-41), $\hat{\varphi}(r)$ can be rewritten as,

$$\hat{\varphi}(r) = \frac{\bar{e}_{31} h_1^2}{8\bar{\Xi}_{33}} \bar{\Delta}\hat{w} - \frac{C_1 h_1}{8\bar{\Xi}_{33}} \bar{\Delta}\bar{\Delta}\hat{w} + \omega^2 \frac{C_2 h_1}{8\bar{\Xi}_{33}} \hat{w} \tag{3-62}$$

The solution of $\hat{\varphi}(r)$ can be obtained by substituting Eqs. (3-57), (3-59) and (3-60) into Eq. (3-61), and is solved as,

$$\begin{aligned}\hat{\varphi}(r) = &\frac{1}{8}\left(\frac{\hat{w}^2 C_2 h_1}{\overline{\overline{\Xi}}_{33}} - \frac{C_1 h_1 \alpha_1^4}{\overline{\overline{\Xi}}_{33}} + \frac{\bar{e}_{31} h_1^2 \alpha_1^2 s_1}{\overline{\overline{\Xi}}_{33}}\right) Z_i(\alpha_1 r) A_1 \\ &+ \frac{1}{8}\left(\frac{\hat{w}^2 C_2 h_1}{\overline{\overline{\Xi}}_{33}} - \frac{C_1 h_1 \alpha_2^4}{\overline{\overline{\Xi}}_{33}} + \frac{\bar{e}_{31} h_1^2 \alpha_2^2 s_2}{\overline{\overline{\Xi}}_{33}}\right) Z_i(\alpha_2 r) A_2 \\ &+ \frac{1}{8}\left(\frac{\hat{w}^2 C_2 h_1}{\overline{\overline{\Xi}}_{33}} - \frac{C_1 h_1 \alpha_3^4}{\overline{\overline{\Xi}}_{33}} + \frac{\bar{e}_{31} h_1^2 \alpha_3^2 s_3}{\overline{\overline{\Xi}}_{33}}\right) Z_i(\alpha_3 r) A_3\end{aligned} \tag{3-63}$$

Eqs. (3-57) and (3-63) are the solution in radial direction for open-circuit piezoelectric coupled circular plate based on Kirchhoff plate model. They can be transformed to the whole cylinder coordination by Eqs. (3-44) and (3-61).

3.3 Displacement and electric fields solution for open-circuit piezoelectric coupled circular plate in different boundary conditions

Based on given boundary condition, the mode shape of the structure can be found from Eqs. (3-57) and (3-63). Two boundary conditions, clamped and simply supported, are discussed as follow.

3.3.1 Clamped circular plate

For clamped circular plate, the boundary condition is expressed as,

$$\hat{w} = 0, \hat{w}' = 0, \hat{\varphi}' = 0\,. \tag{3-64}$$

It is our willing to solve A_i (i=1, 2, 3) in Eq. (3-57) and Eq. (3-63). To make Eq. (3-64) solvable, the characteristic equation is given by

$$\begin{vmatrix} m_{11} & m_{12} & m_{13} \\ m_{21} & m_{22} & m_{23} \\ m_{31} & m_{32} & m_{33} \end{vmatrix} = 0, \tag{3-65}$$

where

$$\begin{aligned}
m_{11} &= Z_1(\alpha_1 r_0) \\
m_{12} &= Z_2(\alpha_2 r_0) \\
m_{13} &= Z_3(\alpha_3 r_0) \\
m_{21} &= \alpha_1 Z_1^{'}(\alpha_1 r_0) \\
m_{22} &= \alpha_2 Z_2^{'}(\alpha_2 r_0) \\
m_{23} &= \alpha_3 Z_3^{'}(\alpha_3 r_0) \\
m_{31} &= \frac{1}{8\bar{\Xi}_{33}}\left(-C_1 h_1 \alpha_1^4 + \bar{e}_{31} h_1^2 \alpha_1^2 s_1 + \omega^2 C_2 h_1\right)\alpha_1 Z_1^{'}(\alpha_1 r_0) \\
m_{32} &= \frac{1}{8\bar{\Xi}_{33}}\left(-C_1 h_1 \alpha_2^4 + \bar{e}_{31} h_1^2 \alpha_2^2 s_2 + \omega^2 C_2 h_1\right)\alpha_2 Z_2^{'}(\alpha_2 r_0) \\
m_{33} &= \frac{1}{8\bar{\Xi}_{33}}\left(-C_1 h_1 \alpha_3^4 + \bar{e}_{31} h_1^2 \alpha_3^2 s_3 + \omega^2 C_2 h_1\right)\alpha_3 Z_3^{'}(\alpha_3 r_0)
\end{aligned} \tag{3-66}$$

From Eq. (3-65), structure resonant frequencies of different modes can be solved. Based on certain frequency, the mode shapes of flexural variable $\hat{w}$ and electric potential $\hat{\varphi}$ are

$$\hat{w} = A_3\left[\frac{m_{13}m_{22} - m_{23}m_{12}}{m_{12}m_{21} - m_{11}m_{22}} Z_1(\alpha_1 r) + \frac{m_{11}m_{23} - m_{13}m_{21}}{m_{12}m_{21} - m_{11}m_{22}} Z_2(\alpha_1 r) + Z_3(\alpha_3 r)\right] \tag{3-67}$$

$$\hat{\varphi} = A_3 \left[\begin{array}{l} \dfrac{m_{13}m_{22} - m_{23}m_{12}}{m_{12}m_{21} - m_{11}m_{22}} \left(\dfrac{\hat{w}^2 C_2 h_1}{\overline{\overline{\Xi}}_{33}} - \dfrac{C_1 h_1 \alpha_1^4}{\overline{\overline{\Xi}}_{33}} + \dfrac{\bar{e}_{31} h_1^2 \alpha_1^2 s_1}{\overline{\overline{\Xi}}_{33}} \right) Z_1(\alpha_1 r) \\ + \dfrac{m_{11}m_{23} - m_{13}m_{21}}{m_{12}m_{21} - m_{11}m_{22}} \left(\dfrac{\hat{w}^2 C_2 h_1}{\overline{\overline{\Xi}}_{33}} - \dfrac{C_1 h_1 \alpha_2^4}{\overline{\overline{\Xi}}_{33}} + \dfrac{\bar{e}_{31} h_1^2 \alpha_2^2 s_2}{\overline{\overline{\Xi}}_{33}} \right) Z_2(\alpha_1 r) + Z_3(\alpha_3 r) \\ + \left(\dfrac{\hat{w}^2 C_2 h_1}{\overline{\overline{\Xi}}_{33}} - \dfrac{C_1 h_1 \alpha_3^4}{\overline{\overline{\Xi}}_{33}} + \dfrac{\bar{e}_{31} h_1^2 \alpha_3^2 s_3}{\overline{\overline{\Xi}}_{33}} \right) \end{array} \right] \quad (3\text{-}68)$$

From Fig. 3-2 illustrates the first four vibration mode shapes of clamped open-circuit piezoelectric coupled plate.

3.3.2 Simply supported circulate plate

For simply supported circulate plate, boundary condition is given by

$$\hat{w} = 0, \hat{M}_{rr} = 0, \hat{\varphi}' = 0 . \quad (3\text{-}69)$$

The characteristic equation is expressed as

$$\begin{vmatrix} n_{11} & n_{12} & n_{13} \\ n_{21} & n_{22} & n_{23} \\ n_{31} & n_{32} & n_{33} \end{vmatrix} = 0 . \quad (3\text{-}70)$$

where

$$
\begin{aligned}
n_{11} &= Z_1(\alpha_1 r_0)\\
n_{12} &= Z_2(\alpha_2 r_0)\\
n_{13} &= Z_3(\alpha_3 r_0)\\
n_{21} &= M_{11} + M_{12} + M_{13}\\
n_{22} &= M_{21} + M_{22} + M_{23}\\
n_{23} &= M_{31} + M_{32} + M_{33}\\
n_{31} &= \frac{1}{8\bar{\Xi}_{33}}\left(-C_1 h_1 \alpha_1^4 + \bar{e}_{31} h_1^2 \alpha_1^2 s_1 + \omega^2 C_2 h_1\right)\alpha_1 Z_1^{'}(\alpha_1 r_0)\\
n_{32} &= \frac{1}{8\bar{\Xi}_{33}}\left(-C_1 h_1 \alpha_2^4 + \bar{e}_{31} h_1^2 \alpha_2^2 s_2 + \omega^2 C_2 h_1\right)\alpha_2 Z_2^{'}(\alpha_2 r_0)\\
n_{33} &= \frac{1}{8\bar{\Xi}_{33}}\left(-C_1 h_1 \alpha_3^4 + \bar{e}_{31} h_1^2 \alpha_3^2 s_3 + \omega^2 C_2 h_1\right)\alpha_3 Z_3^{'}(\alpha_3 r_0)
\end{aligned}
\quad . \text{(3-71)}
$$

M_{ii} is given by (i=1, 2, 3)

$$
\begin{aligned}
M_{i1} &= \left[p^2 \left(\frac{uD_1 + \frac{C_{12}D_2}{C_{11}}}{D_1 + D_2} - 1 \right) - s_i \alpha_i^2 r^2 + \frac{1}{6}\frac{C_1 h_1^2 \bar{e}_{31} \alpha_i^4 r^2}{\bar{\Xi}_{33}(D_1 + D_2)} + \frac{1}{6}\frac{\bar{e}_{31}^2 h_1^3 \alpha_i^2 s_i r^2}{\bar{\Xi}_{33}(D_1 + D_2)} - \frac{1}{6}\frac{\bar{e}_{31} h_1^2 \omega^2 C_2}{\bar{\Xi}_{33}(D_1 + D_2)} \right] Z_i(\alpha_i r)\\
&+ \left(1 - \frac{uD_1 + \frac{C_{12}D_2}{C_{11}}}{D_1 + D_2} \right) \alpha_i r Z_i^{'}(\alpha_i r) \qquad \text{(3-72)}\\
M_{i2} &= \frac{\bar{e}_{31}((h+h_1)^2 - h^2)\left(-C_1 h_1 \alpha_i^4 - h_1^2 \bar{e}_{31} \alpha_i^2 s_i + \omega^2 C_2 h_1\right)}{2\bar{\Xi}_{33} h_1 (D_1 + D_2)} r^2 Z_i(\alpha_i r)\\
M_{i3} &= -\frac{\bar{e}_{31}(h+h_1)((h+h_1)^2 - h^2) s_i \alpha_i^2}{\bar{\Xi}_{33}(D_1 + D_2)} r^2 Z_i(\alpha_i r).
\end{aligned}
$$

The deflection and electrical potential related with ‘r’ are expressed as

$$
\hat{w} = A_3 \left[\frac{n_{13}n_{22} - n_{23}n_{12}}{n_{12}n_{21} - n_{11}n_{22}} Z_1(\alpha_1 r) + \frac{n_{11}n_{23} - n_{13}n_{21}}{n_{12}n_{21} - n_{11}n_{22}} Z_2(\alpha_1 r) + Z_3(\alpha_3 r) \right] \qquad \text{(3-73)}
$$

$$\hat{\varphi} = A_3 \left[\begin{array}{l} \dfrac{n_{13}n_{22} - n_{23}n_{12}}{n_{12}n_{21} - n_{11}n_{22}} \left(\dfrac{\hat{w}^2 C_2 h_1}{\overline{\overline{\Xi}}_{33}} - \dfrac{C_1 h_1 \alpha_1^4}{\overline{\overline{\Xi}}_{33}} + \dfrac{\bar{e}_{31} h_1^2 \alpha_1^2 s_1}{\overline{\overline{\Xi}}_{33}} \right) Z_1(\alpha_1 r) \\ + \dfrac{n_{11}n_{23} - n_{13}n_{21}}{n_{12}n_{21} - n_{11}n_{22}} \left(\dfrac{\hat{w}^2 C_2 h_1}{\overline{\overline{\Xi}}_{33}} - \dfrac{C_1 h_1 \alpha_2^4}{\overline{\overline{\Xi}}_{33}} + \dfrac{\bar{e}_{31} h_1^2 \alpha_2^2 s_2}{\overline{\overline{\Xi}}_{33}} \right) Z_2(\alpha_1 r) + Z_3(\alpha_3 r) \\ + \left(\dfrac{\hat{w}^2 C_2 h_1}{\overline{\overline{\Xi}}_{33}} - \dfrac{C_1 h_1 \alpha_3^4}{\overline{\overline{\Xi}}_{33}} + \dfrac{\bar{e}_{31} h_1^2 \alpha_3^2 s_3}{\overline{\overline{\Xi}}_{33}} \right) \end{array} \right] \quad (3\text{-}74)$$

Fig. 3-4 shows the first four deflections mode shapes of the simply supported couple plate.

3.4 Numerical simulations and discussions

In the following simulations, steel and PZT4 are employed as the host structure and piezoelectric layer, respectively. The material properties and geometric sizes of piezoelectrically coupled plate are provided in table 2-1. The layout of the piezoelectrically coupled plate is shown in Fig. 3-1.

Table 3-1 lists the first four resonance frequencies of both closed and open circuit piezoelectric coupled structures with clamped boundary condition when the thickness ratio (h1 /2h) is 1/10. We can find that the resonant frequencies of the open and closed circuit piezoelectric coupled plates are increased by 6.73% and 3.77% respectively compared to the frequencies of the substrate steel. Such different increases in resonant frequencies of the two plates indicates that the effective stiffness of the open circuit piezoelectric coupled plate is larger than that of the closed circuit one, which coincides with the experimental results by Corr and Clark (2002) and Chevallier *et al* (2008). In order to investigate the physical interpretation of the different increases, Table 3-2 lists the fundamental resonant frequencies of the open and closed circuit piezoelectric coupled plates with host plat thickness of 20 mm and various piezoelectric layers at $h_1 / 2\mathrm{h} = 1/10$, 1/8, and 1/5 respectively. The second column is calculated by removing

the piezoelectric effect, or setting the piezoelectric coefficients to be null, to represent the only stiffening effect of the piezoelectric layer. Therefore, the percentages of the increase in the resonant frequency on columns 4 and 6 establish the piezoelectric effect clearly. From the table it is expectedly seen that the piezo-effect is obvious when the host plate is coupled with thicker piezoelectric layer for both closed and open circuit conditions. In addition, the piezo-effect of closed circuit piezoelectric layer is found to be almost negligible, whereas piezo-effect of open circuit one plays a major role in increasing the frequency of the coupled plate. Such a phenomenon is attributed to the different electric potential distributions along thickness direction of the open and closed circuit of the piezoelectric layers. Fig. 3-3 shows the electric potential distributions in thickness direction of open and closed circuit piezoelectric layers. The electric potential of the closed circuit piezoelectric layer reaches maxima at the mid-plane of piezoelectric layer, then begins to decrease and returns to zero on the surface of piezoelectric layer. On the other hand, for the open circuit electric surface condition, the electric potential keeps growing to maxima towards the surface of piezoelectric layer. The distributions show that when a piezoelectric layer is shortly connected, the electric potential on both surfaces of the piezoelectric layer vanish, and hence the electric energy is released by the closed circuit electrode status, which would reduce the piezo-effect of the piezoelectric layer on the stiffness of the coupled plate. On the other hand, the electric potential of an open circuit piezoelectric layer cannot be released during any vibration of the coupled plate, and is continually converted to mechanical energy because of the piezo-effect. Such a process enlarges the increase of effective stiffness of the coupled structure. Therefore, higher piezo-effect could be observed from the open circuit piezoelectric layer.

The first four resonance frequencies of the piezoelectric coupled plate with simply supported boundary condition are shown in table 3-3. The thickness ratio of piezoelectirc layer to the host beam is 1/10, which is the same as the thickness ratio used in table 3-1. Although the frequencies are found to be much lower than those of the plate with clamped boundary condition, higher increases in resonance frequencies of the open circuit piezoelectric layer than those of the closed circuit piezoelectric plate is again observed. Such a result coincides with that of the clamped coupled plate. Table 3-4 lists the fundamental frequencies of the simply supported open and closed circuit piezoelectric coupled plates with various thickness piezoelectric layers when the thickness of the host beam is 20 mm. Similar observations on the differences of the piezo-effect between open and closed circuit piezoelectric layers are also obtained.

3.5 Conclusions

A mechanical model for the analysis of an open circuit piezoelectric coupled circular plate is developed. The solution for the electric potential along thickness direction of the piezoelectric layer is provided for the first time to strictly satisfy the open circuit electric boundary condition. Based on the developed electric potential solution and the Kirchhoff plate model and Maxwell equation, the free vibration solution for the piezoelectric coupled plate is presented.

The numerical simulations show that the resonance frequencies and stiffness of the open circuit piezoelectric coupled plate are higher than those of the closed circuit counterpart, because the piezoelectric effect of the open circuit piezoelectric layer is larger compared with the closed circuit one. A linear electric potential distribution along the thickness of the piezoelectric layer is found for the first vibration mode of the piezoelectric coupled structure, while non-linear distributions can be seen for higher modes. The piezo-effects of the open and closed circuit

piezoelectric layers are particularly investigated and found that the effect from the open circuit piezoelectric layer is much larger than that from the closed circuit one, which is almost negligible. Such a difference is owing to the different electric energy processes of the two piezoelectric layers during vibrations.

Table 3- 1 First four resonance frequencies of piezoelectric coupled plates with a clamped boundary condition.

Mode No.	Substrate plate	Piezoelectric Coupled Plate			
		Closed circuit (Wang *et al* 2001)	Increments (%) closed circuit	Open circuit	Increments (%) open circuit
1	869.691	902.479	3.77	928.23	6.73
2	1809.87	1878.17	3.77	1931.76	6.73
3	2969.34	3081.08	3.76	3169.00	6.724
4	3385.71	3513.43	3.77	3613.69	6.73

(* Thickness ratio ($h_1/2h$) is 1/10)

Table 3- 2 Effect of the circuit condition on the fundamental resonance frequencies of the piezoelectric coupled plate with clamped boundary condition at different thickness ratios.

Thickness ratio (h_1/2h)	Without piezoelectric effect	With piezoelectric effect			
		Closed circuit	Increment (%)	Open circuit	Increment (%)
1/10	902.40	902.479	0.0087	928.23	2.86
1/8	914.483	914.617	0.0147	946.45	3.50

(* Thickness of host plate is 20mm)

Table 3- 3 First four resonance frequencies of piezoelectric coupled plates with a simply supported boundary condition

Mode No.	Pure Structure	Piezoelectric Coupled			
		Closed circuit (Wang *et al* 2001)	Increments (%) closed circuit	Open circuit	Increments (%) open circuit
1	420.33	435.6	3.63	448.067	6.74
2	1183.75	1227.5	3.70	1262.53	6.66
3	2181.51	2262.4	3.70	2327.03	6.67
4	2531.36	2625.2	3.75	2700.2	6.67

Table 3- 4 Effect of the circuit condition on the fundamental resonance frequencies of the piezoelectric coupled plate with simply supported boundary condition at different thickness ratios.

Thickness ratio (h_1/2h)	Without electric contribution	With electric contribution			
		Closed circuit (Wang *et al* 2001)	Increment (%)	Open circuit	Increment (%)
1/10	435.54	435.63	0.0206	448.067	2.88
1/8	441.30	441.42	0.027	456.91	3.54
1/5	462.04	462.34	0.065	486.73	5.34

(* Thickness of host plate is 20mm)

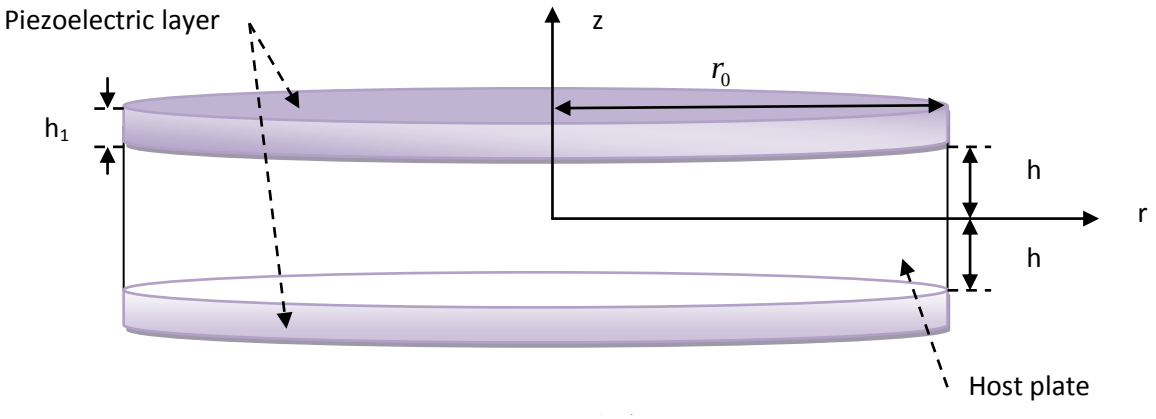

Fig. 3- 1 Layout of a circular plate with two piezoelectric layers mounted on its surfaces.

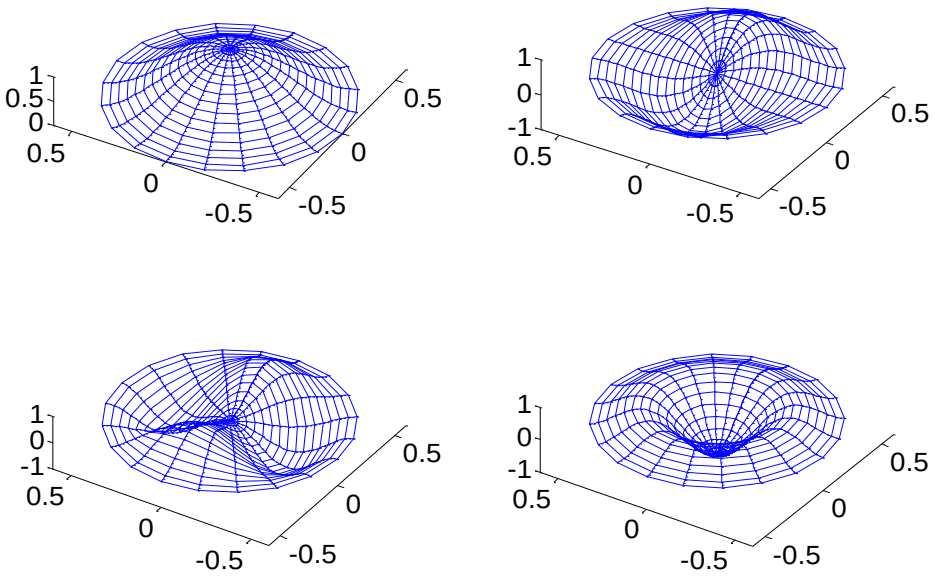

Fig. 3- 2 First four mode shapes of the displacement of the open circuit piezoelectric coupled plate with a clamped boundary condition.

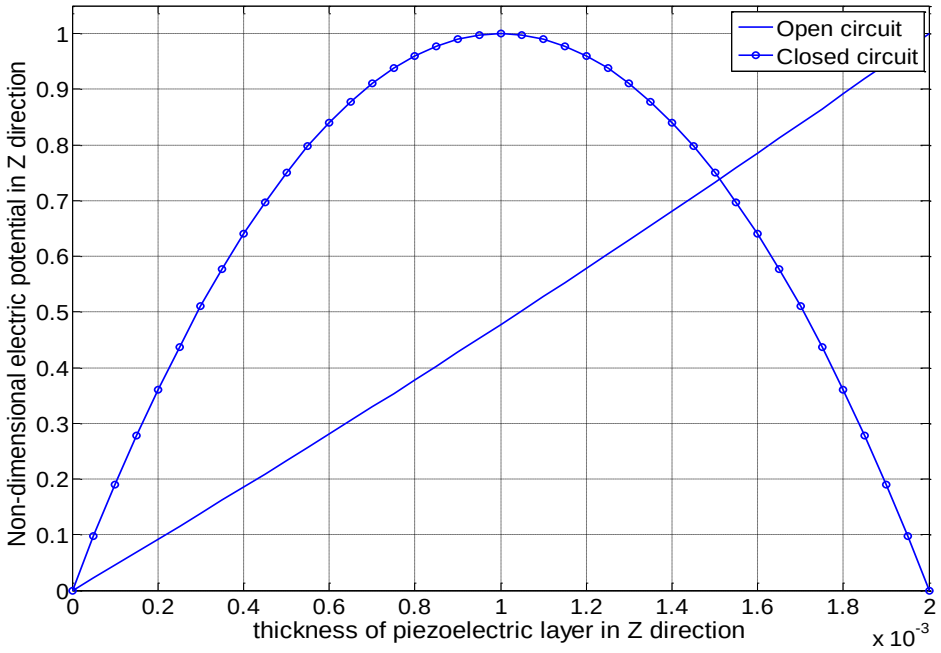

Fig. 3- 3 First mode electric potential distributions in thickness direction of the open and closed circuit piezoelectric layers.

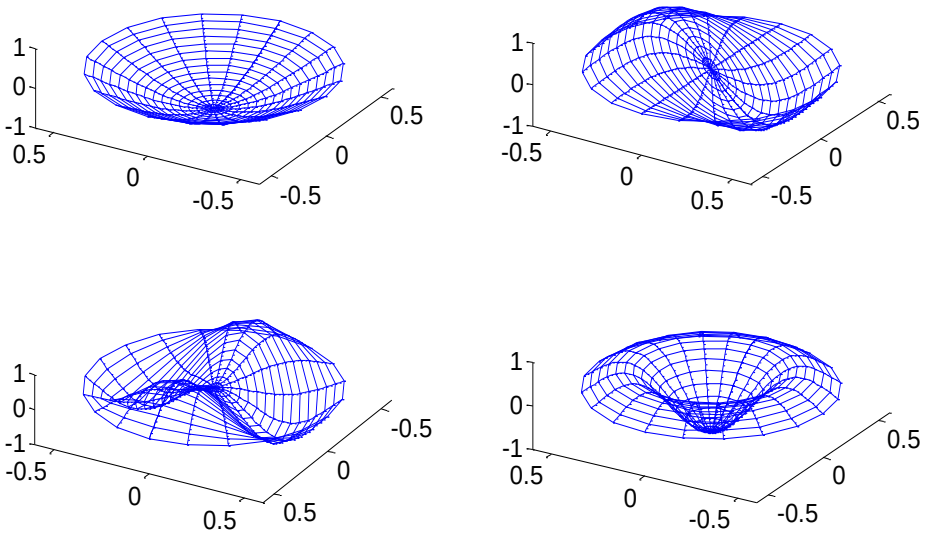

Fig. 3- 4 First four mode shapes of the displacement of the open circuit piezoelectric coupled plate with a simply supported boundary condition.

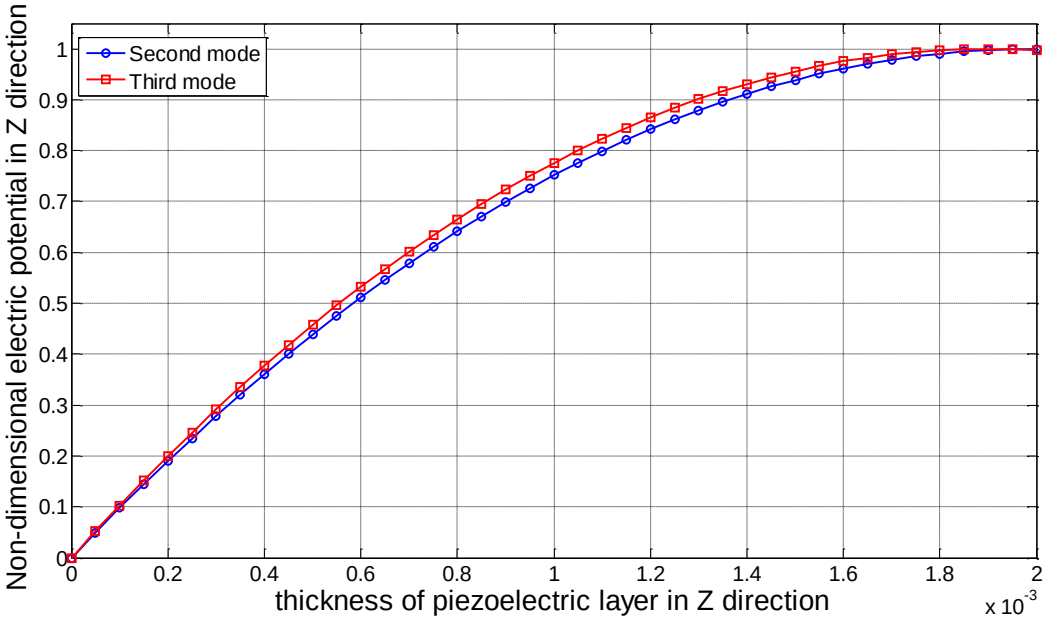

Fig. 3- 5 Electric potential distributions in thickness direction of the open circuit piezoelectric layer at the second and third vibration modes.

4 Study on repair of a vibrating delaminated beam

Following the studies of the dynamic mechanical and electrical responses of the piezoelectric coupled structures, the repair of vibrating engineering structures using surface bonded piezoelectric materials can be conducted. This chapter provides a close-loop feedback control repair methodology for a vibrating delaminated beam structure by use of piezoelectric patches. The electromechanical characteristic of the piezoelectric material is employed to induce a local shear force above the delamination area via an external voltage, which is designed as a feedback of the deflection of the vibrating beam, to reduce the stress singularity around the delamination tips. Moreover, finite element method (FEM) is employed to verify the effectiveness of the proposed design and repair methodology for delaminated beams with various sizes and alignments of delaminations.

4.1 Model of repair of a delaminated beam via piezoelectric patches

A delaminate beam structure is shown by Fig. 4-1. While deflection takes place along the beam structure, axial elongation and compression on the two layers will be induced due to the bending

of the beam. It is assumed that the tensile force p1and compressive force p2 are induced on the top and bottom layers of the delaminate beam. The values of p1 and p2 are given by Wang and Quek (2004)

$$p_1 = p_2 = \frac{EbH\beta}{2a}(w_L'|_{x=x_1} - w_R'|_{x=x_2}) \tag{4-1}$$

where $\beta = \left(\frac{1}{t} + \frac{1}{(H-t)}\right)^{-1}$,

t is the thickness of upper layer of the delaminate beam, E is the young's module of the host beam structure, b and H are the width and height of the beam, respectively. a is the length of the delaminate area, w_L is the flexural deflection of the beam element at the left side of the delaminate area, while w_R is the flexural deflection of the beam element at the right side of the delaminate area.

At the tip of the delaminate area, tensile and compressive forces are induced at the upper and lower parts of the tip due to the bending of the beam, as shown in Fig. 4-1. The induced tensile and compressive forces will lead to the discontinuity of the shear force at the tip of the delaminate area, which will definitely result in shear force singularity and therefore lead to the sliding mode of fracture at the tip of the delaminate area. Therefore, to eliminate the singularity at the tip of the delaminate area and this forms the basis of the proposed repair methodology. Piezoelectric patches will be applied to induce shear force at the interface between the piezoelectric layer and the host delaminated beam by applying a suitable voltage so that the sliding fracture mode at the tip of the delaminate area can be controlled and hence the beam can be repaired accordingly.

4.1.1 Design of repair of vibrating delaminated beam

For the need of active repair and feedback control method, the piezoelectric parches are used as sensor and actuator at the same time. The charge generated by the piezoelectric layer when the beam is deflected is given by Lee and Moon (1990),

$$Q = -e_{31}\int_0^a b(\frac{H+h_1}{2})w''dx \tag{4-2}$$

where H is the height of the repaired beam, h1 is the thickness of piezoelectric layer, b and a are the width and length of the beam structure covered by piezoelectric layer, respectively, e_{31} is the piezoelectric constant and w is transverse displacement. The output voltage of piezoelectric patch, V_o, is given by Lin and Hsu (1999),

$$V_o = \frac{Q}{C_v} = -\frac{e_{31}b(H+h_1)}{2C_v}\int_0^a w''dx \tag{4-3}$$

where C_v is the electric capacitance of piezoelectric patch.

When the piezoelectric layer is used as a collocated sensor and actuator, the voltage applied back to the piezoelectric layer, V_g, can be written as

$$V_g = gV_o = -p\frac{e_{31}b(H+h_1)}{2}\int_0^a w''dx \tag{4-4}$$

where g is the feedback control gain factor and p is defined as repair coefficient ($p = g*b/C_v$). The axial stress along the piezoelectric layer induced by the applied controlled voltage is presented by Sun *et al* (1999),

$$\sigma_{xp} = e_{31}\frac{V_g}{h_1} = -p\frac{e_{31}^2(H+h_1)}{2h_1}\int_0^a w''dx\,. \tag{4-5}$$

The bending moment caused by the piezoelectric layer on the host beam can be written as,

$$M_p = b\int_{\frac{H-h_1}{2}}^{\frac{H+h_1}{2}} y(-E_p y w''+\sigma_{xp})dy\,. \tag{4-6}$$

For the piezoelectric patches bonded on the delaminate beam structure shown in Fig. 4-1, the gained voltage and stress in the piezoelectric layers are given as follow,

$$V_{gru} = -p\frac{e_{31}(t+h_1)}{2}\int_0^a w''dx \quad V_{grl} = -p'\frac{e_{31}(H-t+h_1)}{2}\int_0^a w''dx, \tag{4-7}$$

$$\sigma_{xpu} = -p\frac{e_{31}^2(t+h_1)}{2h_1}\int_0^a w''dx \quad \sigma_{xpl} = -p'\frac{e_{31}^2(H-t+h_1)}{2h_1}\int_0^a w''dx, \tag{4-8}$$

where t is the thickness of upper layer. Depending on eq. (4-1), the repair coefficient of lower layer p' is set to be $p\frac{(t+h_1)}{(H-t+h_1)}$ to generate same value of upper and lower repair forces. The interfaces between the host plate and piezoelectric patches are grounded. As gained voltages are applied on the upper and lower surfaces of the composed plate structure, inverted repair forces will be generated by upper and lower piezoelectric layers.

The bending moments caused by upper and lower piezoelectric patch can be expressed as

$$M_{pu} = b\int_{\frac{t-h_1}{2}}^{\frac{t+h_1}{2}} y(-E_p yw''+\sigma_{xpu})dy \quad M_{pl} = b\int_{-\frac{H-t+h_1}{2}}^{-\frac{H-t-h_1}{2}} y(-E_p yw''-\sigma_{xpl})dy. \tag{4-9}$$

4.1.2 Response of the repaired vibrating delaminated beam

To reveal the effect of the delamination on the sliding fracture mode of the beam structure, a mechanics analysis will be conducted here. The delaminated part will be studied via Euler–Bernoulli beam theory by considering two layers of beam elements connected at the two ends. It is assumed that tiny gap exists between upper and lower layers when delamination takes place in the beam structure so that the two layers can be analyzed as two separated beam elements.

For the analysis of structure dynamic properties, the delaminated beam structure coupled with piezoelectric patches is separated into 4 sections which are illustrated by Fig. 4-1.

The bending moment of the first section is given by,

$$M_1 = 2\int_0^{\frac{H}{2}} -Ey^2 b\frac{d^2w_1}{dx_1^2}dy = -\frac{2Eb(\frac{H}{2})^3}{3}\frac{d^2w_1}{dx_1^2}. \tag{4-10}$$

The subscript of the deflection w stands for the section number.

Based on Euler-Bernoulli beam theory, the governing equation for the first section can be expressed as,

$$\frac{d^2M_1}{dx_1^2} + \rho bH\omega^2 w_1 = 0 \tag{4-11}$$

where ρ is the density of the host beam and ω is the vibration angular velocity of the structure. Similar with the first section, the bending moment and the governing equation for the forth section is given by,

$$M_4 = 2\int_0^{\frac{H}{2}} -Ey^2 b\frac{d^2w_4}{dx_4^2}dy = -\frac{2Eb(\frac{H}{2})^3}{3}\frac{d^2w_4}{dx_4^2}\ , \tag{4-12}$$

$$\frac{d^2M_4}{dx_4^2} + \rho bH\omega^2 w_4 = 0\,. \tag{4-13}$$

Coupled with piezoelectric layer, the bending moment of the second section can be expressed as

$$M_2 = \int_{-\frac{t+h_1}{2}}^{\frac{t-h_1}{2}} -Ey^2 b\frac{d^2w_2}{dx_2^2}dy + \int_{\frac{t-h_1}{2}}^{\frac{t+h_1}{2}} by(-E_p y\frac{d^2w_2}{dx_2^2} + \sigma_{xpu})dy\,, \tag{4-14}$$

where E_p is the effective young's module of the piezoelectric layer, σ_{xpu} is the stress generated by the piezo-effect when extra voltage is applied on the piezoelectric layer, which is given by Eq. (4-8).

With the assumption $t \le \frac{H}{2}$, the bending moment of the third section can be written as,

$$M_3 = \int_{-\frac{H-t+h_1}{2}}^{\frac{H-t+h_1}{2}} -Ey^2 b\frac{d^2w_3}{dx_3^2}dy + \int_{-\frac{H-t+h_1}{2}}^{-\frac{H-t-h_1}{2}} by(-E_p y\frac{d^2w_3}{dx_3^2} - \sigma_{xpl})dy\,. \tag{4-15}$$

Based on Eq. (4-1), the required value of the repair forces generated by piezoelectric layers on upper and lower delaminate layers is the same. Thus, the voltages at the upper and lower piezoelectric layers should be applied with the same magnitude but with different alignments of

the poling direction of the piezoelectric patch so that the inverted forces with same value can be induced (shown by Fig. 4-1).

The governing equations of the second and third sections are given by,

$$\frac{d^2M_2}{dx_2^2}+(\rho bt+\rho_1 bh_1)\omega^2 w_4=0\,, \tag{4-16}$$

$$\frac{d^2M_3}{dx_3^2}+[\rho b(H-t)+\rho_1 bh_1]\omega^2 w_4=0\,, \tag{4-17}$$

where ρ_1 is the density of the piezoelectric layers.

To characterize the dynamic system given by Eqs. (4-11, 4-13, 4-16 and 4-17), the free vibration solution of the delaminate beam is first obtained, which can be written as

$$w_1=C_1\cos k_1x_1+C_2\sin k_1x_1+C_3\cosh k_1x_1+C_4\sinh k_1x_1 \qquad 0\le x_1\le l \tag{4-18}$$

$$w_2=C_5\cos k_2x_2+C_6\sin k_2x_2+C_7\cosh k_2x_2+C_8\sinh k_2x_2 \qquad 0\le x_2\le a \tag{4-19}$$

$$w_3=C_9\cos k_3x_3+C_{10}\sin k_3x_3+C_{11}\cosh k_3x_3+C_{12}\sinh k_3x_3 \qquad 0\le x_3\le a \tag{4-20}$$

$$w_4=C_{13}\cos k_1x_4+C_{14}\sin k_1x_4+C_{15}\cosh k_1x_4+C_{16}\sinh k_1x_4 \qquad 0\le x_4\le L-a-l \tag{4-21}$$

where $k_1^4=\dfrac{12\rho\omega^2}{EH^2}$,

$$k_2^4=\frac{(\rho t+\rho_1h_1)\omega^2}{E[\frac{(H/2)^3}{3}-\frac{(H/2-t)^3}{3}]+E_p[\frac{(t+h_1)^3}{3}-\frac{t^3}{3}]},$$

$$k_3^4=\frac{[\rho(H-t)+\rho_1h_1]\omega^2}{E[\frac{(H/2-t)^3}{3}+\frac{(H/2)^3}{3}]+E_p[\frac{(H/2+h_1)^3}{3}-\frac{(H/2)^3}{3}]},$$ and $C_1\sim C_{16}$ are unknown constants.

Depending on the boundary conditions of cantilever beam and the continue conditions at the two ends of the delaminated layers, the boundary conditions of the four sections of the delaminate beam structure are listed below:

$$w_1 = 0, \frac{dw_1}{dx_1} = 0 \quad \text{at } x_1 = 0, \tag{4-22}$$

$$w_1 = w_2 = w_3, \frac{dw_1}{dx_1} = \frac{dw_2}{dx_2} = \frac{dw_3}{dx_3}, M_1 = M_2 + M_3, \frac{dM_1}{dx_1} = \frac{dM_2}{dx_2} + \frac{dM_3}{dx_3} \text{ at } x_1 = l, x_2 = x_3 = 0 \tag{4-23}$$

$$w_4 = w_2 = w_3, \frac{dw_4}{dx_4} = \frac{dw_2}{dx_2} = \frac{dw_3}{dx_3}, M_4 = M_2 + M_3, \frac{dM_4}{dx_4} = \frac{dM_2}{dx_2} + \frac{dM_3}{dx_3} \text{ at } x_4 = 0, x_2 = x_3 = a \tag{4-24}$$

$$\frac{d^2 w_4}{dx_4^2} = 0, \frac{d^3 w_4}{dx_4^3} = 0 \quad \text{at } x_4 = L - l - a. \tag{4-25}$$

Submitting Eqs. (4-18~4-21) into Eqs. (4-10, 4-12, 4-14 and 4-15) and the boundary conditions, 16 linear equations can be obtained. The solutions for constants $C_1 \sim C_{16}$ with given feedback control repair coefficient *p* are able to be solved based on the agen value problem of the linear system of equations.

4.1.3 Finite element model for verification of repair design

The finite element analysis software ANSYS 10.0 is used to verify the effectiveness of the proposed design and repair methodology. The study of the free vibration process of the delaminated beam is proposed using the transient analysis module provided by Ansys 10.0.

The finite element model is shown in Fig. 4-2 (a). Normal plane element plane 42 and coupled field element plane 223 are used to mesh the host beam structure and the piezoelectric patches. Different colors showed in the Fig. 4-2 stand for different elements and material properties used for the beam and piezoelectric patches. All displacement degrees of freedom of the fixed end of the host beam are restrained. The host beam structure is assumed to be made of metal material, therefore, the voltage of the interfaces between piezoelectric layers and host

beam is set to be zero as the host beam structure is grounded. The piezoelectric patches are poled along the y direction so that, when transverse displacement of the bending beam structure takes place, there will be voltage output on the surfaces of the piezoelectric layers.

Meshing of the delamination tip area is shown in Fig. 4-2 (b). Finer meshing density is applied to the tip area. The determination of the repair coefficient of the feedback control voltage applied to the piezoelectric patches will be determined from the finite element simulations by removal of the stress singularity at the tips of the delamination. The determined repair coefficient from FEM will then be compared with the optimal repair coefficient from the numerical model to verify its effectiveness.

Transient analysis module of ANSYS 10.0 is used for the vibration analysis. A small initial displacement of 0.005 m (the length of the host beam is set to be 0.6m, L=0.6m) is applied to the free end of the cantilever beam for the first 0.1 second of analysis. The free vibration analysis is separated into 150 sub-steps during 0.1 to 0.4 seconds. For each sub-step, the shear stresses on the delamination tips are recorded.

4.2 Numerical simulations and discussions

The host beam is made of aluminum, and the piezoelectric patches are made of PZT4. The material properties and geometric size of the piezoelectric coupled delaminated beam structure are listed in table 4-1.

To verify the accuracy of the analytical model for the repair design of the delaminated beam proposed in section 4.1.2, Table 4-1 provides the comparison of the first three resonant frequencies of delaminated beam with different lengths bonded with the piezoelectric patches, at

l=0.3 m, H=0.015 m, t=0.0075 m and a=0.1 m from the analytical model developed for the repair design and FEM. Deviation between the FEM and repair design model for the first three resonant frequencies is less than 6%. The largest deviation for the fundamental resonant frequency is 3.9% for the longest delaminated beam, at *L= 0.8 m*. Such excellent agreements of the results indicate the accuracy of the analytical model in vibration analysis of delaminated beams.

The non-dimensional gradient difference at the two tips of the delamination is defined as the ratio of the gradient difference of the repaired beam to the un-repaired beam, or given as $\frac{w_2'|_{x=a,p\neq 0} - w_2'|_{x=0,p\neq 0}}{w_2'|_{x=a,p=0} - w_2'|_{x=0,p=0}}$ or $\frac{w_3'|_{x=a,p\neq 0} - w_3'|_{x=0,p\neq 0}}{w_3'|_{x=a,p=0} - w_3'|_{x=0,p=0}}$ which can be solved by Eq. (4-14). Fig. 4-3 illustrates the variation of the non-dimensional gradient differences at the two tips of the delamination versus the repair coefficients at different delamination lengths with L=0.6 m, l=0.3 m, H=0.015 m and t=0.0075 m. The optimal repair coefficients could be identified when the lowest gradient differences are found to be, i.e. 0.062 m/nF, 0.082 m/nF, 0.114 m/nF and 0.164 m/nF with delamination lengths of 0.14 m, 0.12 m, 0.10 m and 0.08 m, respectively. It is found that the repair coefficients are higher for beams with longer delaminations.

Time domain FEM analysis is provided to provide a free vibration analysis in Fig. 4-4 for the first 0.4 s of a delaminated beam to verify the repair coefficients obtained from the analytical model in Fig. 4-3. Fig. 4-4 shows the variation of the shear stresses at the left tip of delamination of the repaired beam structure at L=0.6m, l=0.3m, H=0.015m, t=0.0075m, a=0.1m with different repair coefficients of 0.114 m/nF, 0.155 m/nF and 0.172 m/nF, respectively. It can be seen that the shear stress on the left delamination tip is reduced obviously by the piezoelectric patches at

the optimal repair coefficient 0.114 m/nF that is predicted from Fig. 4-3. Compared with the un-repaired delaminated beam, or with repair coefficient being zero, the shear stress is decreased by 66% at 0.38 s. When the repair coefficient is set to be 0.155 m/nF, the shear stress on the same point is first enlarged in the first 0.18 s, although it finally is reduced obviously after 0.22 s of vibration. At 0.12 s of the vibration of the repaired beam with repair coefficient of 0.155 m/nF, the shear stress on the left delamination tip point is increased even by 140% compared with the un-repaired beam. Moreover, when the repair coefficient is increased to be 0.172 m/nF, the shear stress on the left delamination tip if found to keep growing. At t=0.36 s, the shear stress is found to be increased to be 400% of the un-repaired beam. In summary, the optimal repair coefficient, p=0.114 m/nF, for the delaminated beam structure from the analtyical model in Fig. 4-3 is verified to be very accurate. Fig. 4-5 shows the deflection variation for the same delaminated beam structure in Fig. 4-4 with the repair coefficients. It is noted that the vibration deflection of the free end of the delaminated beam is obviously decreased with all of the repair coefficients of 0.114 m/nF, 0.155 m/nF and 0.172 m/nF, although the stress singularity can only be erased with the optimal repair coefficient of 0.114 m/nF as indicated in Fig. 4-4. Based on the results shown in Figs. 4-4 and 4-5, it can be found that although larger repair coefficients could reduce the vibration deflection of the delaminated beam, the stress singularity cannot be erased simultaneously.

In the following discussions, the effect of some key factors on the optimal repair coefficient will be analysed by both of analytical model for the repair design and FEM. Fig. 4-6 shows the relationship between the optimal repair coefficient and the delamilation length of the beam structure with L=0.6 m, l=0.3 m, H=0.015 m and t=0.0075 m. Both FEM and the design model results indicate that the repair coefficients decrease from 0.089 m/nF to 0.021 m/nF. When the

delamination lengths change from 0.06 m to 0.15 m showing the decrease of the optimal repair coefficient with the increase in the delamination length. Fig. 4-7 shows the variation of the repair coefficient versus the increase in the thickness of the host beam, while other geometry of the host beam is fixed, i.e. L=0.6 m, l=0.3 m, $t=H/2$. The optimal repair coefficients match the FEM results very well when the thickness of host beam is less than 0.015 m. For the beam with the thickness of 0.02 m, the deviation of the repair coefficients between the result from the analytical model and FEM results is only 5.8%. The optimal repair coefficients increase from 0.041 m/nF to 0.114 m/nF when the thickness of host beam is changed to be 0.015 m from 0.005 m. From both the analytical model and FEM results, it can be found that a larger repair coefficient is needed for the repair of a thicker delaminated beam. Fig. 4-8 shows the effect of the location of the delamination in thickness direction of the beam on the repair coefficient. The deviation of the repair coefficients between the analytical model and FEM results vanishes when the delamination is getting closer to the mid-surface of the host beam. The deviation is bigger when the delaminiation is further away from the middle, and the repair coefficient becomes smaller accordingly as evidenced from the figure. From both Figs. 4-7 and 4-8, it is noted that the deviation of the optimal repair coefficients between the analytical model and FEM results is smaller when the ratios of the thickness of the beam sections to the length of the beam sections are smaller. This phenomenon is attributed to the applicability of the Euler–Bernoulli beam theory we used for the repair design. Euler-Bernoulli beam theory is more applicable while the ratio of beam thickness to beam length is smaller.

4.3 Conclusions

The piezoelectric patches are employed for the feedback control repair of vibrating delaminated cantilever beams. The design of the repair coefficient for the voltage induced by the piezoelectric patches by virtue of their electromechanical characteristics is developed to remove the shear stress singularity induced by bending of the delaminated beam. A mechanics analysis model is developed for the design of the feedback control repair of the vibrating delaminated cantilever beam structure bonded with piezoelectric layers, and FEM is conducted to verify the effectiveness of the coefficients from the analytical model. The designed repair coefficient based on Euler-bernoulli beam theory is more accurate for thinner beam with longer delamination, which happens close to the mid-surface of host beam. It is also found that smaller repair coefficient is needed when the delamination area is longer or the host beam is thinner.

Table 4- 1 First three resonant frequencies of the delaminated beam bounded with piezoelectric by FEM and the analytical model.

l=0.3m, H=0.015m, t=0.0075m, a=0.1m (no electric gain on piezoelectric patches)		FEM			analytical model		
		1st	2nd	3rd	1st	2nd	3rd
	L=0.6m	31.63	154.83	522.78	31.82	164.08	533.11
	L=0.7m	22.51	118.51	415.65	23.19	123.06	421.15
	L=0.8m	16.83	96.61	314.01	17.49	98.83	316.07

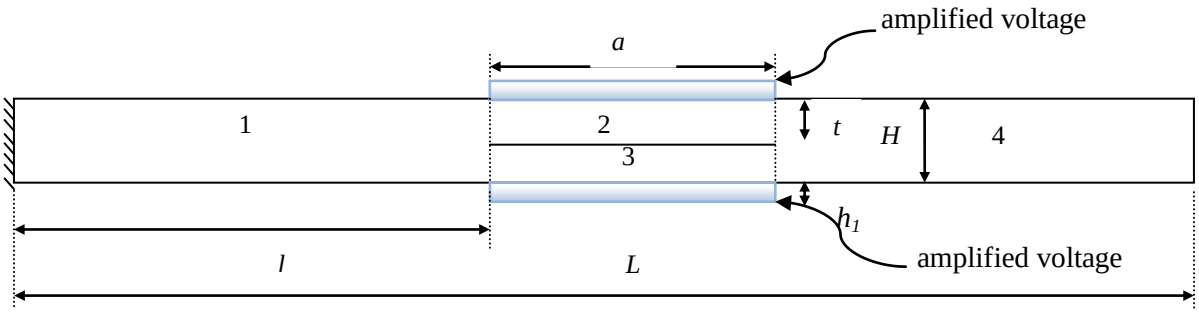

Fig. 4- 1 Layout of the repaired delaminated beam and the piezoelectric patches.

(a)

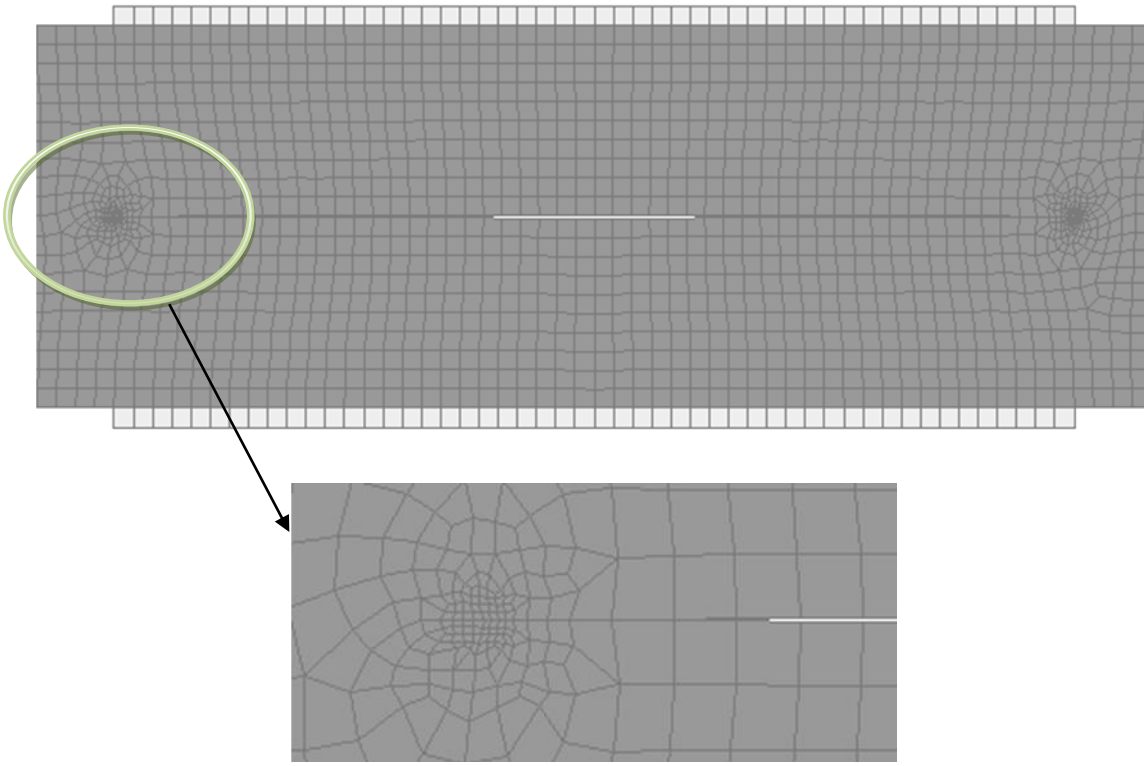

(b)

Fig. 4- 2 Finite element model of the delaminated beam bonded with piezoelectric patches. (a) Overall view of the modeling of the delaminated beam; (b) Meshing of the delamination area.

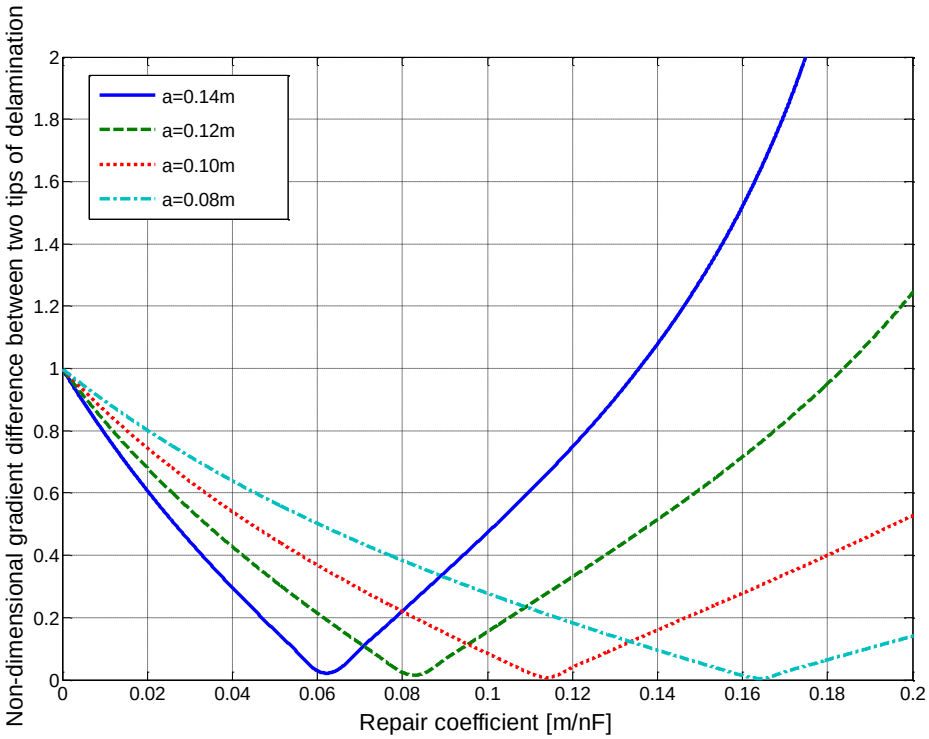

Fig. 4- 3 Variation of the gradient differences versus the repair coefficients with different delamination lengths. (L=0.6 m, l=0.3 m, H=0.015 m, t=0.0075 m)

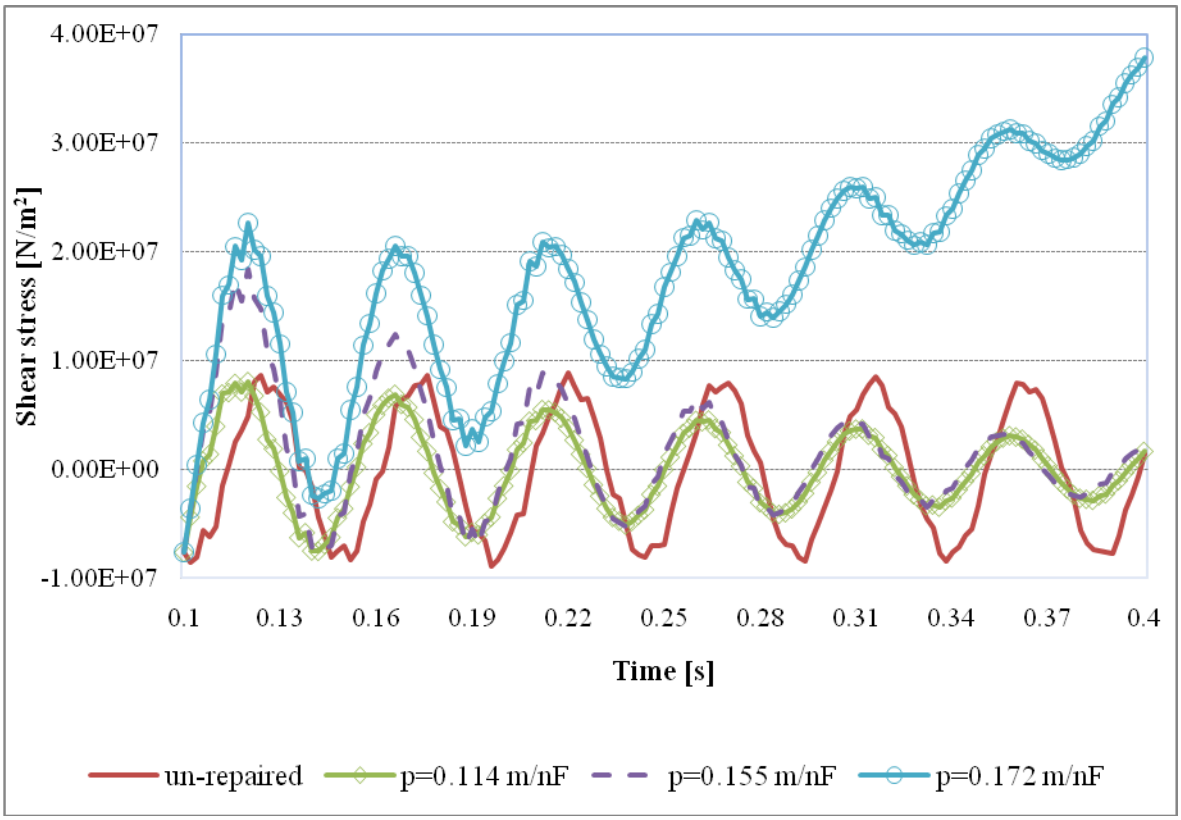

Fig. 4- 4 Shear stresses on the left delamination tip with different repair coefficients. (L=0.6 m, l=0.3 m, H=0.015 m, t=0.0075 m, a=0.1 m)

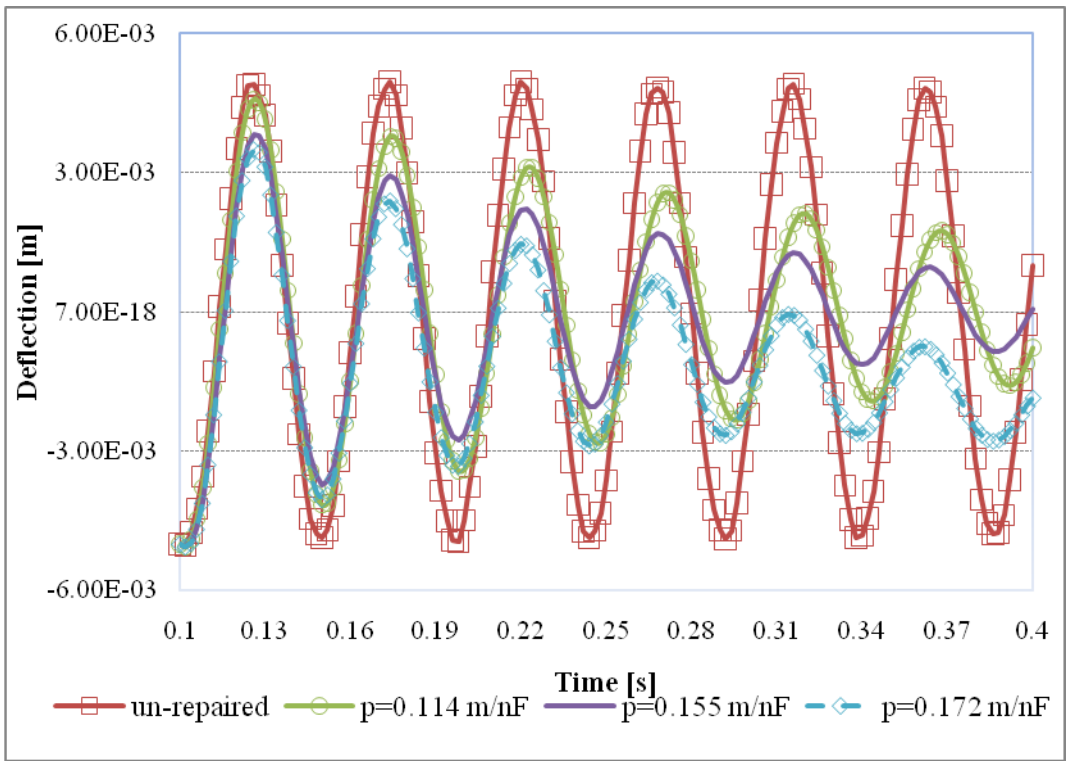

Fig. 4- 5 Deflections at the free end of the vibrating delaminated beam with different repair coefficients. (L=0.6 m, l=0.3 m, H=0.015 m, t=0.0075 m, a=0.1 m)

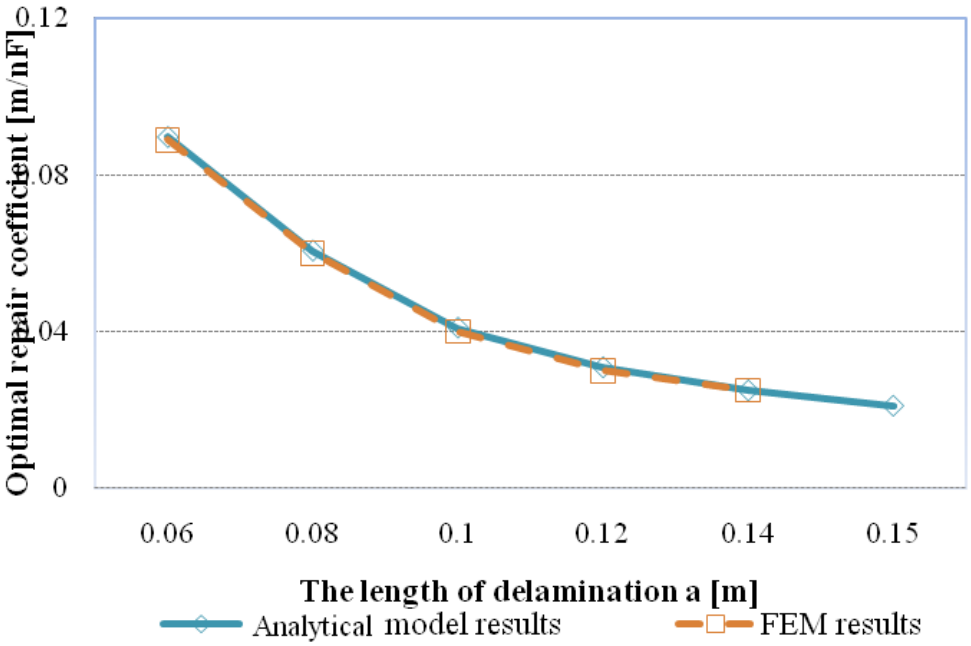

Fig. 4- 6 Variation of the optimal coefficients versus the lengths of the delamination by FEM and the analytical model. (L=0.6m, l=0.3m, H=0.005 m, t=0.0025 m)

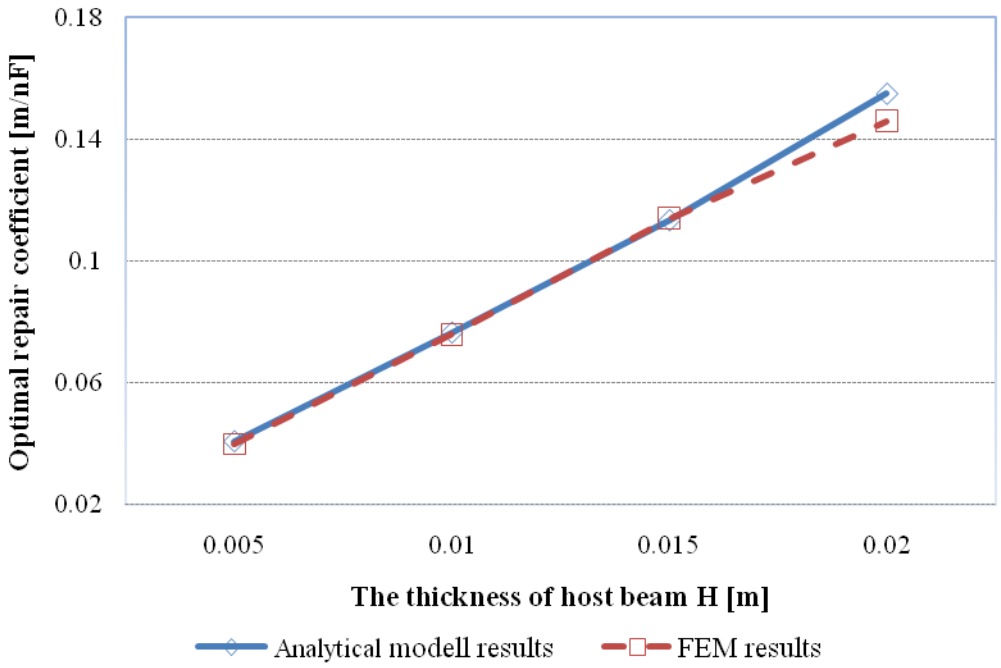

Fig. 4- 7 Variation of optimal repair coefficients versus the thicknesses of the host beam by FEM and the analytical model. (L=0.6 m, l=0.3 m, a=0.1 m, $t=H/2$)

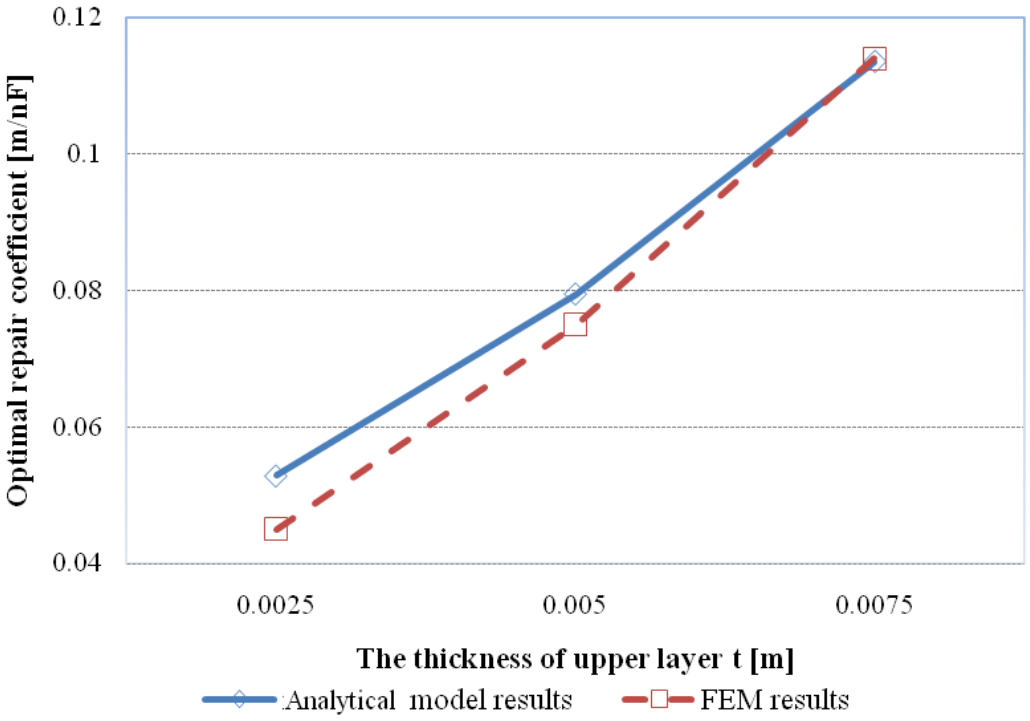

Fig. 4- 8 Variation of optimal repair coefficients versus the thicknesses of the upper layer by FEM and the analytical model. (L=0.6 m, l=0.3 m, a=0.1 m, H=0.015 m)

5 Repair of a delaminated plate under a static loading

After the study on the repair of the delaminated beam, the repair of a delaminated square plate under a transverse static loading via piezoelectric patches is developed through a analytical model and the finite element method (FEM). The axial forces along the upper and lower layers of the rectangular delamination are solved by the analytical model. In order to repair the delaminated plate by reducing the magnitude of the shear stress along the delamiantion edges with the piezoelectric effect, discrete electrodes on piezoelectric layers attached on the surface of the delamination are developed. The design of voltages on individual electrodes is then proposed to achieve the repair purpose. The feasibility of the design of the discrete electrodes and applied voltages is verified by FEM. Simulation results show that larger repair voltages are required when the delamination area is smaller and the loading position is closer to the center of the delamination.

5.1 Analytical model of repair of a delaminated plate via piezoelectric patches

5.1.1 Stress analysis of delamination in plate

A delaminated simply supported square plate subjected to a static loading is shown in Fig. 5-1. Delamination edge numbering is illustrated in Fig. 5-1 (a). Figs. 5-1 (b) and 5-1 (c) show the cross sections of the delaminated plate within XZ and YZ planes, respectively. Piezoelectric patches are surface bounded on the delaminated area. *Lx* and *Ly* are the length and width of the host delaminated plate (for square plate *Lx=Ly*); *H* and t are the thicknesses of the host plate and the upper layer of delamination, respectively; *a* and *b* are the length of delamination edges along X and Y direction; point O is the coordinate origin in XY plane; *c* and *d* stand for the loading position in XY plane. *L1* and *L2* indicate the distance of the left lower corner of the delamination from the coordinate origin. *F* is the vertical static load applied to the surface of delaminated plate. h_1 is the thickness of piezoelectric patches.

While a vertical load is applied to the host plate, deflection will take place along delamination area. Axial elongation and compression along X and Y directions of the two delaminated layers will be induced due to the bending of the host plate (Wang and Quek 2004). Because of the tensile and compression forces induced, shear forces would be initiated at the crack joint of the upper and lower layers of the delamination leading to the second fracture mode at the crack joint. Given the induced stress concentration on the delamination edges, piezoelectric patches are thus employed to induce shear forces between piezoelectric patches and the host delaminated plate by applying suitable voltage to decrease the magnitude of the axial

forces on the upper and lower layers, and hence the shear stress singularity could be erased accordingly.

To find the desirable repair voltage applied to the piezoelectric patches, the tensile/compressive forces on the delamination layers generated by the bending of the host plate need to be estimated first. It is assumed that the compressive force P_{xu} (P_{yu}) and tensile force P_{xl} (P_{yl}) along X (Y) direction are induced on the upper and lower layers of the delamination. Based on the classical elastic plate theory, the compression and elongation displacements of the central axis of upper and lower layers along X direction, Δu_u and Δu_l, can be expressed as follows (Wang and Quek 2004):

$$\Delta u_u = \frac{(H-t)}{2}\left(\left.\frac{\partial w_r(x,y)}{\partial x}\right|_{x=L1+a,y} - \left.\frac{\partial w_l(x,y)}{\partial x}\right|_{x=L1,y} \right), \tag{5-1}$$

$$\Delta u_l = \frac{t}{2}\left(\left.\frac{\partial w_l(x,y)}{\partial x}\right|_{x=L1,y} - \left.\frac{\partial w_r(x,y)}{\partial x}\right|_{x=L1+a,y} \right), \tag{5-2}$$

where $w_r(x,y)\big|_{x,y=L2+b}$ and $w_l(x,y)\big|_{x,y=L2}$ are the deflections on edges 1 and 3 in Fig. 5-1 (a). Following the same idea, the compression and elongation displacements of the central axis of upper and lower layers along Y direction, Δv_u and Δv_l, can be expressed as:

$$\Delta v_u = \frac{(H-t)}{2}\left(\left.\frac{\partial w_r'(x,y)}{\partial y}\right|_{x,y=L2+b} - \left.\frac{\partial w_l'(x,y)}{\partial y}\right|_{x,y=L2} \right), \tag{5-3}$$

$$\Delta v_l = \frac{t}{2}\left(\left.\frac{\partial w_l'(x,y)}{\partial y}\right|_{x,y=L2} - \left.\frac{\partial w_r'(x,y)}{\partial y}\right|_{x,y=L2+b} \right), \tag{5-4}$$

where $w_r(x,y)\big|_{x,y=L2}$ and $w_l(x,y)\big|_{x,y=L2+b}$ are the deflections on edges 2 and 4 in Fig. 5-1 (a).

On the delamination area, the axial forces of an incremental strip along X direction, which starts from position y with a length of 'a' and a width of 'dy', can be defined as $dP_{xu}(y)$ and $dP_{xl}(y)$ for upper and lower delamination layers, respectively, and given as follows:

$$dP_{xu}(y) = \left(\frac{\Delta u_u Et}{a} + \frac{\upsilon P_{yu}}{a} \right) dy, \tag{5-5a}$$

$$dP_{xl}(y) = \left(\frac{\Delta u_l E(H-t)}{a} + \frac{\upsilon P_{yl}}{a} \right) dy, \tag{5-5b}$$

where E is Young's modulus of the host plate and υ is Poisson ratio.

The total compressive force P_{xu} and tensile force P_{xl} on the upper and lower delamination layers along X direction can thus be easily solved to be:

$$P_{xu} = \int_{L2}^{L2+b} \left(\frac{\Delta u_u Et}{a} + \frac{\upsilon P_{yu}}{a} \right) dy, \tag{5-6}$$

$$P_{xl} = \int_{L2}^{L2+b} \left(\frac{\Delta u_l E(H-t)}{a} + \frac{\upsilon P_{yl}}{a} \right) dy. \tag{5-7}$$

Following the same idea, the total compressive force P_{yu} and tensile force P_{yl} along Y direction could be expressed as:

$$P_{\mathrm{yu}} = \int_{L1}^{L1+a} \left(\frac{\Delta v_u Et}{b} + \frac{\upsilon P_{xu}}{b} \right) dx, \tag{5-8}$$

$$P_{yl} = \int_{L1}^{L1+a} \left(\frac{\Delta v_l E(H-t)}{b} + \frac{\upsilon P_{xl}}{b} \right) dx \,. \tag{5-9}$$

The above solutions show total tensile and compressive forces on upper and lower delamination layers when bending takes place on the delaminated plate. Now, we hope to find the force distribution along upper and lower delamination layers for repair purpose. In order to do so, the delamination layers are separated into discrete sections to describe the compressive and tensile forces distribution. The delamination along Y direction (edges 1 and 3) in Fig. 5-1 (a) is separated into N segments, while the delamination along X direction (edges 2 and 4) is separated into M segments. Fig. 5-2 (c) shows the discrete electrodes mounted on the piezoelectric patch. It is assumed that the stress distribution in each of the sections is uniformed. The compressive force and tensile force could be expressed as $P_{xu}{}^{i}$ ($P_{yu}{}^{i}$) and $P_{xl}{}^{i}$ ($P_{yl}{}^{i}$), where i and j (1<=i<=N, 1<=j<=M) are the numbers of the sections on delamination along Y and X directions, respectively. Thus, eqs. (5-6~5-9) could be transformed as follows:

$$P_{\mathrm{xu}}^{\mathrm{i}} = \int_{L2+b(i-1)/N}^{L2+bi/N} \left(\frac{\Delta u_u Et}{a} + \frac{\upsilon \sum_{j=1}^{N} P_{yu}^{j}}{a} \right) dy \,, \tag{5-10}$$

$$P_{\mathrm{xl}}^{\mathrm{i}} = \int_{L2+b(i-1)/N}^{L2+bi/N} \left(\frac{\Delta u_l E(H-t)}{a} + \frac{\upsilon \sum_{j=1}^{N} P_{yl}^{j}}{a} \right) dy \,, \tag{5-11}$$

$$P_{\mathrm{yu}}^{\mathrm{j}} = \int_{L1+a(j-1)/M}^{L1+aj/M} \left(\frac{\Delta v_u Et}{b} + \frac{\upsilon \sum_{i=1}^{M} P_{xu}^{i}}{b} \right) dx \,, \tag{5-12}$$

$$P_{\mathrm{yl}}^{\mathrm{j}} = \int_{L1+a(j-1)/M}^{L1+aj/M} \left(\frac{\Delta v_l E(H-t)}{b} + \frac{\upsilon \sum_{i=1}^{M} P_{xl}^{i}}{b} \right) dx \,. \tag{5-13}$$

where $P_{xu}^{\ i}$ ($P_{yu}^{\ i}$) and $P_{xl}^{\ i}$ ($P_{yl}^{\ i}$) describe the X(Y) direction normal forces of the ith (jth) section from delamination start position [L1, L2] on the edges of upper and lower delaminaiton layers. To solve the linear equations (5-10~5-13), the plate deflection w under a static loading need be found first.

When a transverse load is applied to the surface of the plate, the effect of the delamination on the deflection solution is postulated to be negligible and the deflection of the delaminated plate can be assumed to be the same as the un-delaminated one. The deflection of a simply supported rectangular plate under a point load is given as below (Lowe 1982):

$$W(x,y)=\frac{4F}{\pi^4 DLxLy}\sum_{m=1}^{\infty}\sum_{n=1}^{\infty}\frac{\sin\frac{m\pi c}{Lx}\sin\frac{n\pi d}{Ly}\sin\frac{m\pi x}{Lx}\sin\frac{n\pi y}{Ly}}{\left(\left(\frac{m}{Lx}\right)^2+\left(\frac{n}{Ly}\right)^2\right)^2}, \qquad (5\text{-}14)$$

where the bending rigidity of the plate is given as $D=\frac{EH^3}{12(1-\upsilon^2)}$.

By submitting eq. (5-14) into eqs. (5-1~5-4) and eqs. (5-10~5-13), the force distribution along upper and lower delamination layers, could be expressed as below,

$$-P_{\mathrm{xu}}^{\mathrm{j}}=P_{xl}^{j}=\sum_{m=1}^{\infty}\sum_{n=1}^{\infty}A(m,n,j)+\frac{\upsilon b}{Na}\sum_{j=1}^{N}P_{yu}^{i}, \qquad (5\text{-}15)$$

$$-P_{\mathrm{yu}}^{\mathrm{j}}=P_{yl}^{j}=\sum_{m=1}^{\infty}\sum_{n=1}^{\infty}B(m,n,j)+\frac{\upsilon a}{Mb}\sum_{i=1}^{M}P_{xu}^{i}, \qquad (5\text{-}16)$$

where $A(m,n,i)$ and $B(m,n,j)$ are given as follow:

$$A(m,n,i)=-\frac{1}{\pi^4 D(m^2Ly^2+n^2Lx^2)^2 na}\left(\begin{array}{l}2t(H-t)EF\cdot\sin\dfrac{m\pi c}{Lx}\cdot\sin\dfrac{n\pi d}{Ly}\cdot\\ \dfrac{}{mLx^2Ly^4}\left(\begin{array}{l}-\cos\dfrac{m\pi(L1+a)}{Lx}\cdot\cos\dfrac{n\pi(NL2+bi-b)}{NLy}+\\ \cos\dfrac{m\pi L1}{Lx}\cdot\cos\dfrac{n\pi(NL2+bi-b)}{NLy}+\\ \cos\dfrac{m\pi(L1+a)}{Lx}\cdot\cos\dfrac{n\pi(NL2+bi)}{NLy}-\\ \cos\dfrac{m\pi L1}{Lx}\cdot\cos\dfrac{n\pi(NL2+bi)}{NLy}\end{array}\right)\end{array}\right)$$

$$B(m,n,j)=-\frac{1}{\pi^4 D(m^2Ly^2+n^2Lx^2)^2 mb}\left(\begin{array}{l}2t(H-t)EF\cdot\sin\dfrac{m\pi c}{Lx}\cdot\sin\dfrac{n\pi d}{Ly}\cdot\\ \dfrac{}{nLx^4Ly^2}\left(\begin{array}{l}\cos\dfrac{n\pi(L2+b)}{Ly}\cdot\cos\dfrac{m\pi(ML1+aj-a)}{MLx}-\\ \cos\dfrac{m\pi L2}{Ly}\cdot\cos\dfrac{m\pi(ML1+aj-a)}{MLx}-\\ \cos\dfrac{n\pi(L2+b)}{Ly}\cdot\cos\dfrac{m\pi(ML1+aj)}{MLx}+\\ \cos\dfrac{n\pi L2}{Ly}\cdot\cos\dfrac{m\pi(ML1+aj)}{MLx}\end{array}\right)\end{array}\right).$$

By solving the 20-linear equations. (5-15, 5-16), the force distribution along the delamination layers can be solved.

5.1.2 Repair of delaminated plates using piezoelectric patches

Discrete electrodes concept is developed for the purpose of an optimal repair of delaminated plates, i.e. to decrease the magnitude of the shear stress at the crack joints along the whole edge of the delamination. The discrete electrodes on piezoelectric patches are shown in Fig. 5-2 (c). Depending on the corresponding axis forces distributed on each edge of the delamination layers, voltages on these electrodes will be applied to generate suitable shear forces between the host plate and piezoelectric patches so that the distributed forces on the delamination could be

reduced as a whole. The shear forces on delamination edges at the crack joints of the upper and lower delamination layers will be reduced at the same time so that the slide mode fracture could be controlled.

Piezoelectric patches are polarized by Z direction. The expression of the shear force between a metal substrate and a piezoelectric layer with the assumption of a complete bonding between them was given by Crawley and de Luis (Crawley and Deluis 1987):

$$S = \frac{EHT}{\psi + \alpha}\Lambda \tag{5-15}$$

where $\psi = EH / E_p h_1$, $\alpha = 6$ when a bending bar is considered and $\Lambda = d_{31}V / h_1$; h_1 is the thickness of the piezoelectric patch; d_{31} is the piezoelectric charge coefficient; E_p is the equivalent Young's modulus of the piezoelectric patch; T is the width of distributed electrodes on piezoelectric patch ($T = \frac{a}{M} / \frac{b}{N}$) and V is the input repair voltage; $V = V_i$ when electric potential is applied to the ith electrode.

Shear forces induced by the applied repair voltage to ith/jth electrode between piezoelectric patches and host plate could thus be given to be:

$$S_x^i = \frac{EHb / N}{\psi + 6} \cdot \frac{d_{31}V_i}{h_1}, \tag{5-16}$$

$$S_y^j = \frac{EHa / M}{\psi + 6} \cdot \frac{d_{31}V_j}{h_1}. \tag{5-17}$$

It is expected that S_x^i and S_y^j , are to be used as the repair forces to erase the

tensile/compressive force on the upper/lower delamination layer. The principle of the repair strategy is hence to be developed to apply the repair forces induced by the piezoelectric with the same magnitude but in opposite sign with the calculated normal force distributions on the upper and lower delamination layers, i.e. $S_{\mathrm{x}}^{i} = -P_{\mathrm{xu}}^{\mathrm{i}} = P_{xl}^{i}$ ($S_{\mathrm{y}}^{j} = -P_{\mathrm{yu}}^{\mathrm{j}} = P_{yl}^{j}$). The desired repair voltages are thus obtained by:

$$V_i = \frac{\left(\sum_{m=1}^{\infty} \sum_{n=1}^{\infty} A(m,n,i) + \frac{\upsilon b}{Ma} \sum_{j=1}^{M} P_{yu}^{j} \right) \cdot (\psi + 6) \cdot h_1 \cdot N}{EHbd_{31}}, \tag{5-18}$$

$$V_j = \frac{\left(\sum_{m=1}^{\infty} \sum_{n=1}^{\infty} B(m,n,i) + \frac{\upsilon a}{Nb} \sum_{i=1}^{N} P_{xu}^{i} \right) \cdot (\psi + 6) \cdot h_1 \cdot M}{EHad_{31}}. \tag{5-19}$$

5.2 Finite element model (FEM) of repair of delaminated plates via piezoelectric patches

The finite element model of a delamination plate bounded with piezo-patches is given in Fig. 5-2. Finite element analysis software ANSYS 10 is employed to verify the effectiveness of the proposed analytical model. Solid element 45 and coupled field element 226 are used to mesh the host plate and piezoelectric patches, respectively. Meshing result of the delaminated plate bonded with piezoelectric patches is shown in Fig. 5-2 (d). The meshing of the delamination area is refined to accurate the simulation results.

Two delamination layers are assumed to contact with each other without friction. An area contact pair is built between the two layers to simulate the contact plate delamination. Friction

factor is set to be zero.

The discrete electrodes mounted on the surface of piezoelectric patch are shown in Fig. 5-2 (c) (the electrode is assumed to be divided into ten sections). Different voltages V_i/V_j will be applied to the discrete electrodes to optimize the repair of the delamination.

5.3 Numerical simulations

Based on the developed analytical model and FEM, numerical simulations are conducted to study the repair of a delaminated square plate with four simply supported edges. The delamination edges on both X and Y directions are discredited into 10 sections (N=M=10). The geometry of a delaminated plate and the material properties are given as follows: Lx=Ly=0.3m, E=200e9 N/m^2, H=0.01m, h_1=0.001m, Ep=65e9 N/m^2, d_{31}=256e-12 C/N.

The effectiveness of the analytical model in predicting the axial forces along delamination edges and the voltages applied to the discrete electrodes in reducing the stress concentration is verified by the comparison between the analytical model and FEM. The plate with a delaminition of the following given location and size, $L1$=$L2$=0.1m, a=b=0.1m, t=0.005m, is first investigated. The loading position is given by c=d=0.15m. The normal stresses distribution on the lower layer along the delamination edge 1 and the desired repair voltages applied to the 10 discrete electrodes from both analytical model and FEM are shown in Fig. 5-4. As the structure studied in Fig. 5-4 is symmetrical in XY plane, only the delamination edge 1 is analyzed. The discrete electrodes are distributed along Y direction to provide the reduction of the shear stress magnitude on edges 1 and 3. The largest stress and voltage differences between the analytical model and FEM are 5.3% and 6%, respectively. The largest errors for both stresses and voltages

distributions appear at the ends of the edge 1. Comparison also shows that the highest repair voltage applied to the discrete electrodes by the analytical model needs to be increased by 5% and the lowest repair voltage needs to be decreased by 6% to decrease the shear force between delamination layers as a whole. Fig. 5-3 illustrates the shear stress distribution along the delamination edges 1 and 3 when adjusted voltages are applied to the discrete electrodes. The shear stresses are decreased obviously when suitable voltages are concerned.

Figs. 5-5 to 5-7 illustrate the repair effects by the discrete electrodes on different plate delamination with the upper layer thickness of 0.005m. Fig. 5-5 compares the reduced shear stress on delamination edge 1 by piezo-patches with a single electrode and discrete electrodes for the same structure studied in Fig. 5-4. It can be seen that the largest XZ shear stress on edge 1 could be decreased by 85.4% and the lowest shear stress is decreased by 53.1%, when different voltages are applied to the discrete electrodes. However, only 56.4% the largest shear stress decrease can be seen when an average voltage is applied to the single electrode. The uniform voltage applied to the surface of piezo-patches could, on the other hand, cause an increase in the shear stress on the reverse direction at the ends of delamination edge by 200%, approximately. Obviously, concept of the discrete electrodes could provide efficient repair for the plate delamination while the single patch could not efficiently reduce shear stress along the delamination edges. The repairs of other two un-symmetrical delaminated plates are shown in Figs. 5-6 and 5-7. For the structure with $L1$=0.175m, $L2$=0.1125m, a=b=0.075m and c=d=0.15m, comparison between the repaired and un-repaired YZ shear stress distributions along edge 2 is illustrated in Fig. 5-6. Electrode strips are distributed along X direction aiming to reduce the shear stresses on the edges 2 and 4 mainly, as the largest shear stress distributed along delamination edges is on edges 2 and 4. Our calculations show that shear stresses along edge 2

are decreased by 84%. On the other hand, our results also show that, on the edges 1 and 3, the largest XZ shear stress is decreased from 18000 N/m^2 to 10000 N/m^2. For the structure with *L1*=0.05m, *L2*=0.1m, *a*=0.2m, *b*=0.1m and *c*=*d*=0.15m, the decreased shear stresses on delamination edge 2 by piezo-patches with discrete electrodes are shown in Fig. 5-7. On the repair direction Y, which is parallel with the discrete electrode strips, the largest YZ shear stress on the edges 2 is decreased by 83.3% and the lowest shear stress is reduced by 68%. On the edge 3, the largest shear stress is also decreased by 50%, approximately.

Figs. 5-8 to 5-11 illustrate the variation of the average values of desired repair voltages applied to discrete electrodes versus different delamination structures. The repair voltages versus different length of delamination are given in Fig. 5-8, when *L1*=*L2*=0.1m, *b*=0.1m, *t*=0.005m and *c*=*d*=0.05m. Results show that the repair voltages on electrodes in both X and Y directions decrease along with increase in the lengths of edges 2 and 4. This observation can be explained by eqs. (5-6~5-9). The equations show that the tensile and compressive forces generated on the upper and lower delamination layers decrease with the increase in the delamination length '*a*' or '*b*'. The stress singularity at the crack joints of upper and lower delamination layers will be reduced accordingly. The repair voltages on electrodes in X and Y directions equal with each other when the loaded delamination plate is symmetric with *a*=*b*=0.1m and *c*=*d*=0.05m. The repair voltage variation versus different positions of delamination is shown in Fig. 5-9 with *a*=*b*=0.05m, *c*=*d*=0.15m, *t*=0.005m and *L2*=0.2m. Only repair voltages on electrodes in X direction are shown because the repair voltages on electrodes in X direction is much larger than those in Y direction, when the delamination is moving along *Lx*. The repair is designed based on the shear stress singularity along edges 1 and 3. The repair voltages reach the highest value when the delamination position *L1* is 0.125m, where the loading position is at the center of the

delamination. Fig. 5-10 describes the effect of the loading position on the repair voltage. The delaminated plate is set to be *L1*=*L2*=0.1m, *d*=0.15m, *t*=0.005m and *a*=*b*=0.1m, and the loading position changes from *c*=0.02m to *c*=0.27m along X direction. Our calculation results show that the repair voltages on electrodes in X direction are always smaller than the repair voltages on electrodes in Y direction because the loading position is always located at the centre of delamination on Y direction (*d*=0.15m) and the slop difference between two tips on the Y direction delamination is always larger than the one on X direction. Thus, the repair is designed based on the shear stress singularity along delamination edges 2 and 4. It can be seen that the repair voltages increase to 183v and decrease back to 20v while the loading position is moving through the delamination area. The average repair voltage reaches the highest value of 183v when the loading position is located at the centre of the delaminaiton. Fig. 5-11 illustrates the variation of the repair voltages according to the change of the thickness of upper delamination layer when other geometry parameters are fixed as *L1*=*L2*=0.1m, *a*=*b*=0.1m, *c*=*d*=0.15m. The average value of repair voltages applied to the discrete electrodes increase from 65v to 183v when the thickness of upper delamination layer is changed from 0.001m to 0.005m (H/2). The desired repair voltage is larger when the delamination is closer to the mid-face of the host plate, which can be seen from eqs. (5-15, 5-16). The axial force difference between upper and lower delamination layers decreases while the thickness of the upper layer is reduced from the half thickness of the host plate to 0.001m.

5.4 Conclusions

Piezoelectric patches, which are bonded on the rectangular delamination area, are employed for the repair of a delaminated square plate under a static transverse loading. Discrete electrodes

mounted on the piezoelectric patches are employed to reduce magnitude of the shear stress along the delamiantion edges with the piezoelectric effect. The design of the voltages applied to individual electrodes is proposed by a analytical model to achieve an optimal repair which could reduce the stress concentration on the delamination edges as a whole. In addition, the finite element model is build to verify the analytical model and the repair methodology. The proposed repair method with discrete electrodes is proved efficient. The repair effect is obvious even for the delamination edges which are not designed to be repaired. From numerical simulations, it is found that larger repair voltages applied to the discrete electrodes is needed when the edges of the rectangular delamination along repaired direction are shorter and the loading position is closer to the centre of the delamination area. In additional, the repair voltages will increase when the delamination gets closer to the mid-face of the host delaminated plate.

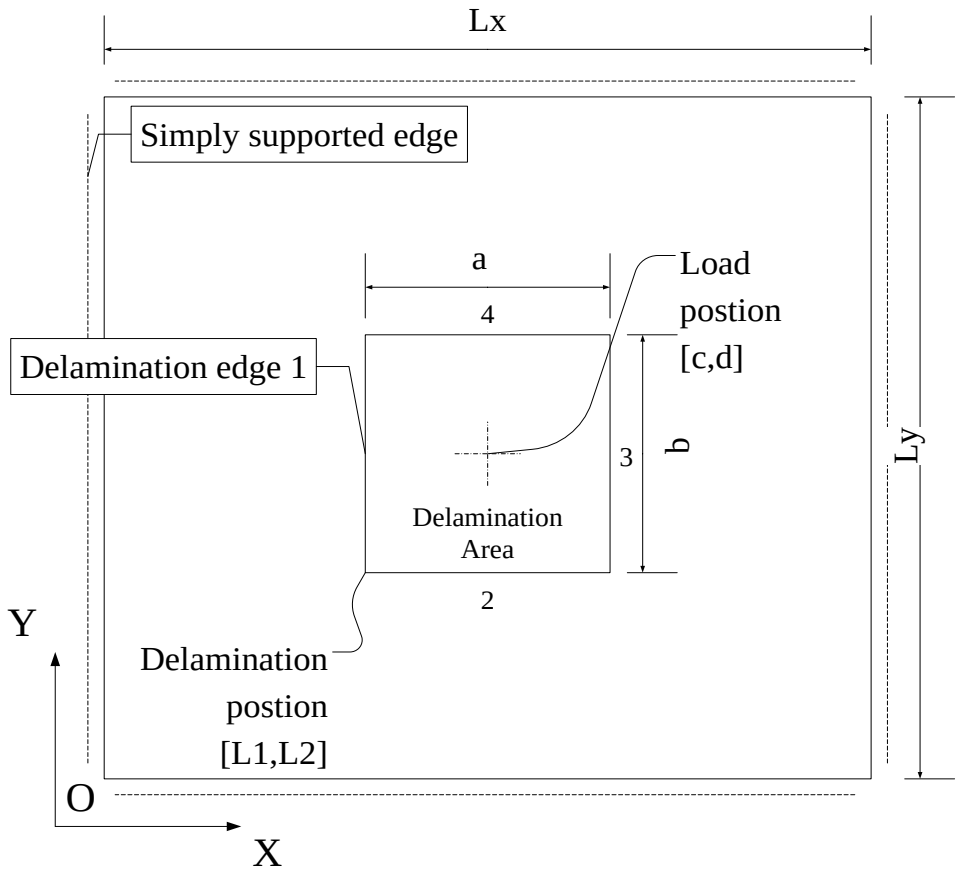

(a) Top view

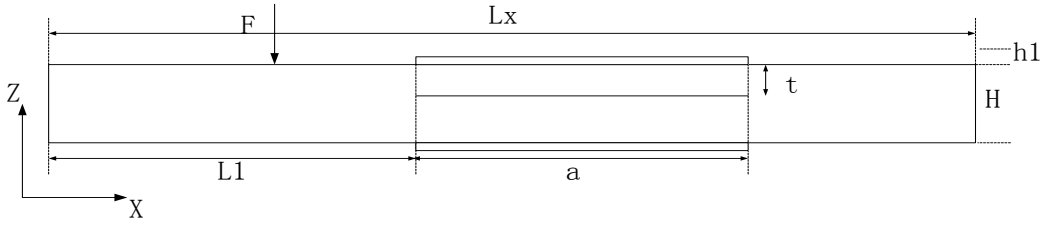

(b) Front view

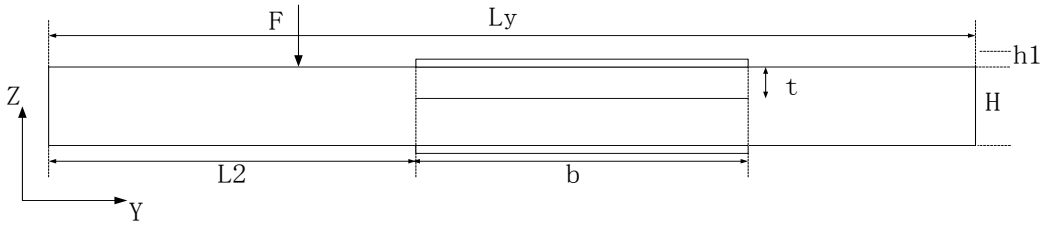

(c) Left view

Fig. 5- 1 A delaminated plate structure

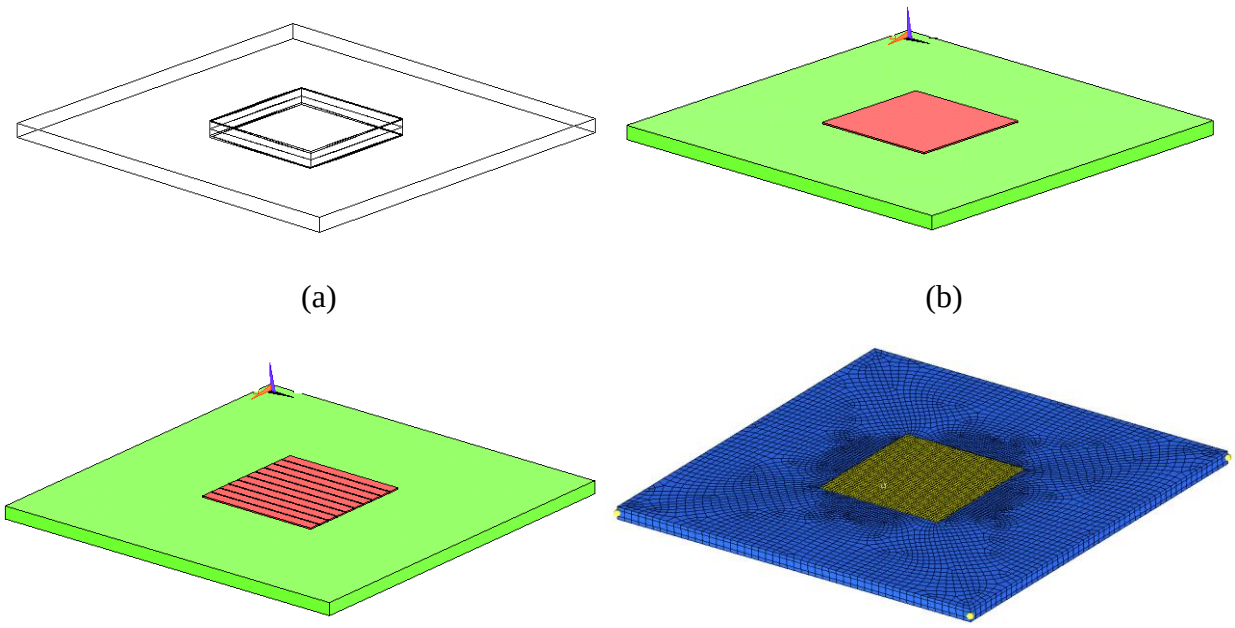

(a) (b)

(c) (d)

Fig. 5- 2 Finite element model of a delaminated plate, distributed electrodes and meshing result.

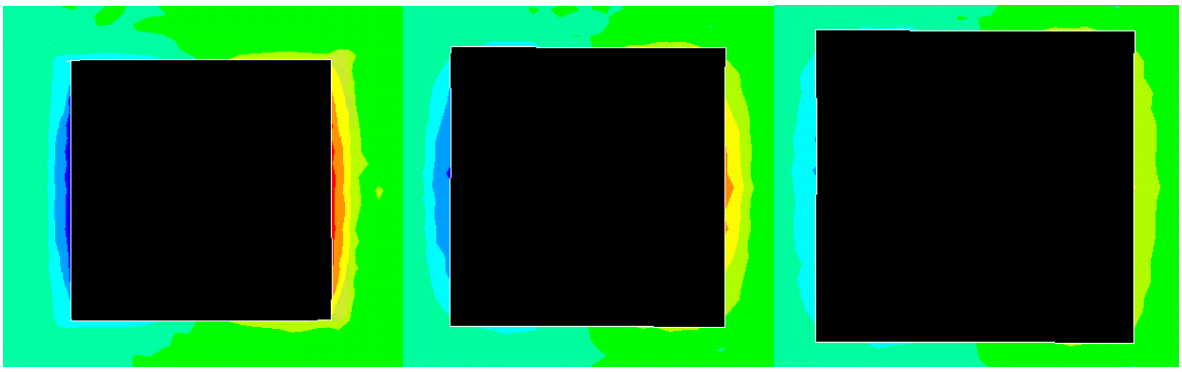

(V=0v) (V=100v~150v) (V=165v~195v)

Fig. 5- 3 Shear stress distributions along delamination edges with different repair voltages. (FEM results) (L1=L2=0.1m, a=b=0.1m, c=d=0.15m, t=0.005m)

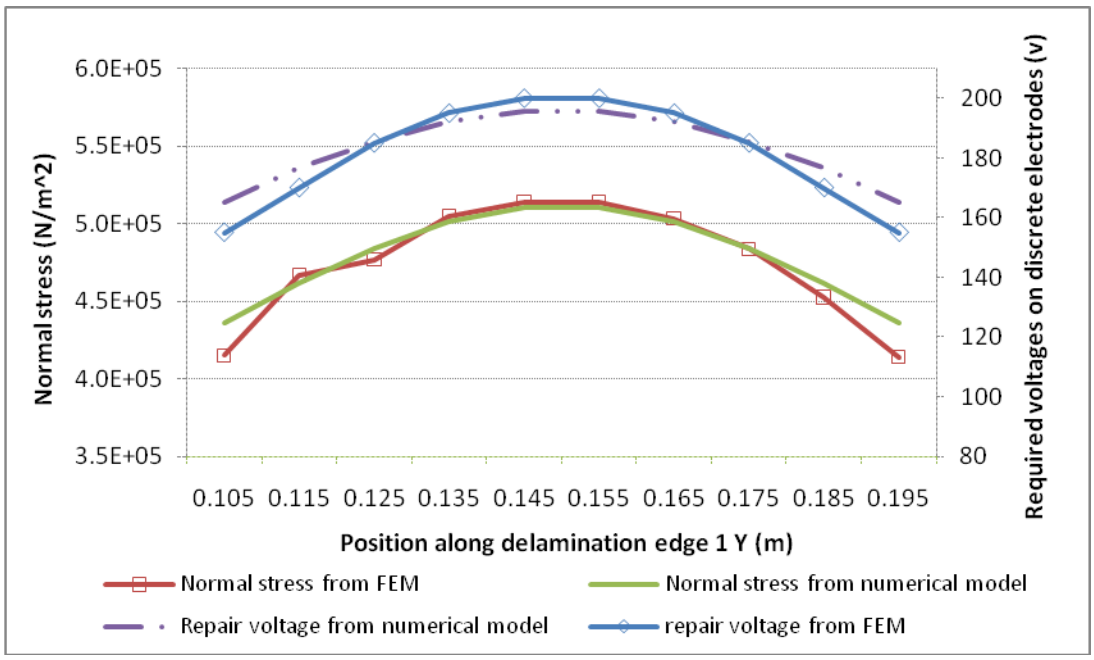

Fig. 5- 4 Nomal stress distributions on the edge 1 of the lower layer and repair voltages for the given structure in Fig. 5-1. (L1=L2=0.1m, a=b=0.1m, c=d=0.15m, t=0.005m)

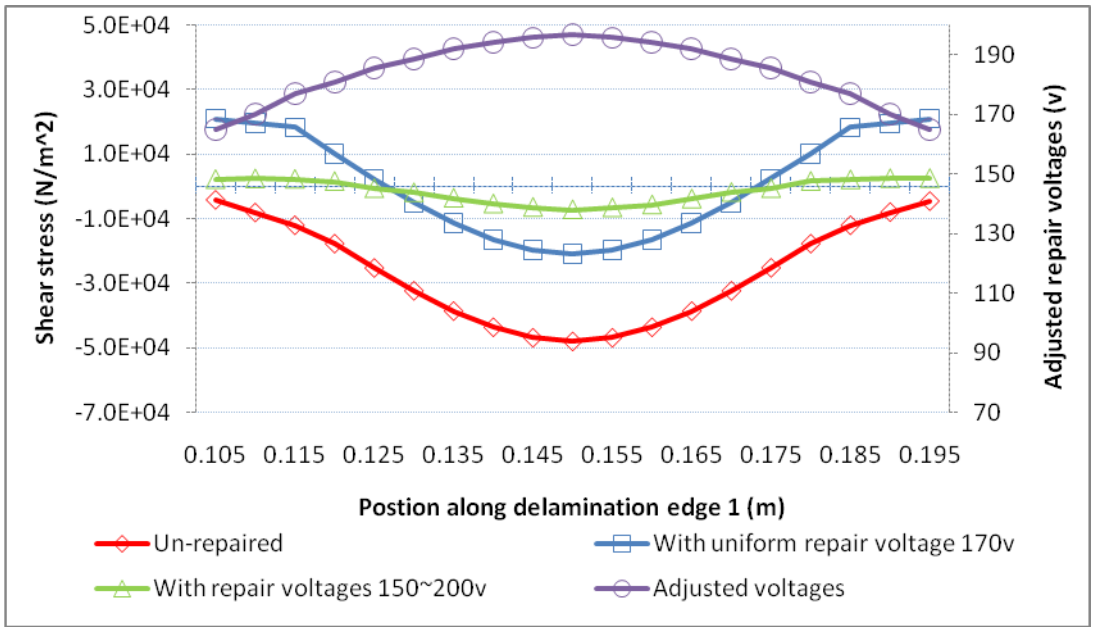

Fig. 5- 5 Shear stress distributions along the delamination edge 1of the structure in Fig. 5-1 before and after the repair by piezoelectric patches with un-distributed eletrode and discrete electrodes. (L1=L2=0.1m, a=b=0.1m, c=d=0.15m, t=0.005m)

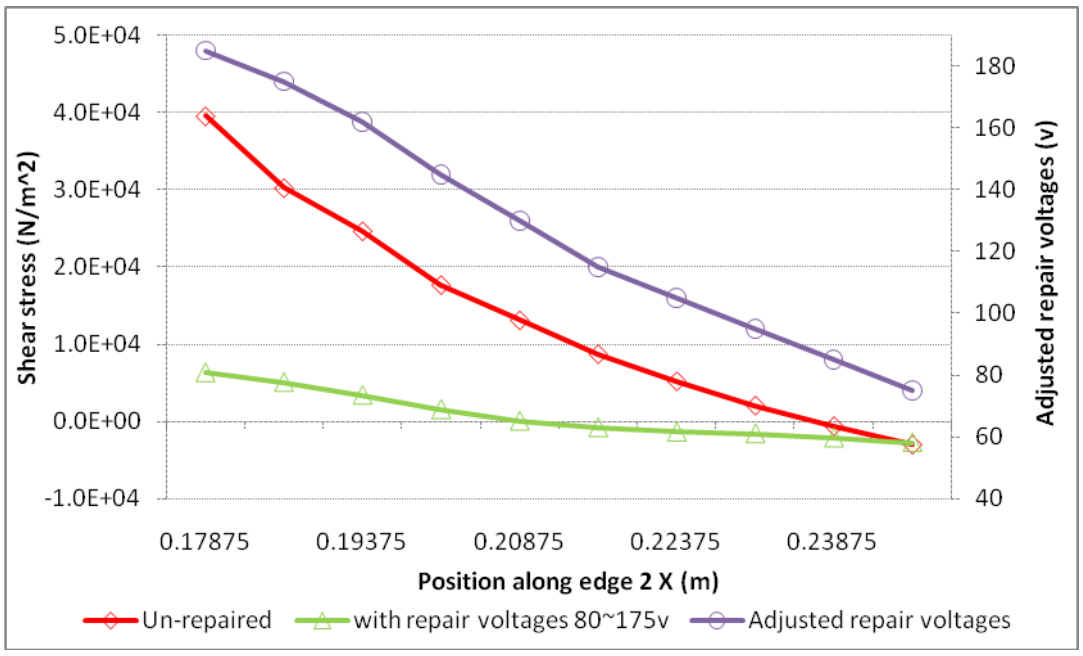

Fig. 5- 6 Shear stress distributions along the delamination edge 2 of the structure in Fig. 5-1 before and after the repair by piezoelectric patches with discrete eletrodes. (L1=0.175m, L2=0.1125m, a=b=0.075m, c=d=0.15m, t=0.005m)

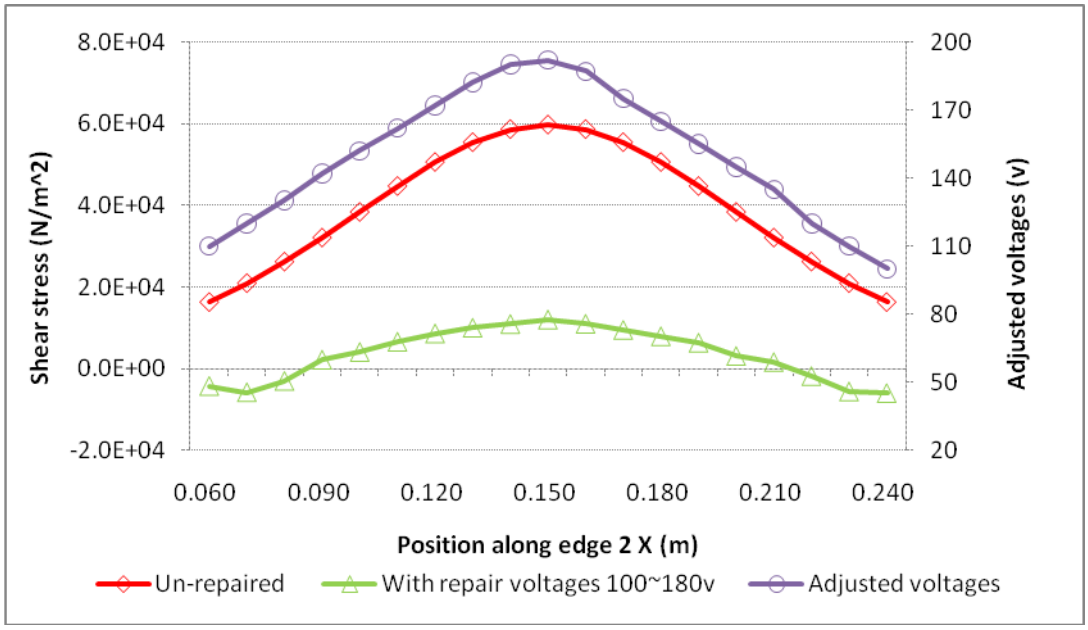

Fig. 5- 7 Shear stress distributions along the delamination edge 2 of the structure in Fig. 5-1 before and after the repair by piezoelectric patches with discrete eletrodes. (L1=0.05m, L2=0.1m, a=0.2m, b=0.1m, c=d=0.15m, t=0.005m)

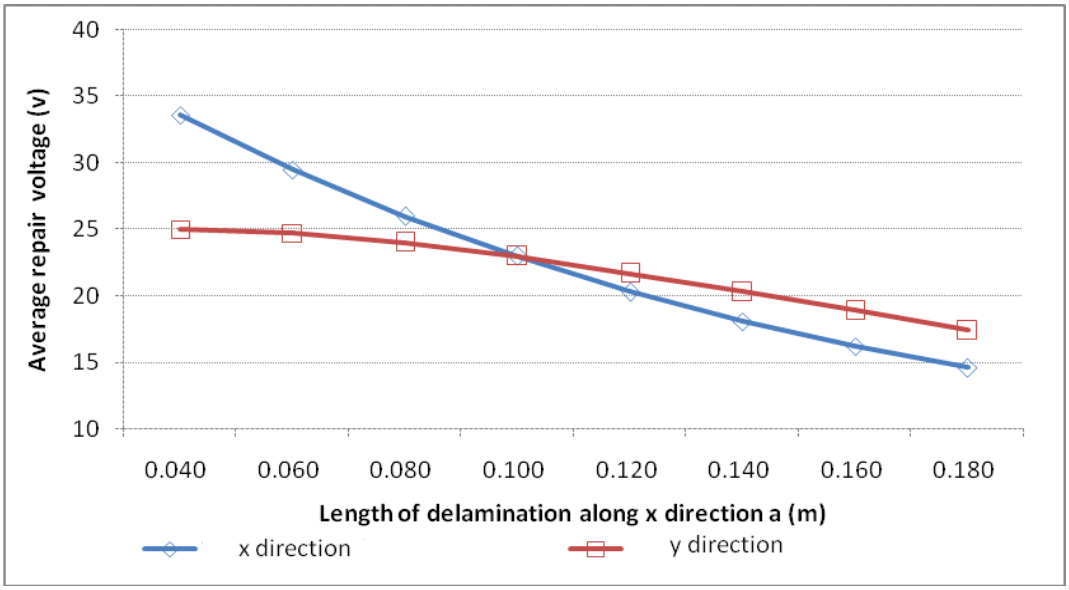

Fig. 5- 8 Relationship between average repair voltages and lengths of delamination. (L1=L2=0.1m, b=0.1m, c=d=0.05m, t=0.005m)

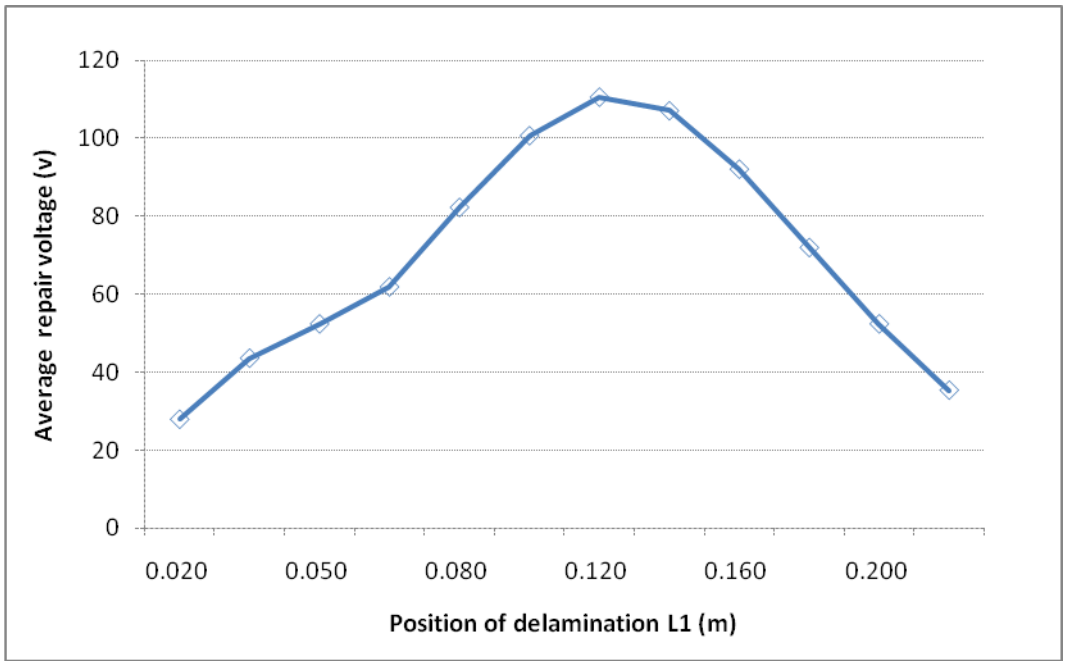

Fig. 5- 9 Relationship between average repair voltages and delamination positions. (L2=0.2m, a=b=0.05m, c=d=0.15m, t=0.005m)

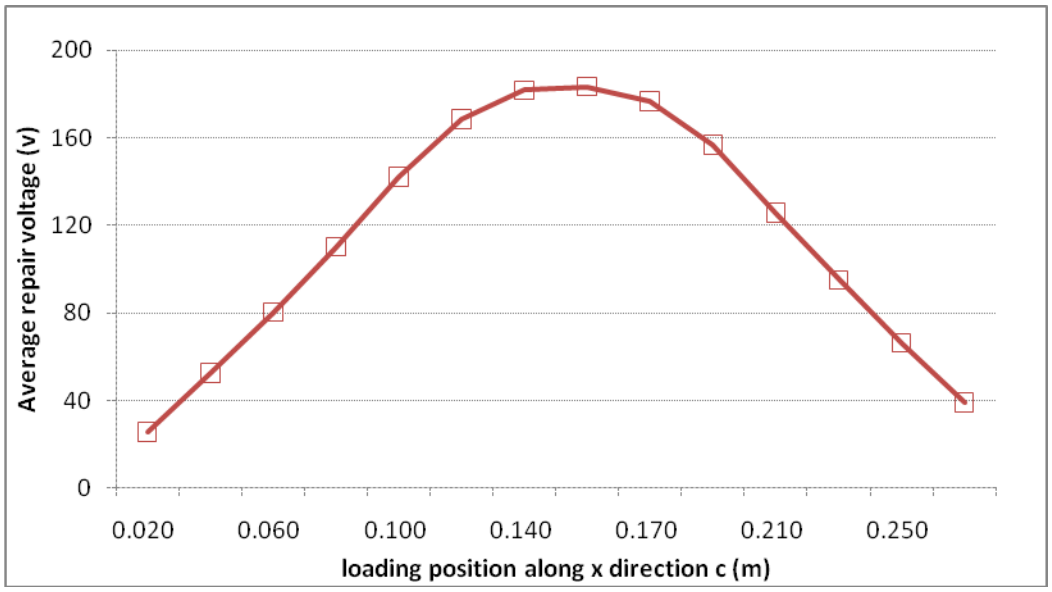

Fig. 5- 10 Relationship between average repair voltages of delamiantion and loading positions. (Lx=Ly=0.3m, L1=L2=0.1m, a=b=0.1m, d=0.15m, t=0.005m)

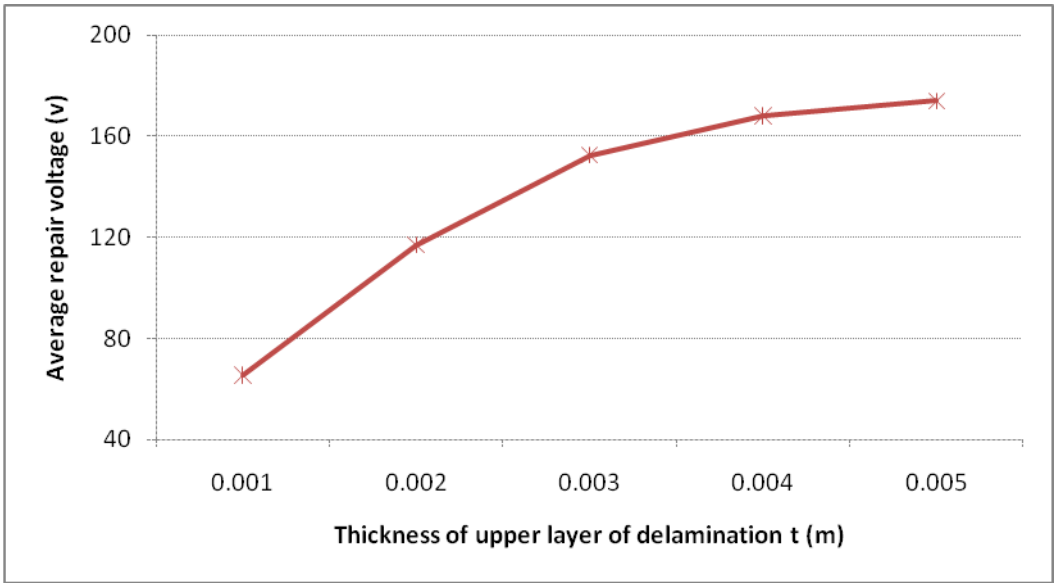

Fig. 5- 11 Relationship between the average repair voltages and the thicknesses of delamination upper layer. (L1=L2=0.1m, a=b=0.1m, c=d=0.15m)

6 An experimental study on repair of a notched beam subjected to dynamic loading with piezoelectric patches

Except the study on the repair of the delaminated structures, an experimental realization of an effective repair of a notched cantilever beam structure subjected to dynamic loading by use of piezoelectric patches is reported. Authors employed a counteracting bending moment induced by piezoelectric patches to decrease the stress concentration at the notch location. Such a principle can also apply to a real cracked structure, as the principle of the structural failure due to both the crack and notch is similar, i.e. the stress concentration occurs at the crack/notch root/tip. In the experiment, a small piezoelectric patch used as a sensor is placed on the notch position to monitor the severity of the stress singularity around the notch area by measuring the output voltage on the sensor, and a patch used as an actuator is located around the notch area to generate a required bending moment by employing an actuation voltage to reduce the stress singularity at the notch position. The actuation voltage on the actuator is designed from a feedback circuit process. An analytical model is first established for the repair process by providing the calculation of the actuation voltage, and then a finite element model (FEM) is conducted to verify the effectiveness of the analytical model. Finally, repair of a notched cantilever beam is

realized experimentally. Both numerical simulations and experimental studies show that the developed practical structural repair technique for notched beams with piezoelectric patches is effective and efficient.

6.1 Analytical model of the repair of the notched beam using piezoelectric patches

The repair technique is illustrated through a repair process of a notched cantilever beam subjected to a dynamic loading at its free end. The notched cantilever beam bonded with a piezoelectric layer is shown in Fig. 6-1. A transverse open notch is located at the upper surface of the beam, while the piezoelectric layer is bonded at the bottom of the beam corresponding to the notch area to reduce the stress singularity at the notch tip. L is the total length of the notched beam, while l is the distance from the fixed end of the cantilever beam to the left end of the piezoelectric layer. The length of the piezoelectric layer is l_1, and the notch is located at the central position of the piezoelectric layer. *de* is the depth of the notch. H and h_1 are thicknesses of the host beam and the piezoelectric layer, respectively. The width of the notched beam is *b*. A periodical dynamic point force, $f(x, t)= F\sin(\omega' t)\delta(x-L)$, is applied at the feed end of the cantilever beam, where ω' is the angular velocity of the external force and $\delta(x-L)$ is the Dirac delta function to model a point loading on engineering structures.

When a bending takes place on the notched beam due to an external force, a slop discontinuity (opening fracture mode) occurs at the notch position. The effect of an open notch can thus be modelled by the discontinuity in the slop of the deflection profile of the beam at the notch position (Krawczuk and Ostachowicz 1995). The model is simply introduced by separating

the notched beam into 4 sections shown in Fig. 6-1 by considering the piezoelectric bonded areas, 2 and 3, connected at the two ends with the non-bonded parts 1 and 4. The sections 2 and 3 are connected at the notch position in the thickness direction. The total change of the slop at the notch position is modelled as follow:

$$w_3'\big|_{x=l+l1/2} - w_2'\big|_{x=l+l_1/2} = \Theta L w_2''\big|_{x=l+l_1/2} \ , \tag{6-1}$$

where $w_1 \sim w_4$ are the deflection of the sections 1~4 of the notched beam, parameter Θ represents the non-dimensional additional flexibility of the beam due to the notch, which is calculated from fracture mechanics and Castigliano's theorem (Krawczuk and Ostachowicz 1995),

$$\Theta = 6\pi \frac{H}{L} \int_0^{de/H} x \left(\frac{0.923 + 0.199(1 - \sin(\frac{\pi}{2}x))^4}{\cos(\frac{\pi}{2}x)} \right)^2 \frac{\tan(\frac{\pi}{2}x)}{\frac{\pi}{2}x} dx \ . \tag{6-2}$$

The stress singularity at the notch tip may cause the growth of the notch leading to a possible failure of the whole beam structure. An idea to repair the notched structure is to apply a piezoelectric patch to remove or decrease the slop discontinuity by applying a bending moment owing to its electromechanical effect at the both sides of the notch.

6.1.1 Design of feedback repair

The design of the feedback repair of the notched beam is illustrated below. The piezoelectric layer shown in Fig. 6-1 can be separated into a sensor and an actuator along its width direction. Thus, we can assume that the piezoelectric sensor and actuator are with the same length of l_1 and mounted above the same area of the beam.

The electrical charge generated on the surface of the piezoelectric sensor, which is perfectly bonded on a bending beam, is given as follow (Lee and Moon 1990):

$$Q = -e_{31}\int_{l}^{l+l1} b_s\left(\frac{H+h_1}{2}\right)\frac{d^2w}{dx^2}dx \ , \tag{6-3}$$

where e_{31} is the piezoelectric constant, b_s is the width of the piezoelectric sensor and w is the transverse displacement of the notched beam. The corresponding output voltage of the piezoelectric sensor, V_o, can be written as (Lin and Hsu 1999):

$$V_o = \frac{Q}{C_v} = -\frac{e_{31}(H+h_1)}{2C_v^{'}}\int_{l}^{l+l1}\frac{d^2w}{dx^2}dx \ , \tag{6-4}$$

where C_v is the electrical capacity of the piezoelectric sensor and $C_v^{'}$ is the electric capacity per unit width of the piezoelectric sensor ($C_v^{'} = C_v / b_s$).

A feedback repair gain factor, g, will be multiplied to the output voltage of the piezoelectric sensor before it is applied to the piezoelectric actuator. The gained voltage, V_g, is given by:

$$V_g = gV_o = -g\frac{e_{31}(H+h_1)}{2C_v^{'}}\int_{l}^{l+l1}\frac{d^2w}{dx^2}dx \ . \tag{6-5}$$

When the gained voltage, V_g, is applied to the piezoelectric actuator, which is made from the same material as the piezoelectric sensor, the shear force generated at the interface between the piezoelectric actuator and the host beam is presented by (Sun *et al* 1999):

$$Fe = \frac{EHb_a}{\psi+\alpha}d_{31}V_g / h_1 = -g\cdot d_{31}e_{31}\frac{EHb_a(H+h_1)}{2C_v^{'}h_1(\psi+\alpha)}\int_{l}^{l+l1}\frac{d^2w}{dx^2}dx \ , \tag{6-6}$$

where E is the Young's modulus of the host beam, b_a is the width of the piezoelectric actuator, $\psi = EH / E_p h_1$, E_p is the equivalent Young's modulus of the piezoelectric patches, d_{31} is the piezoelectric charge coefficient and $\alpha = 6$ when a bending bar is considered. The bending moment induced by the piezoelectric actuator due to the gained feedback voltage, V_g, can thus be obtained by:

$$Me = Fe \cdot \frac{H - h_1}{2} = -g \cdot d_{31} e_{31} \frac{EHb_a\left(H^2 - h_1^2\right)}{4C_v^{'} h_1 (\psi + \alpha)} \int_l^{l+l1} \frac{d^2 w}{dx^2} dx = R \cdot \int_l^{l+l1} \frac{d^2 w}{dx^2} dx \,, \quad (6\text{-}7)$$

where R is defined as the feedback repair coefficient and expressed as:

$$R = -g \cdot d_{31} e_{31} \frac{EHb_a\left(H^2 - h_1^2\right)}{4C_v^{'} h_1 (\psi + \alpha)} . \quad (6\text{-}8)$$

6.1.2 Determination of actuation voltage

To fulfill an effective repair of the notched beam, the slop discontinuity at the notch position of the beam during the vibration is targeted to be erased by the repair moment generated by the piezoelectric actuator. The dynamic response of the notched beam bonded with the piezoelectric sensor and actuator can be solved via the Euler–Bernoulli beam theory. From the dynamic response of the notched beam, the actuation voltage on the actuator would be identified by searching for a repair coefficient, R, that leads to reduction of the slop difference between the two sides of the notch. The process to find the actuation voltage for the repair purpose is illustrated as follows.

Based on the Euler-Bernoulli beam theory, the governing equation for the first and fourth sections can be expressed as:

$$\frac{d^4W_1}{dx^4} + \frac{\rho bH}{EI}\omega_n{}^2 W_1 = 0, \ (x \in 0 \sim l) \tag{6-9}$$

$$\frac{d^4W_4}{dx^4} + \frac{\rho bH}{EI}\omega_n{}^2 W_4 = 0, \ (x \in l + l_1 \sim L) \tag{6-10}$$

where ρ is the density of the host beam; ω_n is the resonant vibration angular velocity of the structure at the *n*th mode. Let $\overline{\omega_n} = \sqrt{\frac{\rho bHL^4\omega_n{}^2}{EI}}$, the non-dimensional expressions of the vibration equation for the first and fourth sections will be:

$$\frac{d^4\overline{W_1}}{d\bar{x}^4} + \overline{\omega_n}^2\overline{W_1} = 0, \ (\bar{x} \in 0 \sim l/L) \tag{6-11}$$

$$\frac{d^4\overline{W_4}}{d\bar{x}^4} + \overline{\omega_n}^2\overline{W_4} = 0, \ (\bar{x} \in (l + l_1)/L \sim 1) \tag{6-12}$$

where $\bar{x}$ is the non-dimensional expression of the position on the notched beam ($\bar{x} = \frac{x}{L}$), and $\overline{W_1}$ and $\overline{W_4}$ are the non-dimensional expression of the amplitude of the mode functions of the first and fourth sections of the beam ($\overline{W_1} = \frac{W_1}{L}, \overline{W_4} = \frac{W_4}{L}$). The non-dimensional governing equations for the second and third sections, which are bonded with piezoelectric patches, are given as follow:

$$\frac{d^4\overline{W_2}}{d\bar{x}^4} + \frac{P}{Q}\overline{\omega_n}^2\overline{W_2} = 0, \ (\bar{x} \in l/L \sim (l + l_1/2)/L) \tag{6-13}$$

$$\frac{d^4\overline{W_3}}{d\bar{x}^4} + \frac{P}{Q}\overline{\omega_n}^2\overline{W_3} = 0, \ (\bar{x} \in (l + l_1/2)/L \sim (l + l_1)/L) \tag{6-14}$$

where $\overline{W_2}=\frac{W_2}{L},\overline{W_3}=\frac{W_3}{L}$, $P=\frac{m'}{\rho Hb}$ and $Q=\frac{(EI)'}{EI}$. m' and $(EI)'$ are the equivalent mass and EI of sections 2 and 3. The expressions of m' and $(EI)'$ are written as:

$$\begin{aligned} m' &= \rho Hb + \rho' h_1 (b_s + b_a) \\ (EI)' &= E\left(\frac{(H-h_1)^3}{24}+\frac{(H+h_1)^3}{24}\right)b + E_p\left(\frac{(H-h_1)^3}{24}-\frac{(H+h_1)^3}{24}\right)(b_s+b_a) \end{aligned} . \quad (6\text{-}15)$$

From eqs. (6-11~6-14), the non-dimensional free vibration solutions of the notched beam bonded with piezoelectric patches can be obtained:

$$\begin{aligned} \overline{W_1} &= C_1\cos\sqrt{\overline{\omega_n}}\bar{x}+C_2\sin\sqrt{\overline{\omega_n}}\bar{x}+C_3\cosh\sqrt{\overline{\omega_n}}\bar{x}+C_4\sinh\sqrt{\overline{\omega_n}}\bar{x}(0\le\bar{x}\le l/L) \\ \overline{W_2} &= C_5\cos\sqrt{\overline{\omega_n}\left(\frac{P}{Q}\right)^{1/4}}\bar{x}+C_6\sin\sqrt{\overline{\omega_n}\left(\frac{P}{Q}\right)^{1/4}}\bar{x}+C_7\cosh\sqrt{\overline{\omega_n}\left(\frac{P}{Q}\right)^{1/4}}\bar{x}+C_8\sinh\sqrt{\overline{\omega_n}\left(\frac{P}{Q}\right)^{1/4}}\bar{x}(l/L\le\bar{x}\le(l+l_1/2)/L) \\ \overline{W_3} &= C_9\cos\sqrt{\overline{\omega_n}\left(\frac{P}{Q}\right)^{1/4}}\bar{x}+C_{10}\sin\sqrt{\overline{\omega_n}\left(\frac{P}{Q}\right)^{1/4}}\bar{x}+C_{11}\cosh\sqrt{\overline{\omega_n}\left(\frac{P}{Q}\right)^{1/4}}\bar{x}+C_{12}\sinh\sqrt{\overline{\omega_n}\left(\frac{P}{Q}\right)^{1/4}}\bar{x}((l+l_1/2)/L\le\bar{x}\le(l+l_1)/L) \\ \overline{W_4} &= C_{13}\cos\sqrt{\overline{\omega_n}}\bar{x}+C_{14}\sin\sqrt{\overline{\omega_n}}\bar{x}+C_{15}\cosh\sqrt{\overline{\omega_n}}\bar{x}+C_{16}\sinh\sqrt{\overline{\omega_n}}\bar{x}((l+l_1)/L\le x_4\le 1) \end{aligned} , \quad (6\text{-}16)$$

where C_1~C_{16} are unknown constants.

For the notched cantilever beam structure bonded with the piezoelectric layer given in Fig. 1, the non-dimensional expressions of boundary conditions of the 4 sections of the beam can be expressed as follow:

$$\begin{aligned} &\bar{x}=0:\overline{W_1}=0,\frac{d\overline{W_1}}{d\bar{x}}=0; \\ &\bar{x}=l/L:\overline{W_1}=\overline{W_2},\frac{d\overline{W_1}}{d\bar{x}}=\frac{d\overline{W_2}}{d\bar{x}},\frac{d^2\overline{W_1}}{d\bar{x}^2}=Q\frac{d^2\overline{W_2}}{d\bar{x}^2}+\frac{Me\cdot L}{EI},\frac{d^3\overline{W_1}}{d\bar{x}^3}=Q\frac{d^3\overline{W_2}}{d\bar{x}^3}; \\ &\bar{x}=(l+l1/2)/L:\overline{W_2}=\overline{W_3},\frac{d\overline{W_2}}{d\bar{x}}+\Theta\frac{d^2\overline{W_2}}{d\bar{x}^2}=\frac{d\overline{W_3}}{d\bar{x}},\frac{d^2\overline{W_2}}{d\bar{x}^2}=\frac{d^2\overline{W_3}}{d\bar{x}^2},\frac{d^3\overline{W_2}}{d\bar{x}^3}=\frac{d^3\overline{W_3}}{d\bar{x}^3}; . \\ &\bar{x}=(l+l1)/L:\overline{W_3}=\overline{W_4},\frac{d\overline{W_3}}{d\bar{x}}=\frac{d\overline{W_4}}{d\bar{x}},\frac{d^2\overline{W_4}}{d\bar{x}^2}=Q\frac{d^2\overline{W_3}}{d\bar{x}^2}+\frac{Me\cdot L}{EI},\frac{d^3\overline{W_3}}{d\bar{x}^3}=Q\frac{d^3\overline{W_4}}{d\bar{x}^3}; \\ &\bar{x}=1:\frac{d^2\overline{W_4}}{d\bar{x}^2}=0,\frac{d^3\overline{W_4}}{d\bar{x}^3}=0 \end{aligned} \quad (6\text{-}17)$$

Submitting eqs. (6-7) and (6-16) into the boundary conditions given by eq. (6-17) leads to sixteen linear equations, from which we can easily solve the *n*th non-dimensional resonance angular velocities of the notched cantilever beam bonded with the piezoelectric patches, $\overline{\omega_n}$, for a given feedback repair coefficient, *R*, depending on the eigan value problem. Submitting $\overline{\omega}_n$ back into eq. (6-17), the unknown constants, $C_1 \sim C_{16}$, and the according *n*th non-dimensional solutions of the normal mode expression of the beam, $\overline{W_1}(x,n) \sim \overline{W_4}(x,n)$, can be found.

The non-dimensional forced vibration solution of the notched cantilever beam bonded with piezoelectric layer shown in figure 1 can be expressed as,

$$\overline{w_{1\sim4}}(x,t) = \sum_{n=1}^{\infty} \overline{W_{1\sim4}}(x,n)\bar{q}(t,n), \tag{6-18}$$

where $\bar{q}(t,n)$ is the non-dimensional generalized coordinate in the *n*th mode. When a point force, $f(x, t) = \begin{cases} F\sin(\omega' t), x = L \\ 0, x \neq L \end{cases}$, is applied at the free end of the cantilever beam, we can obtain the vibration equation of the beam by submitting eq. (6-18) and the non-dimensional normal mode solutions, $\overline{W_1}(x,n) \sim \overline{W_4}(x,n)$, into the forced vibration equation,

$$\sum_{n=1}^{\infty} \frac{d^4 \overline{W_4}(\bar{x},n)}{d\bar{x}^4} \bar{q}(t,n) + \sum_{n=1}^{\infty} \overline{W_4}(\bar{x},n) \frac{d^2 \bar{q}(t,n)}{dt^2} = \overline{f}(\bar{x},t), \tag{6-19}$$

where $\overline{f}(\bar{x},t)$ is the non-dimensional point force applied on the free end of the beam $\overline{f}(\bar{x},t) = \overline{F}\sin(\omega' t) = \frac{f(x,t)L^3}{EI}$. Only $\overline{W_4}(\bar{x},n)$ is included in eq. (6-19) because the external load is zero on the first three sections of the beam. By multiplying eq. (6-19) throughout by $\overline{W_4}(\bar{x},m)$ $(m \neq N)$, integrating from 0 to 1, and using the orthogonality condition of the beam vibration, $\bar{q}(t,n)$ can be solved as,

$$\bar{q}(t,n) = \frac{\overline{F}\,\overline{W_4}(1,n)\sin(\omega' t)}{\rho H b \int_0^1 \overline{W_{1\sim4}}(x,n)dx(\omega_n^2 - \omega'^2)}, \tag{6-20}$$

Then, submitting eq. (6-20) into eq. (6-18), the final non-dimensional vibration solution of the piezoelectric bonded notched cantilever beam subjected to a dynamic force applied at its free end can be expressed as:

$$\overline{w_{1\sim4}}(x,t) = \sum_{n=1}^{\infty} \overline{W_{1\sim4}}(x,n) \frac{\overline{F}\,\overline{W_4}(1,n)\sin(\omega' t)}{\rho H b \int_0^1 \overline{W_{1\sim4}}(x,n)dx(\omega_n^2 - \omega'^2)}. \tag{6-21}$$

In numerical simulations, only the first three modes (n=1~3) are considered to get the vibration deflection of the piezoelectric bonded notched cantilever beam subjected to the dynamic loading with a low frequency. Submitting the solutions of the normal mode expression of the beam, $\overline{W_1}(x,n) \sim \overline{W_4}(x,n)$ (n=1~3), corresponding to a given repair coefficient, R, into eq. (6-15), we can obtain the vibration deflection of the piezoelectric bounded notched beam. The relationship between the repair coefficient and the slop of the vibration deflection of the beam can thus be found accordingly, and an optimal coefficient can thus be identified. In the simulations in Fig. 6-2, the amplitude and angular velocity of the non-dimensional dynamic external force are assumed to be 0.2 and 0.03, respectively ($\overline{F}$ =0.2, $\overline{\omega}'$ =0.03). Figure 6-2 shows the largest non-dimensional slop discontinuities at the notch position of the beam during vibrations versus the repair coefficients. It can be seen that the non-dimensional slop discontinuity at the notch position approaches to zero with the repair coefficient of 366.6. From eq. (6-7), the required gain factor, g, can thus be found for the repair of the notched beam given certain dimensions and material properties of the piezoelectric patches. Finally the actuation voltage is obtained from eq. (6-5).

6.2 FEM simulations

An FEM model is built by Ansys 10.0 to verify the feedback repair of the notched cantilever beam. The structure dimensions and material properties of the notched beam and the piezoelectric layer are given in table 6-1. A transversal dynamic point force with an angular velocity of 1000 rad/s is applied at the free end of the cantilever beam. The amplitude of the point force at the free end of the beam is set as 20N. Normal plane element plane42 and coupled field element plane223 are used to mesh the notched host beam structure and the piezoelectric layer, respectively. From eq. (6-7) and the required repair coefficient given in Fig. 6-2, the satisfied gain factor, *g*, can be found given the structural dimensions and the material properties in table 6-1.

Fig. 6-3 illustrates the Von Mises stress distribution around the notch tip at 0.356s of the vibration of the notched cantilever beam before and after repair. It can be seen that the Von Mises stress at the notch tip point O is decreased from 9.5 MPa to 0.4 MPa, when the gain factor is set as 74, which is provided by the analytical model. 95.8% reduction of the stress singularity can be found at the notch tip of the beam after repair. The effectiveness of the analytical model is hence proven by the FEM simulation.

6.3 Experimental realization of the structural repair

Experimental studies on the feedback repair are carried out based on the electromechanical effect of the piezoelectric material. Fig. 6-4 shows the piezoelectric actuator and sensors mounted on the opposite surface of the notch area of the beam. The width of the notch beam is 0.03m. The piezoelectric actuator and piezoelectric sensor ‘A’ are with the same length of 0.06m and width

of 0.01m. The width and length of the piezoelectric sensor ‘B’ is 0.007m and 0.01m, respectively. A large piezoelectric sensor ‘A’ is used to measure the vibration of the beam around the notch area and generate a large output voltage and the corresponding actuation voltage with reasonable gain factor. The small piezoelectric sensor ‘B’ is mounted just above the notch position to provide an accurate measurement of the slop difference between the two sides of the notch to show the effectiveness of the repair strategy. A final actuation voltage on the piezoelectric actuator can be obtained when the output voltage from piezoelectric sensor ‘B’ approaches to zero.

6.3.1 Experiment setup

Fig. 6-5 gives the experiment setup of the notched beam bonded with the piezoelectric patches. The dimensions and material properties of the notched beam and the piezoelectric patches are given in table 6-1. An aluminum notched beam bonded with piezoelectric patches is fixed on a clamping apparatus, and a steady sinusoidal force excitation is applied at the right end of the cantilever beam by a shaker provided by The Modal Shop INC. (Model 2100E11 100 lbf Modal Shaker). It is noted that the boundary conditions will affect the vibration frequency of the cantilever beam significantly. Thus, the boundary at the fixed end of the beam should be stable enough to get the accurate experiment results. An adjustable operational amplifier, whose gain is variable from 0 to 120, is employed to provide the adaptable gain factor to the output voltage from the surface of the piezoelectric sensor ‘A’. As shown in Fig. 6-4, the aluminum beam bonded with piezoelectric patches is ground connected, and the surface of the piezoelectric sensor ‘A’ is connected with the input pad of the operational amplifier while the output pad of the operational amplifier is connected to the surface of the piezoelectric actuator to build the

feedback repair circuit. The voltage signal from the surface of the piezoelectric sensor ‘B’ is captured by the oscilloscope software provided by LMS International to illustrate the repair effect of the feedback repair.

6.3.2 Observations and discussions

When a steady sinusoidal force excitation is applied to the free end of the cantilever beam, the dynamic voltage signal representing the bending of the vibrating beam is generated on the piezoelectric sensors. The output voltages from the piezoelectric sensors ‘A’ and ‘B’ and the actuation voltages applied to the piezoelectric actuator with the different gain factors are shown in Fig. 6-6. The angular velocity and the amplitude of the sinusoidal force excitation are set to be 1000rad/s and 0.02N, respectively. The overview data on time points 1 and 3 given by the oscilloscope illustrate the voltage signal from the piezoelectric sensor ‘A’ and ‘B’, respectively. The actuation voltage applied to the piezoelectric actuator is shown by the data of the time point 2. The output voltage generated on the piezoelectric sensor ‘B’ is used as the criterion to evaluate the repair efficiency.

From Fig. 6-6 (a), it can be seen that the amplitude of the output voltage generated on the piezoelectric sensor ‘B’ is 1.2e-2V when there is no actuation voltage applied to the piezoelectric actuator, or before repair is conducted. When the gain factor applied to the output voltage from the piezoelectric sensor ‘A’ is set to be 60, amplitude of the actuation voltage of 1.1e-1V is generated and applied to the piezoelectric actuator, and the output voltage from the piezoelectric sensor ‘B’ approaches to zero, shown in Fig. 6-6 (b). At this state, the slop discontinuity on the notch position is removed and the notch effect is removed accordingly, and the repair of the notched beam using the feedback actuated piezoelectric patches is proven to be efficient and

practical experimentally. As the gain factor is increased to 85, the amplitude of the actuation voltage becomes 1.3e-1V, but the amplitude of the output voltage on the piezoelectric sensor 'B' is found to grow back to 1.8e-3V shown in Fig. 6-6 (c). It can be concluded from Fig. 6-6 that the notch can be fully repaired when the gain factor increases to a certain value, but a re-growth of the discontinuity of the slop difference between the two sides of the notch will be found for larger gain factors. The repair is fulfilled only with a certain value of the gain factor. This observation matches the result given by the analytical model.

Fig. 6-7 illustrates the slop discontinuities at the notch position from the analytical simulation and the amplitude of the output voltage generated on the piezoelectric sensor 'B' given by the experimental studies versus the gain factors. It can be seen that the interpolation curve of the experimental data is in agreement with the analytical result. When the gain factor is set to be 74, which is the gain factor provided by the analytical model, the output voltage of piezoelectric sensor B will be reduced to 7e-4 V, which is 5.8% of the reading of the sensor before repair. The analytical model can provide a good guidance and consultation for the design of the practical repair strategy.

6.4 Conclusions

A feedback repair process for a notched cantilever beam structure subjected to a dynamic loading by the use of piezoelectric patches is proposed and realized experimentally. The electromechanical effect of the piezoelectric material is employed to induce a repair bending moment on both sides of the notch with an actuation voltage to reduce the stress singularity at the notch tip. An analytical model is established for the design of the feedback repair strategy for the notched cantilever beam structure subjected to the dynamic loading, and then an FEM is

conducted to verify the efficiency of the design of the repair strategy. Compared with the notched beam before repair, the stress singularity at the notch tip of the beam after repair is found to be reduced by 95.8% in the FEM simulation. In addition, experiments are carried out to study the feedback repair of the notched beam. A small piezoelectric sensor mounted above the notch position is employed to provide an accurate measurement of the reduction of the slop discontinuity at the notch. In experiment studies, the slop discontinuity at the notch position approaches to zero when the designed gain factor is applied. The notched beam is proved to be fully repaired experimentally. When the gain factor is set to be a value given by the analytical model, the slope discontinuity at the notch position is reduced by approximately 95% from experiments. The results from analytical model and the experimental studies are coincided with each other well. The feedback repair of the notched beam using piezoelectric patches is proven to be efficient and practical through both numerical simulations and experimental studies.

Table 6- 1 Material and geometric properties of the piezoelectric coupled beam.

Parameters	Notched Host Beam (Aluminum)	Piezoelectric patches (PZT4)
Young's module (N/m^2)	$E = 69\times10^9$	$E_p=78\times10^9$
Mass density (kg/m^3)	2.8×10^3	7.5×10^3
e_{31} (C/m^2)	–	-2.8
d_{31} (C/N)	–	-1.28×10^{-10}
Cv (nF)	–	0.75 for the piezoelectric patch with the dimension of 0.01m×0.06m×0.0003m
L (m)	0.365	–
l_1 (m)	–	0.06
H(m)	0.003	–
h_1(m)	–	0.0003
l (m)	0.03	–
de (m)	0.0018	–
b(m)	0.03	–
b_s(m)	–	0.01
b_a(m)	–	0.01

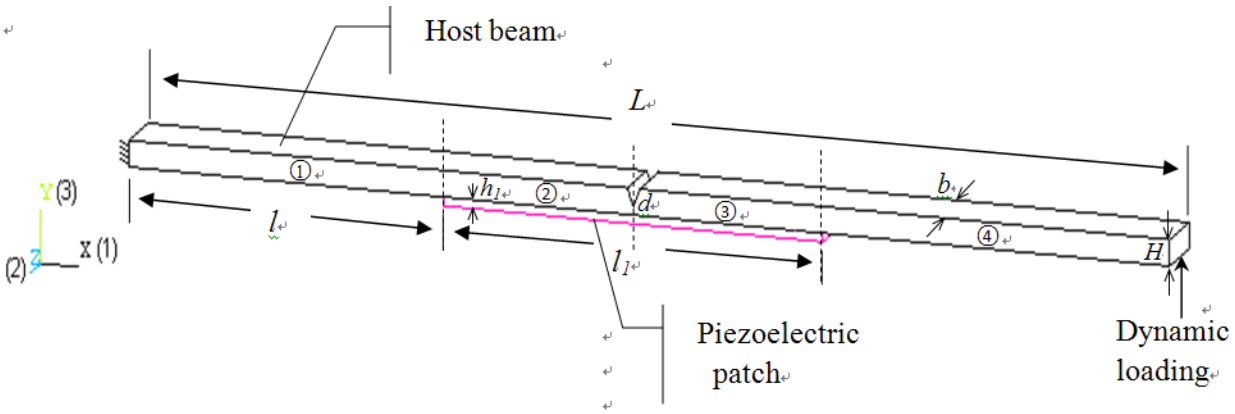

Fig. 6- 1 A notched cantilever beam bonded with a piezoelectric layer subjected to a dynamic loading.

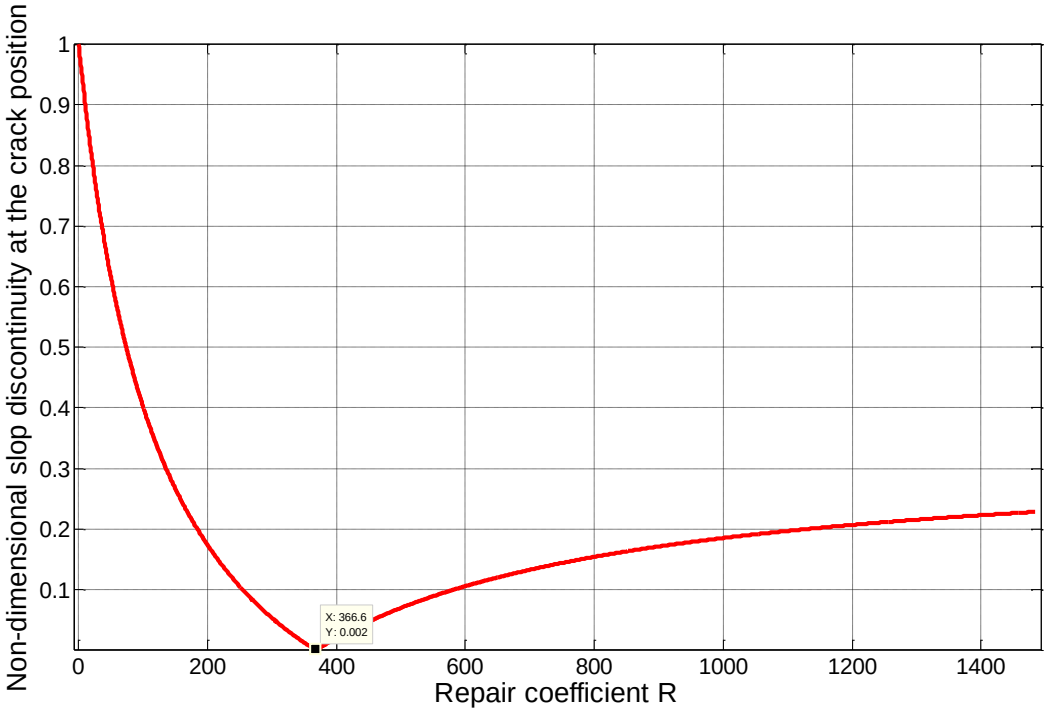

Fig. 6- 2 Variation of the largest slop discontinuity at the notch position during vibration versus the repair coefficient from eq. (6-7).

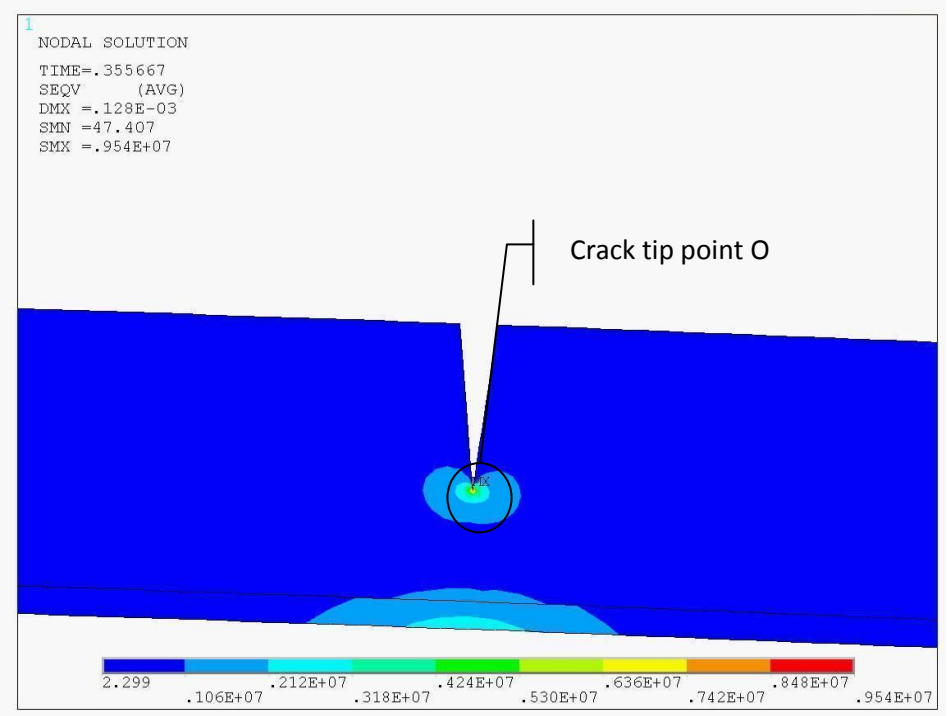

(a)

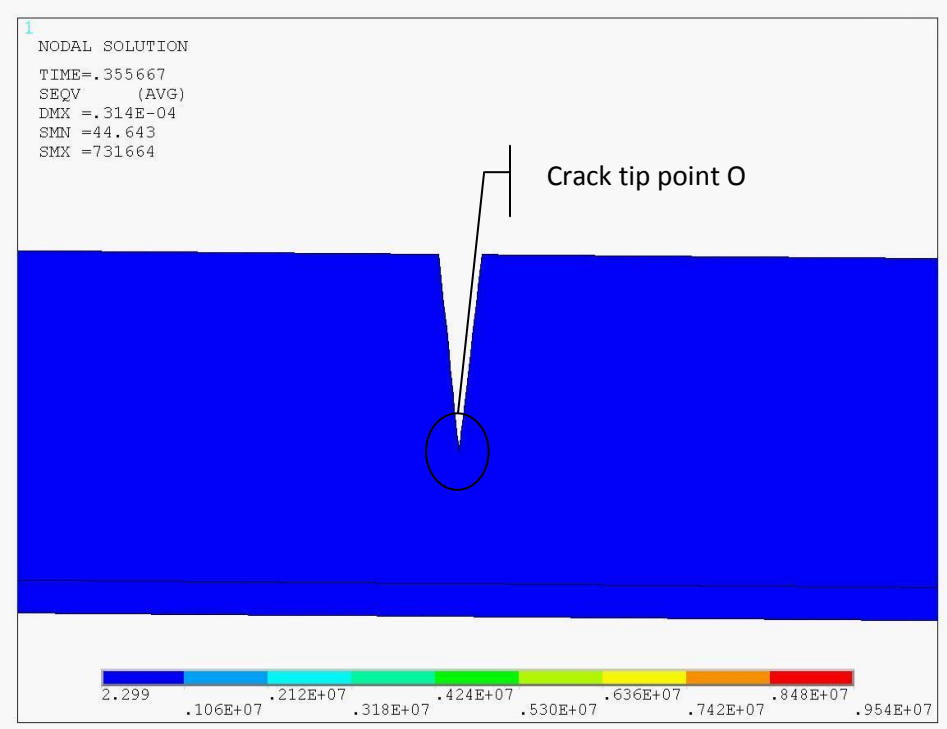

(b)

Fig. 6- 3 Von Mises stress distribution at the notch position of the vibrating cantilever beam with the given dimensions and material properties in table 1 at (a) gain factor=0 and (b) gain factor=74.

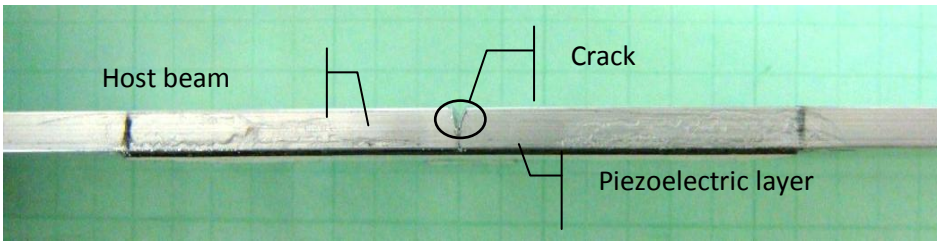

(a) Front view of the notched beam and the piezoelectric layer

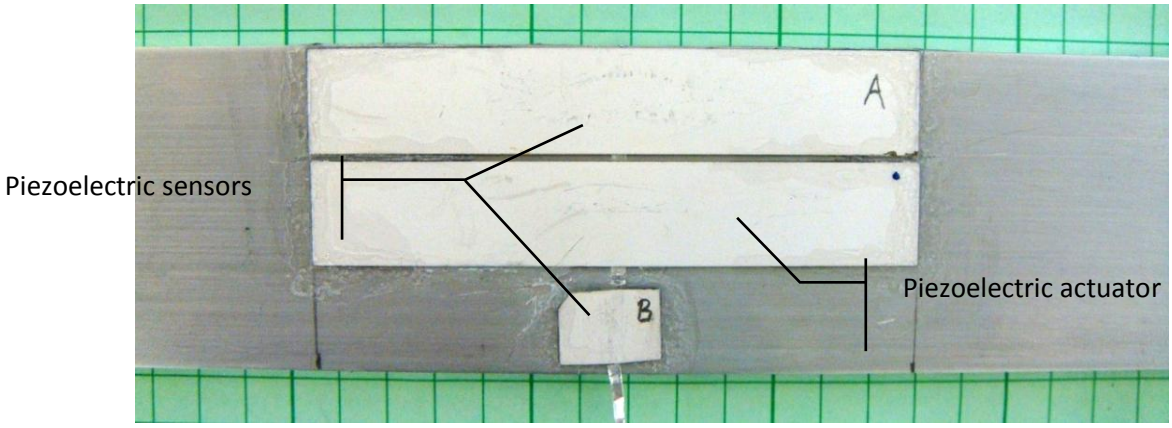

(b) Bottom View of the piezoelectric sensors and actuator

Fig. 6- 4 (a) The notched beam and piezoelectric layer, (b) The piezoelectric sensors and actuator bonded above the notch area.

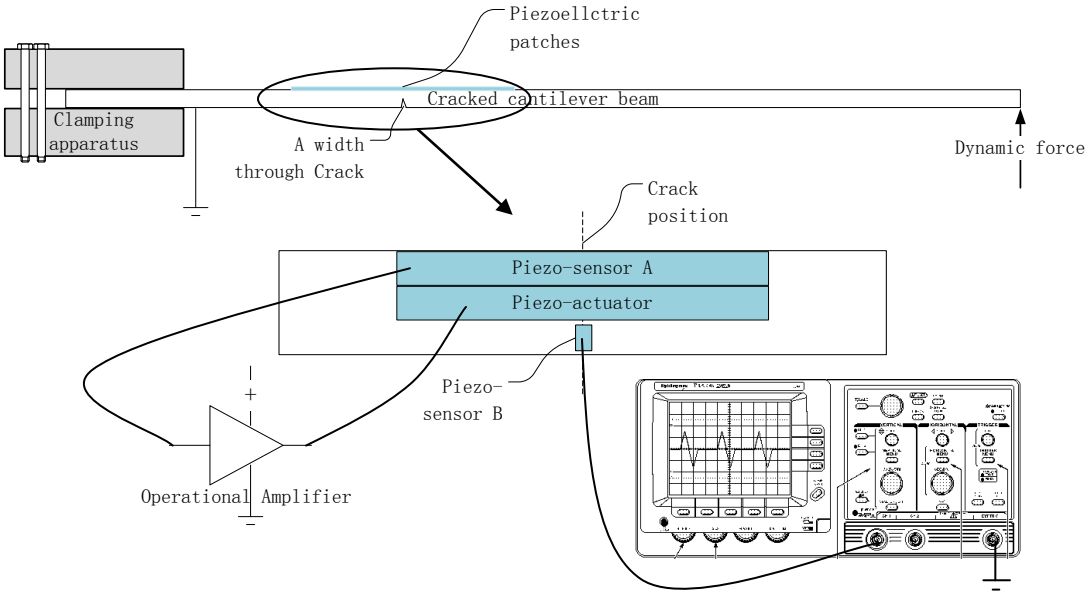

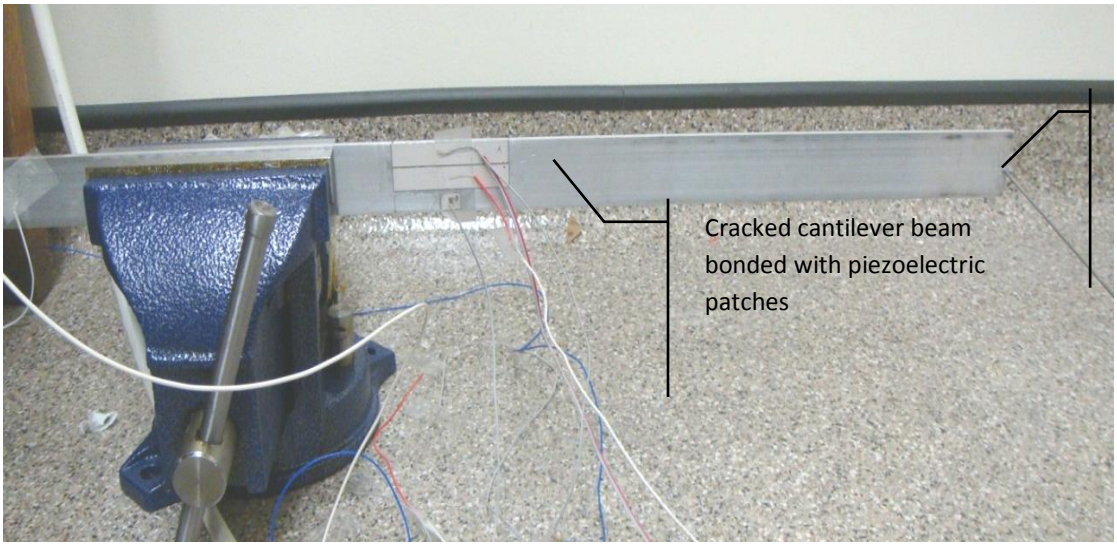

Fig. 6- 5 Experiment set up.

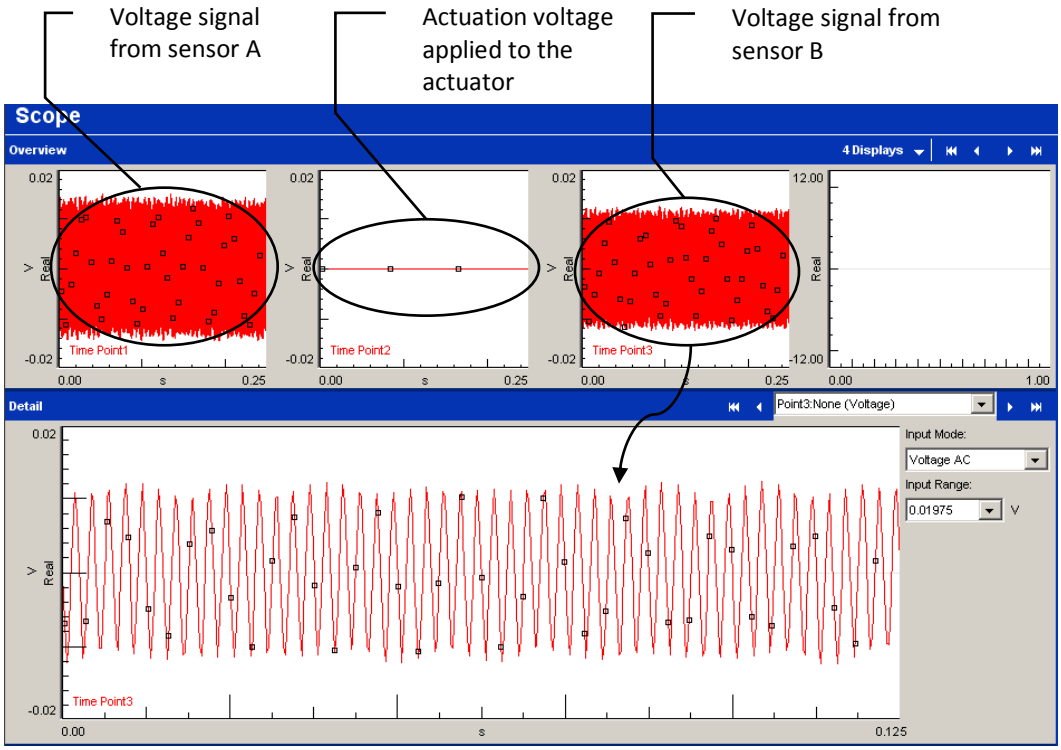
Voltage signal from sensor A
Actuation voltage applied to the actuator
Voltage signal from sensor B
Scope
Overview
4 Displays
Time Point1
Time Point2
Time Point3
Detail
Point3:None (Voltage)
Input Mode:
Voltage AC
Input Range:
0.01975
V

(a)

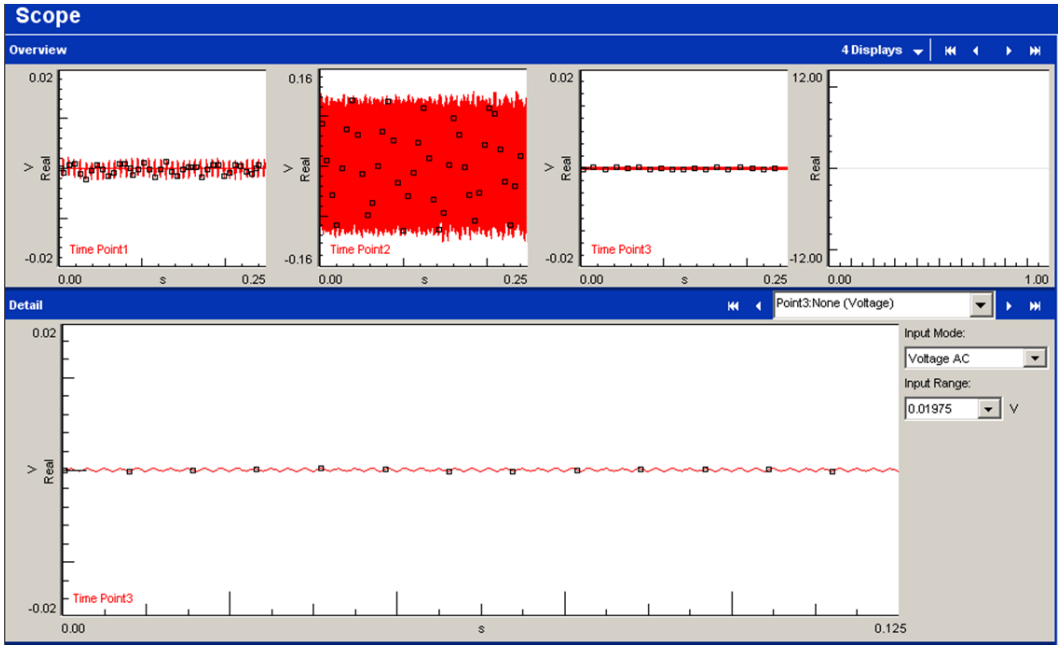
Scope
Overview
4 Displays
Time Point1
Time Point2
Time Point3
Detail
Point3:None (Voltage)
Input Mode:
Voltage AC
Input Range:
0.01975
V

(b)

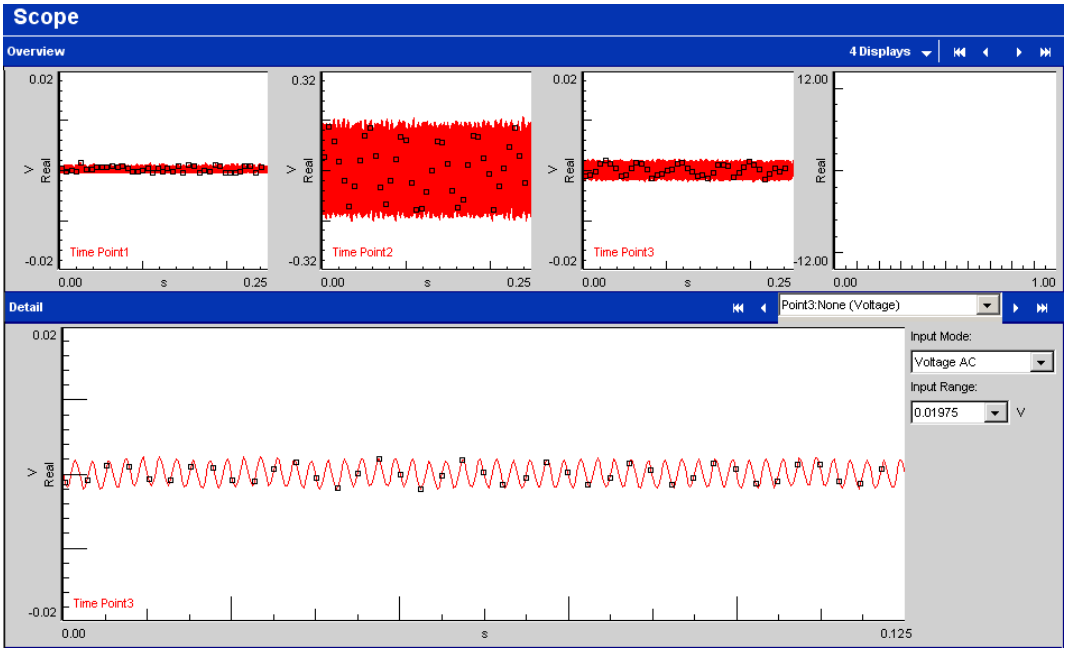

(c)

Fig. 6- 6 Vibration signals from the oscilloscope for the structure in table 1: (a) vibration signal of the beam before repair, (b) vibration signal with the gain factor of 60, (c) vibration signal with the gain factor of 85.

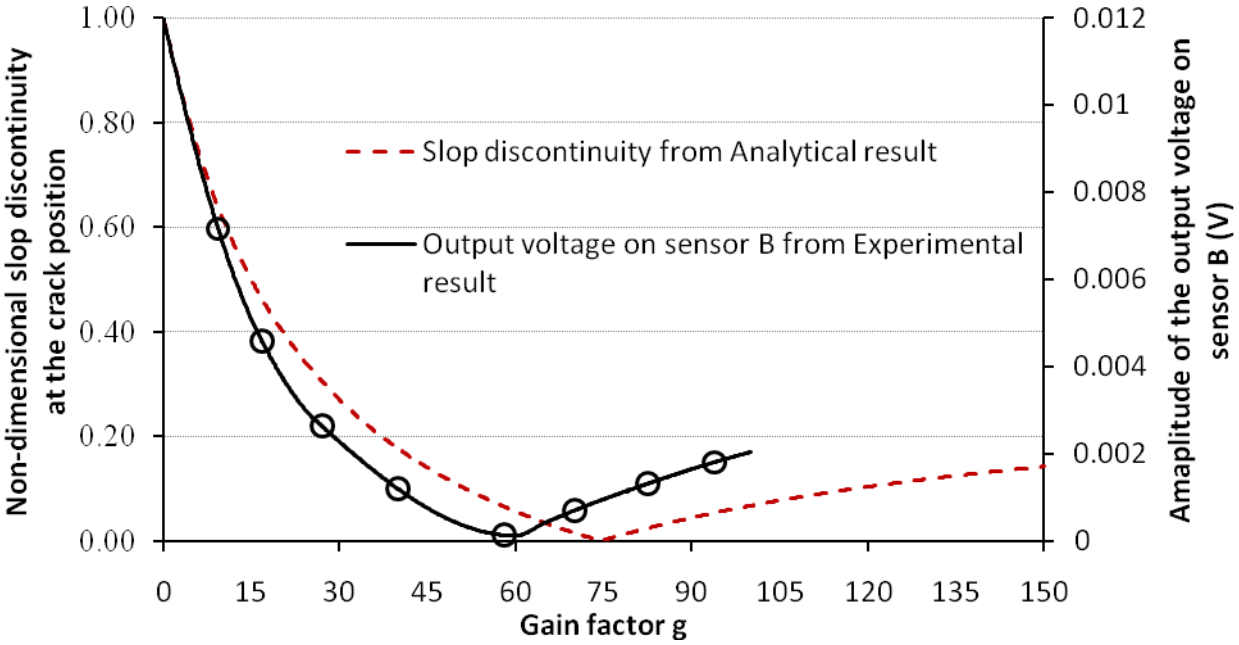

Fig. 6- 7 Comparison of the repair effect versus gain factors given by experiment studies and analytical simulations.

7 Conclusions and future work

In this thesis, the review of the wave propagation and vibration of piezoelectric coupled structures and the structural repair via piezoelectric materials is done first. The studies of wave propagation and vibration of piezoelectric coupled structures with an open circuit electrical boundary condition are followed. The numerical simulation of the shear horizontal (SH) wave propagation in an infinite metal plate surface bonded by a piezoelectric layer is proposed, and the mechanical model for the vibration analysis of a piezoelectric coupled circular plate with the open electrical circuit boundary condition is developed. Electric potential distributions within piezoelectric materials for different piezoelectric coupled structures found in studies of the dynamic responses of piezoelectric coupled structures will provide a guidance on the design of the structural repair via piezoelectric materials.

The main contribution of this research is to propose different design methods for the structural repair of different damages on different engineering structures. Following the studies of the dynamic responses of the piezoelectric coupled structures, a close-loop feedback control repair methodology for a vibrating delaminated beam structure by use of piezoelectric patches is proposed. An analytical model of a piezoelectric coupled delaminated beam structure is provided and verified by FEM. Moreover, a delaminated plate is repaired by piezoelectric patches with distributed electrodes using extra repair voltages applied to different electrodes. The analytical model of the delaminated plate under a static loading is given, results of repair voltages are

solved based on different geometries of the delamination. FEM of the piezoelectric coupled delaminated plate with contact analysis is employed to prove the efficiency of the proposed analytical model and repair method. In addition, an accurate analytical model and FEM simulations with a new repair criterion, which is defined as the slop discontinuity at the notch position, is conducted for the repair of a notched/cracked beam structure. The repair process of a notched beam structure under dynamic loading using the piezoelectric material is proved to be efficient through experimental studies. In summary, from research work during my PhD study, the active structural repair method using piezoelectric patches is realized and proved to be feasible and practical depending on both numerical simulations and experimental studies.

However, my investigations and conversations with other people working in the research field of piezoelectric materials have also lead to a number of interesting questions. Future research will continue to further advance the techniques of the damage detection and structure repair based on smart materials and structures. First, the damage detection of plate structures with the technique using spacial wavelet transforms has not been tested. The detection of multiple collocated delaminations in a composite structure is another challenge of the proposed damage detection technique. This research will be very interesting if the internal stress singularity at the damaged part can be detected from the output electric signal from the piezoelectric fiber, which is embedded inside the composite structures. Second, the repair technique is desired to be improved for its application on composite structures with multiple delaminations, as the surface bonded piezoelectric patches used in my previous studies can only be feasible for the repair of a single delamination. In addition, analytical models, FEM and experimental studies presented by my previous researches were mainly designed for the repair of

isotropic substances. The study on composite materials reinforced by piezoelectric stacks and piezoelectric fibers will be an important research topic in the future.

The research of the piezoelectric fiber reinforced composite materials is still in an initial stage. The application of smart fibers (e.g. piezoelectric fibers) on the active structure repair is a blank research field and opens a new leading-edge research topic for the structural stability enhancement and repair. Further experiments on piezoelectric fiber reinforced composite structures are desired to study the effects of the piezoelectric fibers on the mechanical property of composite structures.

Bibliography

Alaimo A., Milazzo A. and Orlando C., Boundary elements analysis of adhesively bonded piezoelectric active repair, *Engineering Fracture Mechanics* **76** (2009) 500-511.

Ariaei A., Ziaei-Rad S. and Ghayour M., Repair of a cracked Timoshenko beam subjected to a moving mass using piezoelectric patches, *International Journal of Mechanical Sciences* **52** (2010) 1074-1091.

Bailey T. and Hubbard J.E., Distributed Piezoelectric Polymer Active Vibration Control of A Cantilever Beam, *J. Guidance Control Dyn* **8** (1985) 605-611.

Baker A.A. and Jones R., Bonded Repair of Aircraft Structure, (Dordrecht: Martinus Nijhoff), 1988.

Baker A.A., Rose L.R.F. and Jones R., Advances in the Bonded Composite Repair of Metallic Aircraft Structure (Amsterdam: Elsevier) 2002.

Baumhaue J.C. and Tiersten H.F., Nonlinear electroelastic equations for small fields superposed on a bias, *Journal of The Acoustical Society of America* **54** (1973) 1017-1034.

Beck M., Die Knicklast des einseitig eingespannten tangential gedruckten stabes, *Z. Angew. Math. Phys.* **3 (**1952).

Bent A.A., HagoodN.W., RodgersJ.P., Anisotropic actuation with piezoelectric fiber composites, *Journal of Intelligent Material Systems and Structures* **6** (1995) 338-349.

Bleustein J.L., Some simple modes of wave propagation in an infinite piezoelectric plates, *Journal of Acoustics Society of America* **45** (1969) 614-620.

Chattopadhyay A., Dragomir-Daescu D. and Gu H.Z., Dynamics of delaminated smart composite cross-ply beams, *Smart Mater. Struct.* **8** (1999) 92-99.

Chattopadhyay A., Gu H.Z., Dragomir-Daescu D., Dynamics of delaminated composite plates with piezoelectric actuators, *AIAA Journal* **37** (1999) 248-254.

Chee C.Y.K., Tong L.Y. and Steven G.P., A review on the modeling of piezoelectric sensors and actuators incorporated in intelligent structures, *Journal of Intelligent Material Systems and Structures* **9** (1998) 3-19.

Cheng N.C. and Sun C.T., Wave propagation in two-layered piezoelectric plates, *Journal of Acoustics Society of America* **57** (1975) 632-638.

Chevallier G., Ghorbel S. and Benjeddou A., A benchmark for free vibration and effective coupling of thick piezoelectric smart structures, *Smart Materials and Structures* **17** (2008) 065007.

Chrysochoidis N.A. and Saravanos D.A., Assessing the effects of delamination on the damped dynamic response of composite beams with piezoelectric actuators and sensors, *Smart Mater. Struct.* **13** (2004) 733–742.

Chue C.H., Chang L.C. and Tsai J.S., Bonded repair of a plate with inclined central crack under biaxial loading, *Composite Structures* **28** (1994) 39–45.

Corr L.R. and Clark W.W., Comparison of low-frequency piezoelectric switching shunt techniques for structural damping, *Smart Materials and Structure*s **11** (2002) 370-376.

Crawley E. F. and Deluis J., Use of piezoelectric actuators as elements of intelligent structures, *AIAA Journal* **25** (1987) 1373-1385.

Crawley E.F. and Anderson E., Detailed model of piezoelectric actuation of beams *Proceedings of 30th AIAA/ASME/SAE Structures, Structural Dynamics, and Material Conference*, Washington DC, 2000-2010, 1989.

Curtis R.G. and Redwood M., Transverse surface waves in piezoelectric materials carrying a metal layer of finite thickness, *Journal of Applied Physics* **44** (1973) 2002-2007.

Czabaj M.W., Zehnder A.T. and Chuang K.C., Blistering of moisture saturated graphite/polyimide composites due to rapid heating, *Journal of Composite Materials* **43** (2009) 153~174.

Davis C.L. and Lesieutre G.A., An actively tuned solid-state vibration absorber using capacitive shunting of piezoelectric stiffness, *Journal of Sound and Vibration* **232** (2000) 601-617.

De Faria A.R., On buckling enhancement of laminated beams with piezoelectric actuators via stress stiffening, *Composite Structures* **65** (2004) 187-192.

De Faria A.R. and Donadon M.V., The use of piezoelectric stress stiffening to enhance buckling of laminated plates, *Latin American Journal of Solids and Structures* **7** (2010) 167-183.

De Faria A.R. and Almeida S.F., Enhancement of pre-buckling behavior of composite beams with geometric imperfections using piezoelectric actuators, *Composites Part B: Engineering* **30** (1999) 43-50.

Delia C.N. and Shu D.W., Vibration of delaminated composite laminates: A review, *Applied Mechanics Reviews* **60** (2007) 1-20.

Ding H., Xu R. and Chen W., Exact Solutions for Free Vibration of Transversely Isotropic Piezoelectric Circular Plates, *Chinese Journal of Mechanics Press* **16** (2000) 141-147.

Duan W.H., Quek S.T. and Wang Q., Finite element analysis piezoelectric-based repair of a delaminated beam, *Smart Mater. Struct.* **17** (2008) 015017.

Duan W.H., Quek S.T. and Wang Q., Free vibration analysis of piezoelectric coupled thin and thick annular plate, *Journal of Sound and Vibration* **281** (2005) 119-139.

Ehlers S.M. and Weisshaar T.A., Static aeroelastic behavior of an adaptive laminated piezoelectric composite wing, *31st AIAA/ASME/ASCE/AHS/ASC Structures, Structural Dynamics and Materials Conference* Long Beach, CA, USA, 1990.

Etches J.A., Scholey J.J., Williams G.J., Bond I.P., Mellor P.H., Friswell M.I. and Lieven N.A., Exploiting Functional Fibers in Advanced Composite Materials, *Journal of Intelligent Material Systems and Structures* **18** (2006) 449-458.

Guillon O., Thiebaud F., Delobelle F. and Perreux D., Tensile behaviour of PZT in short and open-circuit conditions, *Materials Letters* **58** (2004) 986-990.

Heyliger P. and Saravanos D.A., Exact free vibration analysis of laminated plates with embedded piezoelectric layers, *Journal of Acoustic Society of America* **98** (1995) 1547-1557.

Heyliger P.R. and Ramirez G., Free vibration of laminated circular piezoelectric plates and discs, *Journal of Sound and Vibration* **229** (1999) 935-956.

Ihn J.B. and Chang F.K., Detection and monitoring of hidden fatigue crack growth using a built-in piezoelectric sensor/actuator network: II. Validation using riveted joints and repair patches, *Smart Materials and Structures* **13** (2004) 621-630.

Jaffe B., Cook W.R. and Jaffe H., Piezoelectric Ceramics, Academic Press New York (1971).

Jin J., Excitation and propagation of elastic waves by inter-digital transducer for non-destructive evaluation of plates, A Ph. D thesis National University of Singapore (2003).

Jones R. and Callinan R.J., A design study in crack patching, Fibre Science and Technology 14 (1981) 99–111.

K.T. Chang, M. Ouyang, Open-circuit test of a PZT vibrator and its applications, *Journal of Intelligent Material System and Structures* **11** (2002) 263-271.

Kapuria S., Dumir P.C. and Ahmed A., An efficient coupled layerwise theory for dynamic analysis of piezoelectric composite beams, *Journal of Sound and Vibration* **261** (2003) 927-944.

Kim J., Varadan V.V., Varadan V.K., and Bao X.Q., Finite element modeling of a smart cantilever plate and comparison with experiments, *Smart Materials and Structures* **5** (1996) 165-170.

Kitamura T., Hirakata H. and Itsuji T., Effect of residual stress on delamination from interface edge between nano-films, Eng. Fract. Mech. 70 (2003) 2089–101.

Krawczuk M. and Ostachowicz W.M., Modeling and vibration analysis of a cantilever composite beam with a transverse open crack, *J. Sound Vib.* **183** (1995) 69–89.

Lee C.K. and Moon F.C., Modal sensors and actuators, *J. Appl. Mech.* **57** (1990) 434–441.

Leibowitz and Vinson, The use of Hamilton's principle in laminated piezoelectric and composite structures, *Adaptive Structures and Material Systems* (2003) AD-35.

Li S., Wang J. and Thouless M.D., The effects of shear on delamination in layered materials, J. Mech. Phys. Solids 52 (2004) 193–214.

Liew K.M., He X.Q. and Kitipornchai S., Finite element method for the feedback control of FGM shells in the frequency domain via piezoelectric sensors and actuators, *Computer Methods in Applied Mechanics and Engineering* **193** (2004) 257-273.

Liew K.M., He X.Q., Ng T.Y. and Kitipornchai S., Active control of FGM shells subjected to a temperature gradient via piezoelectric sensor/actuator patches, *International Journal for Numerical Methods in Engineering* **55** (2002) 653-668.

Liew K.M., Lim H.K., Tan M.J. and He X.Q., Analysis of laminated composite beams and plates with piezoelectric patches using the element-free Galerkin method, *Computational Mechanics* **29** (2002) 486-497.

Lin C.C. and Hsu C.Y., Static shape control of smart beam plates laminated with sine sensors and actuators, *Smart Mater. Struct.* **8** (1999) 519–530.

Liu T., Fracture mechanics and crack contact analyses of the active repair of multi-layered piezoelectric patches bonded on cracked structures, *Theoretical and Applied Fracture Mechanics* **47** (2007) 120-132.

Liu T., Crack repair performance of piezoelectric actuator estimated by slope continuity and fracture mechanics, *Engineering Fracture Mechanics* **75 (**2008) 2566-2574.

Liu W.Q., Feng Z.H., Liu R.B. and Zhang J., The influence of preamplifiers on the piezoelectric sensor's dynamic property, *Review of Scientific Instruments* **78** (2007) article number: 125107.

Liu X., Free vibration of thin and thick piezoelectric coupled circular plates, A Thesis for The Degree of Master of Engineering, National University of Singapore, 2001.

Lowe P.G., Basic Principles of Plate Theory, (Scotland: Surry University Press) 1982.

Massabo R. and Cox B.N., Concepts for bridged mode II delamination cracks, *J. Mech. Phys. Solids* **47** (1999) 1265–1300.

Meressi T. and Paden B., Buckling Control of A Flexible Beam Using Piezoelectric Actuators, *Journal of Guidance Control and Dynamics* **16** (1993) 977-980.

Mindlin R.D., Forced thickness-shear and flexural vibrations of piezoelectric crystal plates, *Journal of Applied Physics* **23** (1951) 83-88.

Mukherjee A. and Chaudhuri A., Active control of dynamic instability of piezolaminated imperfect columns, *Smart Materials and Structures* **11** (2002) 847-879.

Mukherjee A. and Chaudhuri A., Nonlinear dynamic response of piezolaminated smart beams, *Computers & Structures* **83** (2005a) 1298-1304.

Mukherjee A. and Chaudhuri A., Active control of piezolaminated columns—exact solutions and experimental validation, *Smart Materials and Structures* **14** (2005b) 475-482.

Nelson D.F., Theory of non-linear electro-acoustics of dielectric, piezoelectric, and pyroelectric crystals, *Journal of The Acoustical Society of America* **63** (1978)1738-1748.

Nilsson K.F., Asp L.E., Alpman J.E. and Nystedt L., Delamination buckling and growth for delaminations at different depths in a slender composite panel, *Int. J. Solids Struct.* **38** (2001) 3039–3071.

ODI R. A., C. M. Friend, A Comparative Study of Finite Element Models for the Bounded Repair of Composite Structure, *Journal of Reinforced Plastics and Composites* **21** (2002) No. 4.

Otsuka K. and Wayman C.M., *Shape Memory Materials* (Cambridge: Cambridge University Press) 1999.

Ouinas D., Bachir Bouiadjra B., Achour B. and Benderdouche N., Modeling of A Cracked Aluminum Plate Repaired with Composite Octagonal Patch in Mode I and Mixed Mode, *Materials and Design* **30** (2009) 590–595.

Pan E. and Heyliger P., Free vibration of simply supported and multilayered magneto-electro-elastic plates, *Journal of Sound and Vibration* **252** (2002) 429-443.

Paradies R. and Schlapfer B., Finite Element Modeling of Piezoelectric Elements with Complex Electrode Configuration, *Smart Materials and Structures* **18** (2009) No. 025015.

Parton V.Z. and Kudryavtser B.A., Electromagnetoelasticity New York: Gordon & Breach Science Publishers (1988).

Platz R., Stapp C. and Hanselka H., Statistical approach to evaluating reduction of active crack propagation in aluminum panels with piezoelectric actuator patches, *Smart Materials and Structures* **20** (2011) 085009.

Quek S.T. and Wang Q., On dispersion relations in piezoelectric coupled plate structures, *Smart Materials and Structures* **9** (2000) 859-867.

Rabinovitch O., Piezoelectric Control of Edge Debonding in Beams Strengthened with Composite Materials: Part I - Analytical Modeling, *Journal of Composite Materials* **41** (2007c) 525-546.

Rabinovitch O., Piezoelectric Control of Edge Debonding in Beams Strengthened with Composite Materials: Part II - Failure Criteria and Optimization, *Journal of Composite Materials* **41** (2007d) 657-677.

Robbins D.H. and Chopra I., Modeling of progressive damage in the adhesive bond layers of actuated plates, *Journal of Intelligent Material Systems and Structures* **18** (2007) 893-921.

Sheinman I., Kardomateas G.A. and Pelegri A.A., Delamination growth during pre-and post-buckling phases of delaminated composite laminates, *Int. J. Solids Struct.* **35** (1998) 19–31.

Sinitses G.J., Sallam S. and Yin W.L., Effect of delamination of axially loaded homogeneous laminated plates, *AIAA Journal* **23** (1985) 1437-1444.

Sprenger W., Gruttmann F. and Wagner W., Delamination growth analysis in laminated structures with continuum-based 3D-shell elements and a viscoplastic softening model, *Comput. Methods Appl. Mech. Eng.* **185** (2000) 123–139.

Suiker A.S.J. and Fleck N.A., Modelling of fatigue crack tunneling and delamination in layered composites, *Composites A* **37** (2006)1722–1733

Sun C.T. and Zhang X.D., Use of thickness shear mode in adaptive sandwich structures, *Smart Material and Structures* **4** (1995) 202-206.

Sun C.T., Klug J. and Arendt C., Analysis of cracked aluminum plates repaired with mounted composite patches, *AIAA J.* **34** (1996) 369–374.

Sun D.C., Wang D.J., Xu Z.L. and Wu H.X., Distributed piezoelectric element method for vibration control of smart plates, *AIAA Journal* **37** (1999) 1459–1463.

Tay T.E., Tan V. and Deng M., Element-failure concepts for dynamic fracture and delamination in low-velocity impact of composites, Int. J. Solids Struct. 40 (2003) 555–571.

Tiersten H.F., Linear piezoelectric plate vibration, Plenum Press, New York, 1969.

Tiersten H.F., Thickness vibrations of piezoelectric, *Journal of Acoustics Society of America* **35** (1963c) 53-58.

Tiersten H.F., Wave propagation in an infinite piezoelectric plate, *Journal of Acoustics Society of America* **35** (1963d) 234-239.

Todoroki A. and Ueda M., Low-cost delamination monitoring of CFRP beams using electrical resistance changes with neural networks, *Smart Mater. Struct.* **15** (2006) 75–84.

Todoroki A., Tanaka M. and Shimamura Y., High performance estimations of delamination of graphite/epoxy laminates with electric resistance change method Compos., Sci. Technol. 63 (2003) 1911–1920.

Turon A., Camanho P.P., Costa J. and Davila C.G., A damage model for the simulation of delamination in advanced composites under variable-mode loading, Mech. Mater. 38 (2006) 1072–1089.

Varadan V.K. and Varadan V.V., Microsensors, microelectromechanical systems (MEMS), and elecctronics for smart structures and systems, *Smart Materials and Structures* **9** (2000) 953-972.

Varadan V.K., Lim Y.H. and Varadan V.V., Close loop finite element modeling of active/passive damping in structural vibration control, *Smart Materials and Structures* **5** (1996) 685-694.

Varelis D. and Saravanos D.A., Coupled buckling and postbuckling analysis of active laminated piezoelectric composite plates, *International Journal of Solids and Structures* **41** (2004) 1519-1538.

Varelis D. and Saravanos D.A., Numerical Analysis of Performances of The Bonded Composite Patch for Reducing Stress Concentration and Repairing Cracks at Notch, *Computational Materials Science* **28** (2003) 41–48.

Viktorov I.A., Rayleigh and Lamb Waves New York: Plenum (1967).

Viktorov I.A., Surface waves in solids Moscow: Nauka Russian (1981).

Wang C.H., *Introduction to Fracture Mechanics* DSTO (Victoria: Aeronautical and Maritime Research Laboratory) 1996.

Wang M. and Meng G., Vibration control of structures treated with delaminated active constrained layer damping, *Proceedings of The International Conference on Mechanical Engineering and Mechanics* **2** (2007) 1518-1521.

Wang Q. and Liew K.M., Analysis of wave propagation in piezoelectric coupled cylinder affected by transverse shear and rotary inertia, *International Journal of Solids and Structures* **40** (2003) 6653-6667.

Wang Q. and Quek S.T., Enhance flutter and buckling capacity of column by piezoelectric layer, *International Journal of Solids and Structures* **39** (2002) 4167-4180.

Wang Q. and Quek S.T., Flexural vibration analysis of sandwich beam coupled with piezoelectric actuator, *Smart Materials and Structures* **9** (2000e) 103-109.

Wang Q. and Quek S.T., On dispersion relations in piezoelectric coupled beams, *AIAA Journal* **38** (2000f) 2357-2361.

Wang Q. and Quek S.T., Repair of delaminated beams via piezoelectric patches, *Smart Mater. Struct.* **13** (2004) 1222–1229.

Wang Q. and Varadan V.K., SH wave propagation in piezoelectric coupled plates, IEEE Transactions on Ultrasonics, *Ferroelectrics, and Frequency Control* **49** (2002g) 596-603.

Wang Q. and Varadan V.K., Wave propagation in piezoelectric coupled plates by use of interdigital transducer Part 1. Dispersion characteristics, *International Journal of Solids and Structures* **39** (2002h) 1119-1130.

Wang Q., Duan W.H. and Quek S.T., Repair of notched beam under dynamic load using piezoelectric patch, *International Journal of Mechanical Science* **46** (2004) 1517-1533.

Wang Q., Quek S.T. and Liew K.M., On the repair of a cracked beam via piezoelectric patches, *Smart Mater. Struct.* **11** (2002) 404-410.

Wang Q., Quek S.T., Sun C.T. and Liu X., Analysis of piezoelectric coupled circular plate, *Smart Materials and Structures* **10** (2001) 229-239.

Wang Q., On buckling of column structures with a pair of piezoelectric layers, *Engineering Structures* **24** (2001) 199-205.

Wang Q., On The Jump of Buckling Capacity of Beams via Piezoelectric Layers, *Advances in Structural Engineering* **7** (2004) 363-370.

Wang Q., A note on possible flutter of piezoelectric layers, *International Journal of Structural Stability and Dynamics* **5** (2005) 125-133.

Wang Q. and Quek S.T., Repair of cracked column under axially compressive load via piezoelectric patch, *Computers & Structures* **83** (2005) 1355-1363.

Wang Q. and Quek S.T., Enhancing flutter and buckling capacity of column by piezoelectric layers, *International Journal of Solids and Structures* **39** (2002i) 4167-4180.

Wang Q. and Quek S.T., Repair of delaminated beams via piezoelectric patches, *Smart Materials and Structures* **13** (2004) 1222-1229.

Wang Q. and Varadan V.K., Transition of the buckling load of beams by the use of piezoelectric layers, *Smart Materials and Structures* **12** (2003) 696-702.

Wang Q. and Wu N., A review on repair of cracked and delaminated structures with piezoelectric materials, *CSME Bulletin* (2011).

Wang Q.S. Active buckling control of beams using piezoelectric actuators and strain gauge sensors, *Smart Materials and Structures* **19** (2010) 065022.

Wang Q., Duan W. and Quek S.T., Repair of notched beam under dynamic load using piezoelectric patch, *International Journal of Mechanical Sciences* **46** (2004) 1517-1533.

Wang Q., Liew K.M., He X.Q. and Xiang Y., Local buckling of carbon nanotubes under bending *Applied Physics Letters* **91** (2007) 093128.

Wang Q., Zhou G.Y. and Quek S.T., Repair of delaminated beams subjected to compressive force via piezoelectric layers, *Advances in Structural Engineering* **8** (2005) 411-425.

Wells G.N., de Borst R. and Sluys L.J., A consistent geometrically non-linear approach for delamination, *Int. J. Numer. Methods Eng.* **54** (2002) 1333–1355.

Wilkins D.J., Eisenmann J.R., Camin R.A., W.S. Margolis and R.A. Benson Characterizing delamination growth in graphite-epoxy *Damages in Composite Materials ASTM Special Technical Publication* (1982) 168–183.

Wu N. and Wang Q., An experimental study on repair of a notched beam subjected to dynamic loading with piezoelectric patches, *Smart Materials and Structures* (2011) **In Review.**

Wu N. and Wang Q., Repair of a delaminated plate under static loading with piezoelectric patches, *Smart Materials and Structures* **19** (2010j) 105025.

Wu N. and Wang Q., Repair of vibrating delaminated beam structures using piezoelectric patches, *Smart Materials and Structures* **19** (2010k) 035027.

Young A., Rooke D.P. and Cartwright D.J., Analysis of patched and stiffened cracked panels using the boundary element method, *Int. J. Solids Struct.* **29** (1992) 2201–2216.

Yu H.H., He M.Y. and Hutchinson J.W., Edge effects in thin film delamination, *Acta Mater.* **49** (2001) 93–107.

Zhang Z., Feng C. and Liew K.M., Three-dimensional vibration analysis of multilayered piezoelectric composite plates, *International Journal of Engineering Science* **44** (2006) 397-408.

Zou Y., Tong L. and Steven G.P., Vibration-based model-dependent damage (delamination) identification and health monitoring for composite structures—a review, J. Sound Vib. 230 (2000) 357–378.

Appendix: List of publications in PhD research

Referred Journal Papers (9)

Accepted (9):

Q. Wang and N. Wu, 2012, An review on structure enhancement and repair using piezoelectric materials and shape memory alloys, *Smart Materials and Structures*, Vol. 21 013001.

N. Wu and Q. Wang, 2011, An experimental study on repair of a cracked beam subjected to dynamic loading with piezoelectric patches, *Smart Materials and Structures*, Vol.20 115023.

Q. Wang and N. Wu, 2011, A review on repair of cracked and delaminated structures with piezo electric materials, *CSME Bulletin*, June 2011.

N. Wu and Q. Wang, Experimental study of damage detection of beam structures with wavelets t ransform International, *Journal of Engineering Science*, Vol.49 pp. 253-261 2011.

Q. Wang and N. Wu, Detecting delamination location of a beam with wavelet transform: An exp erimental study, *Smart Materials and Structures (Feature article)*, Vol. 20 012002 2011.

N. Wu and Q. Wang, Repair of a delaminated plate under static loading with piezoelectric patche s, *Smart Materials and Structures*, Vol.19 105025 2010.

N. Wu and Q. Wang, Repair of vibrating delaminated beam structures using piezoelectric patche s, *Smart Materials and Structures*, Vol.19 035027 2010.

N. Wu, Q. Wang and S.T. Quek, Free Vibration Analysis of Piezoelectric Coupled Circular Plate with Open Circuit, *Journal of Sound and Vibration*, Vol. 329 pp. 1126-1136 2010.

Q. Wang, N. Wu and S.T. Quek, Acoustic Wave in Piezoelectric Coupled Plates with Open Circ uit, *International Journal of Structural Stability and Dynamics*, Vol.10 pp. 1-15 2010.

Referred Conference Papers (2):

N. Wu and Q. Wang, Repair of A Square Delaminated Plate Under A Static Loading, *5th World Conference on Structural Control and Monitoring*, July 12-July 14, 2010, Tokyo, Japan

N. Wu and Q. J. Peng, Maintainability evaluation based on product disassembly analysis, *Procee dings of the ASME 2009 International Design Engineering Technical Conferences & Computers and Information in Engineering Conference*, August 30 - September 2, 2009, San Diego, Califor nia, USA

Patent (1):

Q. Wang and N. Wu, Repair of Delaminated Plates with piezoelectric materials, UNITED STATES PATENT APPLICATION, 2010.